Transport phenomenon in a lowdimensional quantum system

Ph.D. Thesis



Hemant Kumar Sharma

Supervised by

Prof. Ashok Chatterjee

School of Physics
University of Hyderabad
Hyderabad -500046
Telangana
India

December 2021

Transport phenomenon in a low-dimensional quantum system

A thesis submitted for the award of the degree of

Doctor of Philosophy in Physics

by

Hemant Kumar Sharma

(Reg. No. 15PHPH15)

Supervised by

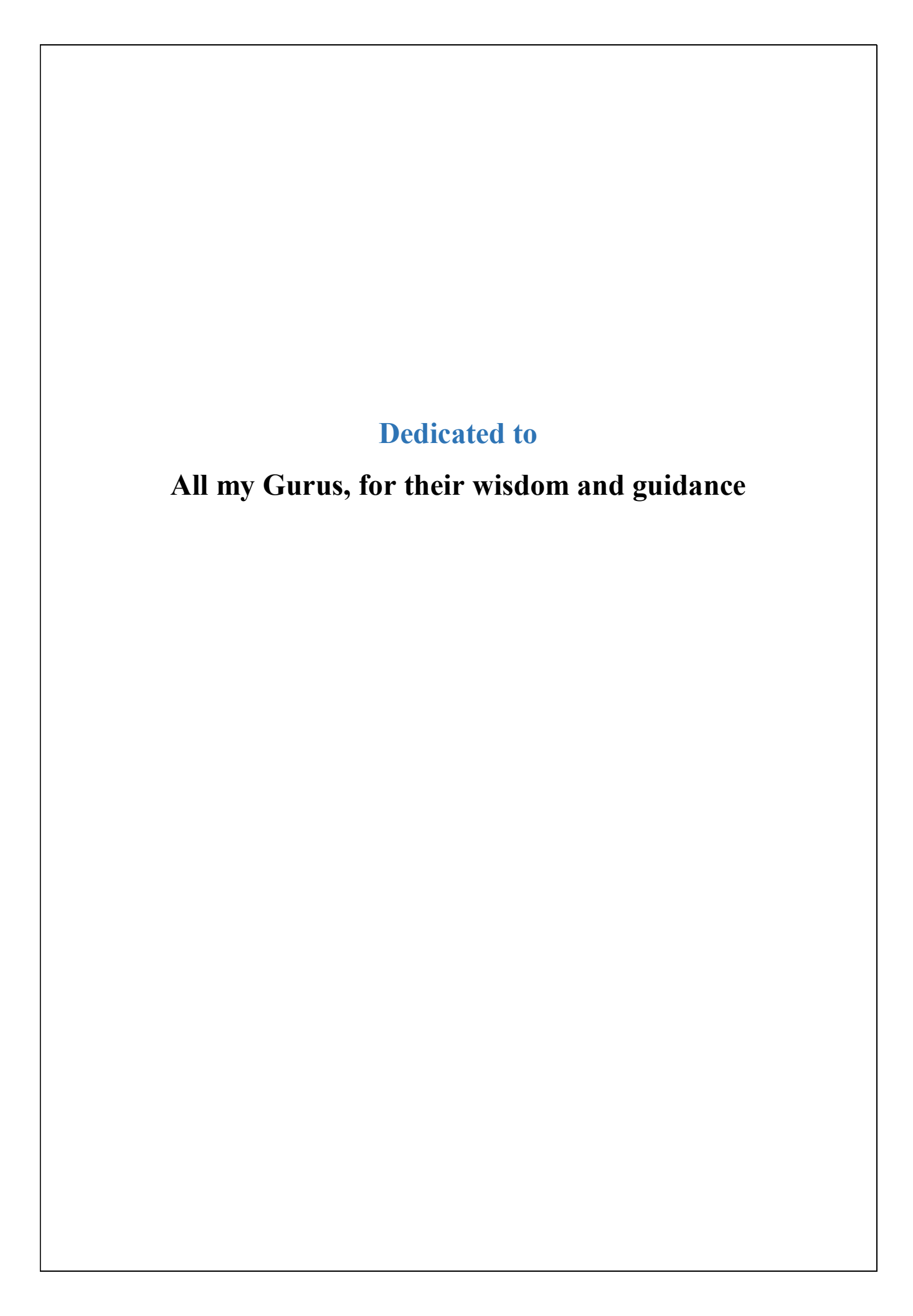
Prof. Ashok Chatterjee





School of Physics
University of Hyderabad
Hyderabad -500046
Telangana
India

December 2021







Declaration

I, Hemant Kumar Sharma hereby declare that, the work reported in this thesis entitled, "Transport phenomenon in a low-dimensional quantum system", is original and has been carried out by me under the supervision of Prof. Ashok Chatterjee, School of Physics, University of Hyderabad, Telangana, India, as per the Ph.D. ordinances of the University. I also declare that, this work is free from plagiarism and it has not submitted for the award of a research degree at any other University. I hereby agree that my thesis can be deposited in Shodhganga or INFLIBNET. A report on plagiarism statistics from the university librarian is enclosed.

(Hemant Kumar Sharma)

Reg. No: 15PHPH15

Date: 29/12/2021

Hyderabad





Certificate

This is to certify that, the thesis entitled "Transport phenomenon in a low-dimensional quantum system", submitted to the University of Hyderabad by Mr. Hemant Kumar Sharma bearing Reg. No. 15PHPH15 in partial fulfilment of the requirements for the award of Doctor of Philosophy in Physics, is a bonafide work carried out by him under my supervision and guidance, which is a plagiarism free thesis. The thesis has not been submitted previously in part or in full to this or any other University or Institution for the award of any degree or diploma.

Further, the student has the following publications before submission of the thesis for adjudication:

- 1) "Spin torque induced spin current in a two-dimensional tight-binding system with Rashba coupling in the presence of random impurities". **H. Sharma**, S. Sil, and A. Chatterjee, J Mag Mag Mat, **500**, 166329, (2020): (Chapter 2)
- 2) "Spin transport in a two-dimensional tight-binding system with Rashba and Dresselhaus spin-orbit interactions in the presence of static random disorder".**H. K Sharma**, S. Sil and A. Chatterjee, J Mag Mag. Mat, **529**, 167711, (2021). (Chapter 3)

Manuscripts under preparation/review

- 1) Torque-dependent Spin-Hall conductivity and Hall angle in presence of Rashba and Dresselhaus spin-orbit interactions and static random disorder for a two-dimensional tight-binding system. **Hemant K. Sharma**, S. Sil and A. Chatterjee (**in Review**): (Chapter -4)
- 2) Torque-dependent Spin-Hall conductivity and Hall angle in presence of Rashba and Dresselhaus spin-orbit interactions and static random disorder for a two-dimensional tight-binding system at finite temperature. **Hemant K. Sharma**, S. Sil and A. Chatterjee (**To be communicated**). (Chapter -5)
- 3) Magneto-transport through a Quantum Dot Dimer in presence of quantum dissipation, electron-electron and electron-phonon interaction. H. K
 Sharma, M. Kalla and A. Chatterjee (To be communicated). (Chapter -6)

List of publications (not part of the thesis work):

- "Electronic and magnetic properties of a two-electron Gaussian GaAs quantum dot with spin-Zeeman term: A study by numerical diagonalization".
 Hemant K. Sharma, Aalu Boda, Bahadir Boyacioglu, Ashok Chatterjee J Mag Mag Mat, 469, 171, (2020).
- 2) "Nature of localization-delocalization transition in a two-level system interacting with a phonon bath: A variational treatment with an improved wave function" **Hemant K. Sharma**, M. Yadaiah, Soma Mukhopadhyay and Ashok Chatterjee, IJTP **59**, 596 (2020)

Also, made presentations in the following conferences:

1. Q-Mat

Spin Transport in presence of Rashba Spin orbit Interaction in Two Dimension System

5th - 27th July, 2018. IISER Mohali.

2. Annual Conference on Quantum Condensed matter

Nature of localization-delocalization transition in a two-level system interacting with a phonon bath: A variational treatment with an improved wave function

Indian Institute of Science, Bangalore, India, 8th-10th July, 2019

3. International Conference on Condensed Matter Physics

Spin Hall Conductance in a two-dimensional tight-binding model in the presence of Rashba spin-orbit interaction and random impurities. (IJIIP, Vol. 1, Issue 2, 2020)

Oral talk

Kolkata, West Bengal, India, 14th-16th Nov, 2019

The following courses have taken as part of the course work:

Course No.	Course Offered at	Title of Course Credit	Pass/Fail
PY801	School of Physics	Advanced Quantum	Pass
		Mechanics	
PY803	School of Physics	Advanced Electromagnetic	Pass
		Theory	
PY804	School of Physics	Advanced Statistical	Pass
		Mechanics	
PY821	School of Physics	Research Methodology	Pass

(Prof. Ashok Chatterjee)
Thesis Supervisor,
School of Physics,

University of Hyderabad.

Dean M. Thauashyam. School of Physics, University of Hyderabad. Date: 29 | 12 | 202 |

School of Physics
University of Hyderabad
Avderabad-500 046, INDIA

Prof. ASHOK CHATTERJEE SCHOOL OF PHYSICS UNIVERSITY OF HYDERABAD HYDERABAD - 500 046. INDIA

ACKNOWLEDGEMENTS

First of all, I would like to express my sincere gratitude to my supervisor Prof. Ashok Chatterjee for his immense support in my research work. His passion and devotion toward the wok always inspired me. His guidance helped me in all the time of research and writing this thesis. A special thanks to Dr. Soma Mukhopadhyay, who helped me tremendously in my research work and the personal problem all these years. I had a great time, and I learned a lot from them. It always brings peace to my mind whenever I am with them. I am indebted to Prof. S. Srinath and Prof. V S Nageswara Rao for being my Doctoral Committee members. Their insightful comments and questions lead me to improve my knowledge of physics. My heartfelt thanks to Dr. Shreekantha Sil for his help in my scientific calculations. I am deeply grateful to Prof. Vinod Nautiyal, who taught me every subject during my undergraduate and was always there whenever I needed moral support. It is a genuine pleasure to express my deep sense of thanks to Dr. Vaitheeswaran G. S, and Dr. Shyamal Biswas, for their care and unfailing support. I had the great pleasure to have friends like Deepak, Bhuvan, Neeraj, Dhananjay, Ajay, Dr. Raghay, and Dr. Vipin, who always cheered me up and motivated me when things were not on my sides. I thank my group members Zahid, Manasa, Kuntal, Pooja, and Debika for our fruitful discussions and my seniors Uma Lavonia and Dr. Lulu Jahan. I am incredibly grateful to my super senior Dr. Allu Boda for his enormous help in my research work. I am grateful to Dr. Konda Srinivas, Vineet, Subrata, Parveen, Bappa, Pawan, Shanti, Susmita, Rakshit, Karishma, and Sarthak for standing by me through good or bad times. I offer my profuse thanks to all the School Of Physics staff for their kind help and co-operation throughout my entire Ph. D. program. It was a remarkable and joyful journey with many ups and downs. It became memorable because of the love and care of so many people. I want to thank all those people I met somewhere, and somehow they made me smile and taught me beautiful life lessons. Life was not

easy, but my friends, family, and professors gave me a chance to enjoy it. Furthermore, I would like to thank my family for their patience and support. I hope their patience brings fruitful results. Lastly, I want to pay my regard to Ziyad Kadir for his love and care.

CONTENTS

Chapter 1: Introduction	
1.1 Spintronics	2
1.2 Spin Orbit interactions	2
1.3 Spin Hall effect	4
1.4 Single Molecular Transistor	5
1.5 Outline	6
1.6 References	7
Chapter 2: Torque-dependent Spin and ch presence of Rashba spin-orbit interaction disorder for a two-dimensional tight-bindi	s and static random
2.1 Introduction	11
2.2 Model	12
2.2.1 Spin Current	14
2.2.2 Charge Current	18

2.2.4 Longitudinal Charge Conductivity	27
2.2.5 Longitudinal Spin Conductivity	31
2.3 Numerical Result	32
2.4 Conclusion	39
2.5 References	40
Chapter 3: Torque-dependent Spin and charge con presence of Rashba and Dresselhaus spin-orbit i and static random disorder for a two-dimensi binding system.	nteractions
3.1 Introduction	42
3.2 Model	42
3.2.1 Spin Current	45
3.2.2 Charge Current	48
3.2.3 Relaxation Time	52
3.2.4 Longitudinal Charge Conductivity	54
3.2.5 Longitudinal Spin Conductivity	56
3.3 Numerical Result and Discussion	58
3.4 Conclusion	66
3.5 References	67

Chapter 4: Torque-dependent Spin-Hall conductivity and Hall angle in presence of Rashba and Dresselhaus spin-orbit interactions and static random disorder for a two-dimensional tight-binding system

4.1 Introduction	68
4.2 Formalism	69
4.3 Result	70
4.4 Conclusion	75

Chapter 5: Torque-dependent Spin-Hall conductivity and Hall angle in presence of Rashba and Dresselhaus spin-orbit interactions and static random disorder for a two-dimensional tight-binding system at finite temperature.

76
76
78
78
82
86
92
92

Chapter 6: Magneto-transport through a Quantum Dot Dimer in presence of quantum dissipation, electron-electron and electron-phonon interaction.

6.1 Introduction	93
6.2 Model	95
6.3 Result and Discussion	116
6.4 Conclusion	132
6.5 References	133
Chapter 7: Conclusion	137
List of publications	141

CHAPTER 1

Introduction

Presently, science and technology is on a new path of accelerated growth for faster and better performance of electronics devices. This has been possible because of the advanced fabrication technology which can produce electronic components in ultra-small sizes. The density with which transistors and resistors are fabricated on the memory devices or computer chips has reached a remarkably high value. This has led to a tremendous increase in the performance of electronic devices. But the performance of the devices due to the small sizes of its components has its limits. These limits are mainly caused by quantum mechanical factors, due to which electron motion can no longer be controlled. One serious difficulty that arises at very small length scale in the compact devices is the Joule heating which leads to a decrease in the lifetime and efficiency of the devices. This problem arises when the charge of the electron is the main focus of study. Thus one has to go for other alternative properties of the electron, such as spin. It was first shown by Dirac [2] that the electron has not only charge and mass but also an intrinsic angular momentum, namely 'spin,' which arises from relativistic effect. This new concept has generated a new field where both the charge and spin play a crucial role. This new field is referred to as 'Spin-electronics' or more commonly as "Spintronics."

1.1 Spintronics

Spintronics [3, 4] is a relatively new emerging field of condense field physics that promises increasing speed, faster computation, and less power consumption while minimizing electronic circuits. Spintronics uses electron degree of freedom in addition to or in place of the electron charge. The first encounter with spintronics comes when researchers observe a change in electrical resistance when current passes through a non-magnetic and magnetic layers in the presence of a magnetic field. This led to the discovery of the giant magnetoresistance effect (GMR) [5] in 1988 by Fert and Grunberg, for which they got the Nobel Prize in 2007. Further work showed that with the change in magnetic and non-magnetic layer thickness, one could control GMR [6], and it could be used for commercial purposes and for storing data in electrical devices. In 1990, Datta and Das proposed the spin filter concept [7], which suited well as an example for a spintronic device. These spin transistors are quite similar to a conventional transistor. Of course, there are also some differences. In conventional transistors, the gate voltage influences electron motion. However, in a spin transistor, the gate voltage modifies the electron's spin by controlling its precession. This manipulation of spin makes the device far more energetically efficient and provides a faster switching time.

Besides having profound applications, the field of Spintronics also has intrinsic interest because the working of a spintronic device depends profoundly on the fundamental understanding of spin properties and its transport mechanism. It also provides a new challenge and chance to understand the basic quantum nature of matter.

1.2 Spin-Orbit Interaction

Spin-orbit interaction results from relativistic Quantum theory, where along with the electronic charge, spin is a fundamental and integral part of the electron, as illustrated in the Dirac theory. In the non-relativistic regime, Dirac equation can be written as Schrodinger equation along with some relativistic corrections. These relativistic corrections couple the momentum of the electron and its spin to the external potential gradient. This forms the fundamental origin of spin-orbit coupling, which includes both L.S couplings. Firstly, it links the spin-orbital momentum S to orbital angular momentum L in atomic and molecular physics. Secondly, it connects all the phenomena of spin-orbit interactions in the condense matter system.

In atomic and molecular physics, the spin-orbit coupling is a very familiar term. It gives the coupling between the spin of an electron and its angular momentum around the nucleus and leads to the fine structure splitting. Spin-orbit coupling can be explained in terms of $-\mu$. B Zeeman interaction, which acts between the μ magnetic moment of a particle and a magnetic field B present in the particle's moving frame. In a material, a momentum-dependent Zeeman term arises when a static electric field $E = E_0 e_z$ gives rise to spin-orbit magnetic field $B_{SO} = (E_0 \hbar/mc^2) \times (k_x e_y - k_x e_y)$ in the moving frame of the electron having momentum $\hbar k$, where σ_x and σ_y are x and y component of spin matrices, m is the mass of the electron, and c is the speed of light. The momentum-dependent Zeeman term is known as Rashba spin-orbit coupling [8], which can be written as follows:: $-\mu B = \sigma_x k_y - \sigma_y k_x$, and often comes from the asymmetry of confinement potential in a twodimensional heterostructure. So, whenever the electron moves in a crystal having a potential gradient, spin-orbit coupling (SOC) plays a prominent role. SOC mainly originates either from lack of mirror symmetry causing Rashba type SOC in two-dimensional system as discussed above or from

the lack of bulk inversion symmetry, known as Dresselhaus SOC [9] which is given by Zeeman interaction term: $-\mu B = \sigma_x k_x - \sigma_y k_y$.

Since the early days of quantum mechanics, the phenomenon of SOC was well known. However, recent development in spintronics has made it a subject of intense interest. Apart from many applications, The SOC performs a vital role in the Anomalous Hall effect, Spin Hall effect [10, 11], and Topological insulators [12].

1.3 Spin Hall Effect

The Spin Hall effect (SHE) acquires its concept from the Anomalous Hall effect and is possibly the best illustration of spin-orbit interaction. In the Anomalous Hall Effect (AHE), SOC causes an asymmetric scattering of charge carriers depending on their orientations and in ferromagnetic material it can be determined electrically because of a population difference in the majority and the minority carrier causing a transverse potential drop [13]. Spin Hall Effect is a pure SOC phenomenon and can be observed in non-magnetic materials. Due to SOC, the up spin and down spin charge carriers becomes different in number leading to non-zero transverse voltage drop. The spin Hall Effect was first proposed by Dyakonov and Perel [14, 15] based on the skew scattering mechanism (Mott scattering) some five decades ago. They observed that a nonpolarized electric current produced a transversely polarized current due to external spin-orbit interaction. Similarly, the Inverse spin Hall Effect leads to a transverse electric current when polarized spin current is passed. Three decades later, the intrinsic Spin Hall Effect was predicted by Mukami [16] and Sinova [17] which initiated an intense debate in this field [See [18-20] and references therein].

In recent years, there has been a flurry of investigations on Spin Hall devices that have the potential for application in spintronics, like optical and spin injection and detection in non-magnetic systems. In metallic spin Hall devices [21, 22], it was seen that a non-magnetic electrode could be utilized to generate and detect spin current [23]. In semiconductors spin Hall devices, attention has been concentrated on optical detection [24, 25, 26], and it was seen that polarized light can be electrically detected by inverse spin Hall Effect, which produces electric current from the optically induced spin current [27, 28]. Some devices can connect the externally-controlled SOC with inverse Hall Effect to detect electric spin [29, 30]. This provides the basis for devices like spin field-effect transistors.

1.4 Single Molecular Transistors

Transistors are the vital parts of electronic devices and have constituted the main role in the digital revolution. Since the development of the first model, many new designs have been proposed, but the basic idea has remained the same. A transistor is a three-terminal device. By applying voltage or injecting charge at one terminal, one can manipulate current through the remaining terminals. The transistor acts as an amplifier when the output power is higher than the input power. Another transistor application would be its manifestation as a switch, in which one terminal regulates voltage between the other two.

In 1974 [31], the first proposal of using single molecular transistors in an electronic device came and since then, considerable effort has been made to downsize the device to a single molecular level. The first single molecular device was fabricated by H. Park .et. al in 2000 [32] and understandably the interest in the subject grew enormously after that. A typical single molecular device contains a central molecule linking a source and a drain, and the whole structure is placed on a gate electrode. In this device, the gate electrode regulates the current between

the source and the drain. Besides being used for switching and amplification functions, a single molecular transistor can also be used for spectroscopy information i.e. by changing the gate voltage, the shift in the energy level of the central molecule can be observed. From this observation one can achieve further information about the molecule or the quantum dot such the presence of excites states and vibrational modes [32, 33] and also the effects like frank-condon blockage [34], Kondo effect [35, 36] and superconductivity [37]. Furthermore, the gate electrode terminal can be used to reduce, oxidize, and explore the properties of Molecular transport for various charge states by attracting and repelling electrons. Also, the fine structure of single-molecule magnets and magnetic anisotropy can also be revealed using three terminal devices [39-41]. Additionally, they facilitate the driving [42] and read out [43] of single nuclear spins, which can act as molecular quantum bits.

1.5 Outline

This thesis is arranged in the following order. In the present chapter i. e., Chapter 1, we have introduced some basic terminologies and a brief overview of spintronics and single molecular transistor.

In the following chapter i. e., in Chapter 2, we have shown our calculation of the torque-dependent spin and charge conductivity in the presence of Rashba spin-orbit interaction and impurity for a two-dimensional system. We have used spin and charge polarization operators to calculate spin and charge current and the Matsubara Green function technique to relaxation time due to random impurity. We further calculate the charge and spin conductivity using Kubo's current-current correlation function.

In Chapter 3, we discusses the effect of both Rashba and Dresselhaus spin-orbit interactions and study how the interplay between Rashba and Dresselhaus interactions affects our system when the impurity is present.

In Chapter 4, we extend the formalism used in Chapters 2 and 3 to investigate the effect of Rashba and Dresselhaus spin orbit interactions on torque dependent spin Hall conductivity in the presence of impurities.

From the point of view of experiments, it is important to have results at finite temperatures. Therefore to make our work more realistic and practical, we study in Chapter 5, the longitudinal and transverse spin and charge conductivity at finite temperature.

In Chapter 6 we investigates non-equilibrium quantum transport in a quantum dot dimer, situated on a non-conducting substrate and attached to a source and a drain by two metallic rods. Here, we computed the tunneling current and differential conductivity of a quantum dot dimer using the Keldysh non-equilibrium Green function formalism.

Finally in Chapter 7, we summarize our findings and make concluding remarks.

1.6 References

- 1. G. E. Moore. Cramming more components onto integrated circuits. Electronics, **38**,114, (1965).
- 2. P. A. M. Dirac. The quantum theory of the electron. Proc. R. Soc. Lond. A, 17, 610, (1928).

- 3. S. A. Wolf *et. al.*, Science **294**, 1488 (2001).
- 4. I. Žutić, J. Fabian, and S. D. Sarma, Rev. Mod. Phys. **76**, 323 (2004).
- 5. W. P. McCray. How spintronics went from the lab to the ipod. Nat. Nano., 4:4, 2009
- 6. S. S. P. Parkin, N. More, and K. P. Roche. Phys. Rev. Lett., **64**, 2304 (1990).
- 7. S. Datta and B. Das. Appl. Phys. Lett., **56**, 665, (1990).
- 8. Y.A. Bychkov, & E.I Rashba, J. Phys. Chem. 17, 6039 (1984).
- 9. G. Dresselhaus, G. Phys. Rev. 100, 580 (1955).
- 10. J. Sinova, et al. Rev. Lett. **92**, 126603 (2004).
- Y. K. Kato, R.C. Myers, A. C. Gossard, &D. D. Awschalom.. Science 306, 1910(2004).
- 12. M. Z. Hasan, & C. L. Kane, Rev. Mod. Phys. 82, 3045 (2010).
- N. Nagaosa., J. Sinova, S. Onoda, A. H. MacDonald, and N. P. Ong, Rev. Mod. Phys. 82, 1539 (2010).
- 14. M. I. Dyakonov and V. I. Perel. JETP Lett. 13:467 (1971).
- 15. M. I. Dyakonov and V. I. Perel. Phys. Lett. A, **35**:459, (1971).
- 16. S. Murakami, N. Nagaosa, and S.-C. Zhang.. Science, **301**, 1348,(2003).
- 17. J. Sinova, D. Culcer, Q. Niu, N. A. Sinitsyn, T. Jungwirth, and A. H. MacDonald. Phys. Rev. Lett., **92**, 126603, (2004).
- H.-A. Engel, E. I. Rashba, and B. I. Halperin. Theory of spin hall effects in semiconductors. In H. Kronmuller and S. Parkin, editors, Handbook of Magnetism and Advanced Magnetic Materials, volume 5, pages 2858–2877. Wiley, Chichester, (2007).
- 19. J. Sinova and A. H. MacDonald. Theory of spin-orbit effects in semiconductors. volume 82 of Semiconductors and Semimetals, chapter 2, pages 45–87. Elsevier, (2008).
- 20. R. Raimondi, P. Schwab, C. Gorini, and G. Vignale. Ann. Phys., **524**, 153, (2012).
- 21. S. O. Valenzuela and M. Tinkham. Nature, **442**, 176, (2006).

- 22. E. Saitoh, M. Ueda, H. Miyajima, and G. Tatara. Appl. Phys. Lett., **88**, 182509, (2006).
- 23. T. Kimura, Y. Otani, T. Sato, S. Takahashi, and S. Maekawa. Phys. Rev. Lett., **98**, 156601, (2007).
- 24. Y. K. Kato, R. C. Myers, A. C. Gossard, and D. D. Awschalom. Science, **306**, 1910, (2004).
- 25. V. Sih, R. C. Myers, Y. K. Kato, W. H. Lau, A. C. Gossard, and D. D. Awschalom. Nat. Phys., 1, 31, (2005).
- J. Wunderlich, B. Kaestner, J. Sinova, and T. Jungwirth. Phys. Rev. Lett.,
 94, 047204, (2005).
- 27. J. Wunderlich, A. C. Irvine, J. Sinova, B. G. Park, L. P. Zarbo, X. L. Xu, B. Kaestner, V. Novak, and T. Jungwirth. Nat. Phys., 5, 675 (2009).
- 28. K. Ando, M. Morikawa, T. Trypiniotis, Y. Fujikawa, C. H. W. Barnes, and E. Saitoh.. Appl. Phys. Lett., **96**, 082502 (2010).
- 29. C. Br"une, A. Roth, E. G. Novik, M. Konig, H. Buhmann, E. M. Hankiewicz, W. Hanke, J. Sinova, and L. W. Molenkamp. Nat. Phys., **6** 448, (2010).
- 30. J. Wunderlich, B.-G. Park, A. C. Irvine, L. P. Z^arbo, E. Rozkotov'a, P. Nemec, V. Nov'ak, J. Sinova, and T. Jungwirth. Science, **330**(6012):1801–1804, (2010).
- 31. A. Aviram and M. A. Ratner, Chem. Phys. Lett. 29, 277, (1974).
- 32. H. Park, J. Park, A. K. L. Lim, E. H. Anderson, A. P. Alivisatos and P. L. McEuen, Nature, **407**, 57,(2000).
- 33. E. A. Osorio, K. O'Neill, N. Stuhr-Hansen, O. F. Nielsen, T. Bjørnholm and H. S. J. van der Zant, Adv. Mater., **19(2)**, 281, (2007)(a).
- 34. E. Burzuri', Y. Yamamoto, M. Warnock, X. Zhong, K. Park, A. Cornia and H. S. J. van der Zant, Nano Lett., 14, 3191 (2014).
- 35. J. Park, A. N. Pasupathy, J. I. Goldsmith, C. Chang, Y. Yaish, J. R. Petta, M. Rinkoski, J. P. Sethna, H. D. Abruna, P. L. McEuen and D. C. Ralph, Nature, 417, 722, (2002).

- 36. W. J. Liang, M. P. Shores, M. Bockrath, J. R. Long and H. Park, Nature, 417, 725, (2002).
- 37. C. B. Winkelmann, N. Roch, W. Wernsdorfer, V. Bouchiat and F. Balestro, Nat. Phys. **5**, 876, (2009).
- 38. S. Kubatkin, A. Danilov, M. Hjort, J. Cornil, N. Bredas, J. L. Stuhr-Hansen, P. Hedegard and T. Bjørnholm, Nature, **425**, 698, (2003).
- 39. H. B. Heersche, Z. de Groot, J. A. Folk, H. S. J. van der Zant, C. Romeike, M. R. Wegewijs, L. Zobbi, D. Barreca, E. Tondello and A. Cornia, Phys. Rev. Lett., **96**, 206801, (2006).
- A. S. Zyazin, J. W. G. van den Berg, E. A. Osorio, H. S. J. van der Zant, N. P. Konstantinidis, M. Leijnse, M. R. Wegewijs, F. May, W. Hofstetter, C. Danieli and A. Cornia, Nano Lett. 10, 3307 (2010).
- 41. E. Burzuri', A. S. Zyazin, A. Cornia and H. S. J. van der Zant, Phys. Rev. Lett. **109**, 147203 (2012).
- 42. S. Thiele, F. Balestro, R. Ballou, S. Klyatskaya, M. Ruben and W. Wernsdorfer, Science, **344**, 6188 (2014).
- 43. R. Vincent, S. Klyatskaya, M. Ruben, W. Wernsdorfer and F. Balestro, Nature, **488**, 357 (2012).

CHAPTER 2

Torque-dependent Spin and charge conductivity in presence of Rashba spin-orbit interactions and static random disorder for a two-dimensional tight-binding system.

2.1 Introduction

The main concern in spintronics is to generate and manipulate spin current [1, 2] and employ its effects in different systems, ranging from semiconductor paramagnets to ferromagnetic metals. Ideally, the spin current is defined as the difference between the up-spin current and the down-spin current. But in the presence of spin-orbit interactions, spin is no longer a conserved quantity, though this difficulty is usually circumvented by focusing on spin relaxation time. Over the last few years, it has been discovered that spin-orbit coupling can be used to achieve electric control of spin generation and its transport [3, 9]. So, defining a spin current in a general situation i.e., in the presence and absence of spin-orbit interactions, becomes important.

In most of the earlier works on spin transport, the spin current has been determined by calculating the expectation value of the product of spin and the velocity observable. But this conventional definition $[(vs^z + s^zv)/2]$ suffers from serious flaws. First, the spin current, according to this definition, is not a conserved quantity. This problem motivated numerous alternative definitions [10–11]. Secondly, the spin current obtained using the above definition turns out to be finite in insulators with localized eigenstates only [12]. Finally, as there is no mechanical or thermodynamic force associated with this current, the usual near-equilibrium transport theory cannot account for it. To overcome the

problems mentioned above, Shi et al. [13] has provided a new definition spin current. They have defined the spin current as the time derivate of the spin displacement, and it differs by a torque dipole term [14, 15] from the conventional definition of spin current. This torque dipole term arises when the spin magnetic moment of the system is not conserved and is given by the expectation value of the rate of change of spin.

In the present chapter, we investigate the role of Rashba spin-orbit (RSO) interaction (RSOI) on the torque-dependent longitudinal charge and spin conductivity for a two-dimensional tight-binding model in the presence of random impurities.

2.2 The Model

We consider a two-dimensional electronic system in the presence of Rashba spinorbit coupling and random impurities. The Hamiltonian consists of the onsite energy term, the hopping term, the Rashba spin-orbit interaction term and the electron-impurity interaction term. Thus the Hamiltonian of the system is given by

$$H = H_0 + H_{imp}. (2.1)$$

$$H_{0} = \sum_{i} \epsilon_{0} c_{i}^{\dagger} c_{i} + t \left[\sum_{i_{x}, i_{y}} c_{i_{x}, i_{y}} c_{i_{x+1}, i_{y}} + c_{i_{x}, i_{y}}^{\dagger} c_{i_{x}, i_{y+1}} + h.c \right]$$

$$-i\alpha_{R} \left[\sum_{i_{x}, i_{y}} c_{i_{x}, i_{y}}^{\dagger} \sigma_{y} c_{i_{x+1}, i_{y}} + h.c \right] + i\alpha_{R} \left[+ \sum_{i_{x}, i_{y}} c_{i_{x}, i_{y}}^{\dagger} \sigma_{x} c_{i_{x}, i_{y+1}} + h.c \right].$$

$$(2.2)$$

$$H_{imp} = \sum_{i,l} v \delta(r_i - r_l) c_i^{\dagger} c_i.$$
 (2.3)

where ϵ_0 is the onsite energy, t gives the hopping coefficient and α_R is the Rashba spin-orbit interaction strength. In the Impurity Hamiltonian H_{imp} , r_i and r_l give he position vectors of the electron and the impurity respectively and v the electron-impurity interaction strength. We will refer to v as the impurity potential strength or loosely impurity strength. Writing the Hamiltonian (2.2) in Fourier basis, we obtain

$$H_0 = \sum_{\mathbf{k}_x, \mathbf{k}_y} c_{\mathbf{k}_x, \mathbf{k}_y}^{\dagger} \left[\epsilon_{\mathbf{k}} + 2\alpha_R \left(sink_x \sigma_y - sink_y \sigma_x \right) \right] c_{\mathbf{k}_x, \mathbf{k}_y}. \tag{2.4}$$

where

$$\epsilon_{\mathbf{k}} = \epsilon_0 + 2t(\cos \mathbf{k}_{\mathbf{x}} + \cos \mathbf{k}_{\mathbf{y}}).$$
 (2.5)

To diagonalize the Hamiltonian (2.2), we perform a unitary transformation using operator U_k which satisfies the condition: $U_k^{\dagger} = U_k^{-1}$ and is given by

$$U = \frac{1}{\sqrt{2}} \begin{bmatrix} 1 & p_{k_x, k_y} \\ -p_{k_x, k_y}^* & 1 \end{bmatrix}. \tag{2.6}$$

where we define

$$p_{k_{x},k_{y}} = \frac{\sin k_{y} + i\sin k_{x}}{\sqrt{\sin^{2}k_{y} + \sin^{2}k_{x}}}, p_{k_{x},k_{y}}^{*} = \frac{\sin k_{y} - i\sin k_{x}}{\sqrt{\sin^{2}k_{y} + \sin^{2}k_{x}}}.$$
 (2.7)

The diagonalized operator is given by

$$\begin{pmatrix} \alpha_{1,k} \\ \alpha_{2,k} \end{pmatrix} = U_k \begin{pmatrix} c_{k\uparrow} \\ c_{k\downarrow} \end{pmatrix} , \quad (\alpha_{1,k}^{\dagger} \quad \alpha_{2,k}^{\dagger}) = \begin{pmatrix} c_{k\uparrow}^{\dagger} & c_{k\downarrow}^{\dagger} \end{pmatrix} U_k^{\dagger}, \qquad (2.8)$$

and the Hamiltonian (2.2) transforms to

$$H_0 = \sum_{\mathbf{k}_{\mathbf{x}}, \mathbf{k}_{\mathbf{y}}} \left[\epsilon_{1,k} \alpha_{1,k}^{\dagger} \alpha_{1,k} + \epsilon_{2,k} \alpha_{1,k}^{\dagger} \alpha_{1,k} \right], \tag{2.9}$$

where $\epsilon_{1,k}$ and $\epsilon_{2,k}$ are given by

$$\epsilon_{1,k} = \left(\epsilon_k - 2\alpha_R \sqrt{\sin^2 k_y + \sin^2 k_x}\right), \epsilon_{2,k} = \left(\epsilon_k + 2\alpha_R \sqrt{\sin^2 k_y + \sin^2 k_x}\right).$$

Thus in the presence of Rashba Spin-orbit coupling, single energy state splits into two spin states, each one defining one particular spin state.

2.2.1 SPIN CURRENT

To get the spin current operator, we start from the spin polarization operator:

$$\vec{P}^{s_z} = \sum_{i_x, i_y} \vec{R}_{i_x, i_y} c_{i_x, i_y}^{\dagger} \sigma_z c_{i_x, i_y}.$$
 (2.10)

where \vec{R}_{i_x,i_y} is the lattice point and σ_z is the spin matrix along z-direction. The spin current density \vec{J}^{s_z} is given by time derivative of Spin polarization operator. Thus we can write

$$\vec{J}^{s_z} = \frac{\partial \vec{P}^{s_z}}{\partial t} = i \left[H_0^1 + H_0^R, \sum_{j_x, j_y} \vec{R}_{j_x, j_y} c_{j_x, j_y}^{\dagger} \sigma_z c_{j_x, j_y} \right],$$
(2.11a)

$$= i \left[H_0^1, \sum_{j_{x}, j_{y}} \vec{R}_{j_{x}, j_{y}} c_{j_{x}, j_{y}}^{\dagger} \sigma_z c_{j_{x}, j_{y}} \right] + i \left[H_0^R, \sum_{j_{x}, j_{y}} \vec{R}_{j_{x}, j_{y}} c_{j_{x}, j_{y}}^{\dagger} \sigma_z c_{j_{x}, j_{y}} \right] (2.11b)$$

where H_0 has been written as: $H_0 = H_0^1 + H_0^R$, H_0^1 and H_0^R being given by

$$H_0^1 = \sum_{i_x, i_y} \epsilon_0 c_i^{\dagger} c_i + t \left[\sum_{i_x, i_y} (c_{i_x, i_y}^{\dagger} c_{i_{x+1}, i_y} + c_{i_x, i_y}^{\dagger} c_{i_x, i_{y+1}} + h.c) \right]$$
(2.12)

$$H_0^R = -i\alpha_R \left[\sum_{i_x, i_y} (c_{i_x, i_y}^{\dagger} \sigma_y c_{i_{x+1}, i_y} - c_{i_x, i_y}^{\dagger} \sigma_x c_{i_x, i_{y+1}}) + \text{h.c}) \right]$$
(2.13)

The first term of (2.11b) is calculated as:

$$\begin{split} \left[H_{0}^{1},\vec{P}^{s_{z}}\right] &= \ t\sum_{\mathbf{i}_{x},\mathbf{i}_{y}} (\vec{R}_{\mathbf{i}_{x+1},\mathbf{i}_{y}} - \vec{R}_{\mathbf{i}_{x},\mathbf{i}_{y}}) \left[c_{\mathbf{i}_{x},\mathbf{i}_{y}}^{\dagger}\sigma_{z}c_{\mathbf{i}_{x+1},\mathbf{i}_{y}} - c_{\mathbf{i}_{x+1},\mathbf{i}_{y}}^{\dagger}\sigma_{z}c_{\mathbf{i}_{x},\mathbf{i}_{y}}\right] \\ &+ t\sum_{\mathbf{i}_{x},\mathbf{i}_{y}} \left(\vec{R}_{\mathbf{i}_{x},\mathbf{i}_{y+1}} - \vec{R}_{\mathbf{i}_{x},\mathbf{i}_{y}}\right) \left[c_{\mathbf{i}_{x},\mathbf{i}_{y}}^{\dagger}\sigma_{y}c_{\mathbf{i}_{x},\mathbf{i}_{y+1}} - c_{\mathbf{i}_{x},\mathbf{i}_{y+1}}^{\dagger}\sigma_{y}c_{\mathbf{i}_{x},\mathbf{i}_{y}}\right] \end{split} \tag{2.14}$$

To calculate the second term of equation (2.11b), we first write it as follows.

$$[H_0^R, \vec{P}^{S_z}] = , [H_{01}^R + H_{02}^R, \vec{P}^{S_z}]$$
(2.15)

Using Eq.(2.13) and using the relations

$$c_{i_{x+1},i_{y}} = \begin{pmatrix} c_{i_{x+1},i_{y}\uparrow} \\ c_{i_{x+1},i_{y}\downarrow} \end{pmatrix} \quad and \quad c_{i_{x+1},i_{y}}^{\dagger} = \begin{pmatrix} c_{i_{x+1},i_{y}\uparrow}^{\dagger} & c_{i_{x+1},i_{y}\downarrow}^{\dagger} \end{pmatrix} \quad (2.16)$$

we can write H_{01}^R and H_{02}^R as

$$H_{01}^{R} = -i\alpha_{R} \sum_{i_{x}, i_{y}} \left[-i(c_{i_{x}, i_{y}\uparrow}^{\dagger} c_{i_{x+1}, i_{y}\downarrow} - c_{i_{x}, i_{y}\downarrow}^{\dagger} c_{i_{x+1}, i_{y}\uparrow}) + \text{h.c.} \right] \quad (2.17)$$

$$H_{02}^{R} = i\alpha_{R} \sum_{i_{x}, i_{y}} \left[(c_{i_{x}, i_{y}\uparrow}^{\dagger} c_{i_{x}, i_{y+1}\downarrow} - c_{i_{x}, i_{y}\downarrow}^{\dagger} c_{i_{x}, i_{y+1}\uparrow}) + \text{h.c.} \right]$$
 (2.18)

Calculating the commutation of H_{01}^R and H_{02}^R with \vec{P}^{s_z} , we get

$$\begin{split} \left[H_{01}^{R} , \vec{P}^{S_{Z}} \right] &= -\mathrm{i} \alpha_{R} \left[\sum_{i_{x}, i_{y}} (c_{i_{x}, i_{y}\uparrow}^{\dagger} c_{i_{x+1}, i_{y}\downarrow} - c_{i_{x}, i_{y}\downarrow}^{\dagger} c_{i_{x+1}, i_{y}\uparrow}) + \mathrm{h.c.}, \right. \\ & \left. \sum_{j_{x}, j_{y}} \vec{R}_{j_{x}, j_{y}} (c_{j_{x}, j_{y}\uparrow}^{\dagger} c_{j_{x}, j_{y}\uparrow} - c_{j_{x}, j_{y}\downarrow}^{\dagger} c_{j_{x}, j_{y}\downarrow}) \right] \\ & = \alpha_{R} \sum_{i_{x}, i_{y}} (\vec{R}_{i_{x+1}, i_{y}} + \vec{R}_{i_{x}, i_{y}}) \left[c_{i_{x}, i_{y}}^{\dagger} \sigma_{x} c_{i_{x+1}, i_{y}} - c_{i_{x+1}, i_{y}}^{\dagger} \sigma_{x} c_{i_{x}, i_{y}} \right] \quad (2.19) \end{split}$$

$$\begin{split} \left[H_{02}^R , \vec{P}^{s_z}\right] &= \mathrm{i}\alpha_\mathrm{R} \left[\sum_{\mathrm{i}_\mathrm{x}, \mathrm{i}_\mathrm{y} \uparrow} (c_{\mathrm{i}_\mathrm{x}, \mathrm{i}_\mathrm{y+1} \downarrow}^\dagger + c_{\mathrm{i}_\mathrm{x}, \mathrm{i}_\mathrm{y} \downarrow}^\dagger c_{\mathrm{i}_\mathrm{x}, \mathrm{i}_\mathrm{y+1} \uparrow}) + \mathrm{h.c.}, \\ & \sum_{\mathrm{j}_\mathrm{x}, \mathrm{j}_\mathrm{y}} \vec{R}_{\mathrm{j}_\mathrm{x}, \mathrm{j}_\mathrm{y}} (c_{\mathrm{j}_\mathrm{x}, \mathrm{j}_\mathrm{y} \uparrow}^\dagger c_{\mathrm{j}_\mathrm{x}, \mathrm{j}_\mathrm{y} \uparrow} - c_{\mathrm{j}_\mathrm{x}, \mathrm{j}_\mathrm{y} \downarrow}^\dagger c_{\mathrm{j}_\mathrm{x}, \mathrm{j}_\mathrm{y} \downarrow}) \right] \end{split}$$

$$= \alpha_{\rm R} \sum_{{\bf i}_{\rm x}, {\bf i}_{\rm y}} (\vec{R}_{{\bf i}_{\rm x}, {\bf i}_{\rm y+1}} + \vec{R}_{{\bf i}_{\rm x}, {\bf i}_{\rm y}}) \left[c^{\dagger}_{{\bf i}_{\rm x}, {\bf i}_{\rm y}} \sigma_{y} c_{{\bf i}_{\rm x}, {\bf i}_{\rm y+1}} - c^{\dagger}_{{\bf i}_{\rm x}, {\bf i}_{\rm y+1}} \sigma_{y} c_{{\bf i}_{\rm x}, {\bf i}_{\rm y}} \right]$$
(2.20)

Using Eqns. (2.19), (2.20), (2.15) and (2.14) in (2.11), we have

$$\vec{J}^{s_{z}} = \frac{\partial \vec{P}^{s_{z}}}{\partial t} = i \left[H_{0}^{1}, \vec{P}^{s_{z}} \right] + i \left[H_{01}^{R}, \vec{P}^{s_{z}} \right] + i \left[H_{02}^{R}, \vec{P}^{s_{z}} \right]
= it \sum_{i_{x}, i_{y}} (\vec{R}_{i_{x+1}, i_{y}} - \vec{R}_{i_{x}, i_{y}}) \left[c_{i_{x}, i_{y}}^{\dagger} \sigma_{z} c_{i_{x+1}, i_{y}} - c_{i_{x+1}, i_{y}}^{\dagger} \sigma_{z} c_{i_{x}, i_{y}} \right]
+ it \sum_{i_{x}, i_{y}} (\vec{R}_{i_{x}, i_{y+1}} - \vec{R}_{i_{x}, i_{y}}) \left[c_{i_{x}, i_{y}}^{\dagger} \sigma_{y} c_{i_{x}, i_{y+1}} - c_{i_{x}, i_{y+1}}^{\dagger} \sigma_{y} c_{i_{x}, i_{y}} \right]
+ i\alpha_{R} \sum_{i_{x}, i_{y}} (\vec{R}_{i_{x+1}, i_{y}} + \vec{R}_{i_{x}, i_{y}}) \left[c_{i_{x}, i_{y}}^{\dagger} \sigma_{x} c_{i_{x+1}, i_{y}} - c_{i_{x+1}, i_{y}}^{\dagger} \sigma_{x} c_{i_{x}, i_{y}} \right]
+ i\alpha_{R} \sum_{i_{x}, i_{y}} (\vec{R}_{i_{x}, i_{y+1}} + \vec{R}_{i_{x}, i_{y}}) \left[c_{i_{x}, i_{y}}^{\dagger} \sigma_{y} c_{i_{x}, i_{y+1}} - c_{i_{x}, i_{y+1}}^{\dagger} \sigma_{y} c_{i_{x}, i_{y}} \right]$$
(2.21)

So the spin current density.

Along x- direction

$$J_{x}^{s_{z}} = \operatorname{it} \sum_{i_{x}, i_{y}} \left[c_{i_{x}, i_{y}}^{\dagger} \sigma_{z} c_{i_{x+1}, i_{y}} - c_{i_{x+1}, i_{y}}^{\dagger} \sigma_{z} c_{i_{x}, i_{y}} \right]$$

$$+ i \alpha_{R} \sum_{i_{x}, i_{y}} (2i_{x} + 1) \left[c_{i_{x}, i_{y}}^{\dagger} \sigma_{x} c_{i_{x+1}, i_{y}} - c_{i_{x+1}, i_{y}}^{\dagger} \sigma_{x} c_{i_{x}, i_{y}} \right]$$

$$+ i \alpha_{R} \sum_{i_{x}, i_{y}} (2i_{x}) \left[c_{i_{x}, i_{y}}^{\dagger} \sigma_{y} c_{i_{x}, i_{y+1}} - c_{i_{x}, i_{y+1}}^{\dagger} \sigma_{y} c_{i_{x}, i_{y}} \right]$$

$$(2.22)$$

Along y-direction

$$J_{y}^{s_{z}} = \operatorname{it} \sum_{i_{x}, i_{y}} \left[c_{i_{x}, i_{y}}^{\dagger} \sigma_{z} c_{i_{x}, i_{y+1}} - c_{i_{x}, i_{y+1}}^{\dagger} \sigma_{z} c_{i_{x}, i_{y}} \right]$$

$$+ i \alpha_{R} \sum_{i_{x}, i_{y}} (2i_{y}) \left[c_{i_{x}, i_{y}}^{\dagger} \sigma_{x} c_{i_{x+1}, i_{y}} - c_{i_{x+1}, i_{y}}^{\dagger} \sigma_{x} c_{i_{x}, i_{y}} \right]$$

$$+ i \alpha_{R} \sum_{i_{x}, i_{y}} (2i_{y} + 1) \left[c_{i_{x}, i_{y}}^{\dagger} \sigma_{y} c_{i_{x}, i_{y+1}} - c_{i_{x}, i_{y+1}}^{\dagger} \sigma_{y} c_{i_{x}, i_{y}} \right]$$

$$(2.23)$$

Using Eqn. [2.8] the x-direction spin current density can be written as

$$J_{x}^{2z} = -2t \sum_{\mathbf{k}_{x}, \mathbf{k}_{y}} \frac{\sin k_{x} \sin k_{y}}{\sqrt{\sin^{2}(k_{y}) + \sin^{2}(k_{x})}} \alpha_{\mathbf{k}_{x}, \mathbf{k}_{y}}^{\dagger} \sigma_{x} \alpha_{\mathbf{k}_{x}, \mathbf{k}_{y}}$$

$$+ 2t \sum_{\mathbf{k}_{x}, \mathbf{k}_{y}} \frac{\sin^{2}k_{x}}{\sqrt{\sin^{2}(k_{y}) + \sin^{2}(k_{x})}} \alpha_{\mathbf{k}_{x}, \mathbf{k}_{y}}^{\dagger} \sigma_{y} \alpha_{\mathbf{k}_{x}, \mathbf{k}_{y}}$$

$$+ \alpha_{R} \sum_{\mathbf{k}_{x}, \mathbf{k}_{y}} \frac{2i\cos(k_{x})\sin^{2}(k_{y})}{\sin^{2}(k_{y}) + \sin^{2}(k_{x})} \alpha_{\mathbf{k}_{x}, \mathbf{k}_{y}}^{\dagger} \begin{bmatrix} p_{k_{x}, k_{y}}^{*} & -p_{k_{x}, k_{y}}^{*2} \\ -p_{k_{x}, k_{y}}^{*} & -p_{k_{x}, k_{y}}^{*2} \end{bmatrix} \alpha_{\mathbf{k}_{x}, \mathbf{k}_{y}}$$

$$(2.24)$$

2.2.2 Charge current

To get the charge current operator, we start from the definition of charge polarization operator:

$$\vec{P}^c = \sum_{i_x, i_y} \vec{R}_{i_x, i_y} c_{i_x, i_y}^{\dagger} I c_{i_x, i_y} . \qquad (2.25)$$

The time derivative of charge polarization will give the charge current density \vec{l}^c .

$$\vec{J}^c = \frac{\partial \vec{P}^c}{\partial t} = i \left[H_0 , \sum_{\mathbf{j}_{\mathbf{x}}, \mathbf{j}_{\mathbf{y}}} \vec{R}_{\mathbf{j}_{\mathbf{x}}, \mathbf{j}_{\mathbf{y}}} c_{\mathbf{j}_{\mathbf{x}}, \mathbf{j}_{\mathbf{y}}}^{\dagger} I c_{\mathbf{j}_{\mathbf{x}}, \mathbf{j}_{\mathbf{y}}} \right]$$
(2.26)

$$\begin{split} &= it \sum_{\mathbf{i}_{\mathbf{x}}, \mathbf{i}_{\mathbf{y}}} (\vec{R}_{\mathbf{i}_{\mathbf{x}+1}, \mathbf{i}_{\mathbf{y}}} - \vec{R}_{\mathbf{i}_{\mathbf{x}}, \mathbf{i}_{\mathbf{y}}}) \left[c^{\dagger}_{\mathbf{i}_{\mathbf{x}}, \mathbf{i}_{\mathbf{y}}} c_{\mathbf{i}_{\mathbf{x}+1}, \mathbf{i}_{\mathbf{y}}} - c^{\dagger}_{\mathbf{i}_{\mathbf{x}+1}, \mathbf{i}_{\mathbf{y}}} c_{\mathbf{i}_{\mathbf{x}}, \mathbf{i}_{\mathbf{y}}} \right] \\ &+ it \sum_{\mathbf{i}_{\mathbf{x}}, \mathbf{i}_{\mathbf{y}}} (\vec{R}_{\mathbf{i}_{\mathbf{x}}, \mathbf{i}_{\mathbf{y}+1}} - \vec{R}_{\mathbf{i}_{\mathbf{x}}, \mathbf{i}_{\mathbf{y}}}) \left[c^{\dagger}_{\mathbf{i}_{\mathbf{x}}, \mathbf{i}_{\mathbf{y}}} c_{\mathbf{i}_{\mathbf{x}}, \mathbf{i}_{\mathbf{y}+1}} - c^{\dagger}_{\mathbf{i}_{\mathbf{x}}, \mathbf{i}_{\mathbf{y}}} \right] \\ &+ i\alpha_{\mathbf{R}} \sum_{\mathbf{i}_{\mathbf{x}}, \mathbf{i}_{\mathbf{y}}} (\vec{R}_{\mathbf{i}_{\mathbf{x}+1}, \mathbf{i}_{\mathbf{y}}} - \vec{R}_{\mathbf{i}_{\mathbf{x}}, \mathbf{i}_{\mathbf{y}}}) \left[c^{\dagger}_{\mathbf{i}_{\mathbf{x}}, \mathbf{i}_{\mathbf{y}}} \sigma_{\mathbf{y}} c_{\mathbf{i}_{\mathbf{x}+1}, \mathbf{i}_{\mathbf{y}}} - c^{\dagger}_{\mathbf{i}_{\mathbf{x}+1}, \mathbf{i}_{\mathbf{y}}} \sigma_{\mathbf{y}} c_{\mathbf{i}_{\mathbf{x}}, \mathbf{i}_{\mathbf{y}}} \right] \\ &\cdot -\mathbf{i}\alpha_{\mathbf{R}} \sum_{\mathbf{i}_{\mathbf{x}}, \mathbf{i}_{\mathbf{y}}} \left(\vec{R}_{\mathbf{i}_{\mathbf{x}}, \mathbf{i}_{\mathbf{y}+1}} - \vec{R}_{\mathbf{i}_{\mathbf{x}}, \mathbf{i}_{\mathbf{y}}} \right) \left[c^{\dagger}_{\mathbf{i}_{\mathbf{x}}, \mathbf{i}_{\mathbf{y}}} \sigma_{\mathbf{x}} c_{\mathbf{i}_{\mathbf{x}}, \mathbf{i}_{\mathbf{y}+1}} - c^{\dagger}_{\mathbf{i}_{\mathbf{x}}, \mathbf{i}_{\mathbf{y}+1}} \sigma_{\mathbf{x}} c_{\mathbf{i}_{\mathbf{x}}, \mathbf{i}_{\mathbf{y}}} \right]. (2.27) \end{split}$$

So, in the α – operator, the charge current density in x-direction is:

$$J_{x}^{c} = \sum_{k} f_{1}^{x}(k) \alpha_{1,k}^{\dagger} \alpha_{1,k} + \sum_{k} f_{2}^{x}(k) \alpha_{2,k}^{\dagger} \alpha_{2,k} + \sum_{k} f_{3}^{x}(k) \alpha_{1,k}^{\dagger} \alpha_{2,k}$$
$$+ \sum_{k} f_{3}^{*x}(k) \alpha_{2,k}^{\dagger} \alpha_{1,k} , \qquad (2.28)$$

where

$$f_1^x(k) = 2tsink_x - \frac{2\alpha_R cosk_x sink_x}{\sqrt{sin^2(k_y) + sin^2(k_x)}} , \qquad (2.28a)$$

$$f_2^{x}(k) = 2tsink_x + \frac{2\alpha_R cosk_x sink_x}{\sqrt{sin^2(k_y) + sin^2(k_x)}} , \qquad (2.28b)$$

$$f_3^x(k) = \frac{2\alpha_R cosk_x sink_x (sink_x - isink_y)}{sin^2(k_y) + sin^2(k_x)} , \qquad (2.28c)$$

$$f_3^{x*}(k) = \frac{2\alpha_R cosk_x sink_x (sink_x + isink_y)}{sin^2(k_y) + sin^2(k_x)}$$
 (2.28d)

Similarly charge current in y- direction is:

$$J_{y}^{c} = \sum_{\mathbf{k}} f_{1}^{y}(k) \alpha_{1,\mathbf{k}}^{\dagger} \alpha_{1,\mathbf{k}} + \sum_{\mathbf{k}} f_{2}^{y}(k) \alpha_{2,\mathbf{k}}^{\dagger} \alpha_{2,\mathbf{k}} + \sum_{\mathbf{k}} f_{3}^{y}(k) \alpha_{1,\mathbf{k}}^{\dagger} \alpha_{2,\mathbf{k}} + \sum_{\mathbf{k}} f_{3}^{y}(k) \alpha_{1,\mathbf{k}}^{\dagger} \alpha_{2,\mathbf{k}} + \sum_{\mathbf{k}} f_{3}^{y}(k) \alpha_{2,\mathbf{k}}^{\dagger} \alpha_{2,\mathbf{k}}, \qquad (2.29)$$

where

$$f_1^{y}(k) = 2tsink_y - \frac{2\alpha_R cosk_y sink_y}{\sqrt{sin^2(k_y) + sin^2(k_x)}}, \qquad (2.29a)$$

$$f_2^{y}(k) = 2tsink_y + \frac{2\alpha_R cosk_y sink_y}{\sqrt{sin^2(k_y) + sin^2(k_x)}} , \qquad (2.29b)$$

$$f_3^{y}(k) = \frac{-2\alpha_R \cos k_y \sin k_x (\sin k_x - i \sin k_y)}{\sin^2(k_y) + \sin^2(k_x)} , \qquad (2.29c)$$

$$f_3^{y*}(k) = -\frac{2\alpha_R \cos k_y \sin k_x (\sin k_x + i \sin k_y)}{\sin^2(k_y) + \sin^2(k_x)} . \tag{2.29d}$$

2.2.3 Relaxation Time

In the k-space the impurity Hamiltonian (2.3) can be written as

$$H_{imp} = \sum_{\substack{i,l\\k,k'}} ve^{iq(r_l - r_i)} e^{ik.r_i} e^{ik'.r_i} c_k^{\dagger} c_{k'} = \frac{1}{\aleph} \sum_{\substack{l\\k,k'}} ve^{iq(k-k').R_l} c_k^{\dagger} c_k , \quad (2.30)$$

And from the unitary transformation Eqn. (2.6) can be written as:

$$H_{imp} = \frac{1}{N} \sum_{k,k'} \left[V_{kk'}^{11} \alpha_{1,k}^{\dagger} \alpha_{1,k'} + V_{kk'}^{12} \alpha_{1,k}^{\dagger} \alpha_{2,k'} + V_{kk'}^{21} \alpha_{2,k}^{\dagger} \alpha_{1,k'} + V_{kk'}^{22} \alpha_{2,k}^{\dagger} \alpha_{2,k'} \right], \tag{2.31}$$

where

$$V_{kk'}^{11} = \frac{1}{2} \sum_{l} v e^{i(k-k') \cdot R_l} \left[\left(1 + p_k p_{k'}^* \right) \right], \tag{2.31a}$$

$$V_{kk'}^{12} = \frac{1}{2} \sum_{l} v e^{i(k-k') \cdot R_l} [(p_k - p_{k'})], \qquad (2.31b)$$

$$V_{kk'}^{21} = \frac{1}{2} \sum_{l} v e^{i(k-k') \cdot R_l} [(p_{k'}^* - p_k^*)], \qquad (2.31c)$$

$$V_{kk'}^{22} = \frac{1}{2} \sum_{l} v e^{i(k-k') \cdot R_l} \left[(1 + p_{k'} p_k^*) \right], \tag{2.31d}$$

When impurities are present, electrons will acquire relaxation time. We calculate relaxation time from the imaginary part of the self-energy. The relevant Green function is given by

$$G(\boldsymbol{p},\tau) = \sum_{l=1}^{\infty} (-1)^l \int_0^{\beta} d\tau_1 \dots \dots \int_0^{\beta} d\tau_n$$

$$* \langle Tr[\alpha_{1,\boldsymbol{p}}^{\dagger}(\tau)V(\tau_1)V(\tau_2) \dots \dots V(\tau_l)\alpha_{1,\boldsymbol{p}}(0)] \rangle$$
(2.32)

Here we calculate the Green function to second order, as in the first order i.e. for l = 1, we get a constant shift in the energy. The second-order Green function for our Hamiltonian is given by

$$G(p,\tau) = \sum_{k,k'} \iint_{00}^{\beta\beta} d\tau_{1} d\tau_{2} \langle T_{\tau} \left[\alpha_{1,p} \left(V_{kk_{1}}^{11} \alpha_{1,k}^{\dagger}(\tau_{1}) \alpha_{1,k_{1}}(\tau_{1}) + V_{kk_{1}}^{12} \alpha_{1,k}^{\dagger}(\tau_{1}) \alpha_{2,k_{1}}(\tau_{1}) + V_{kk_{1}}^{21} \alpha_{1,k}^{\dagger}(\tau_{1}) \alpha_{1,k_{1}}(\tau_{1}) + V_{kk_{1}}^{22} \alpha_{2,k}^{\dagger}(\tau_{1}) \alpha_{2,k_{1}}(\tau_{1}) \right]$$

$$+ V_{kk_{1}}^{22} \alpha_{2,k}^{\dagger}(\tau_{1}) \alpha_{2,k_{1}}(\tau_{1})$$

$$+ \left(V_{k_{2}k'}^{11} \alpha_{1,k_{2}}^{\dagger}(\tau_{2}) \alpha_{1,k'}(\tau_{2}) + V_{k_{2}k'}^{12} \alpha_{1,k_{2}}^{\dagger}(\tau_{2}) \alpha_{2,k'}(\tau_{2}) + V_{k_{2}k'}^{21} \alpha_{2,k_{2}}^{\dagger}(\tau_{2}) \alpha_{2,k'}(\tau_{2}) \right)$$

$$+ V_{k_{2}k'}^{22} \alpha_{2,k_{2}}^{\dagger}(\tau_{2}) \alpha_{2,k'}(\tau_{2}) \right) \alpha_{1,p}^{\dagger}(0) .$$

$$(2.33)$$

Using Wicks theorem, equation (2.34) reduces to

$$G(p,\tau) = \sum_{k_1} \int_{00}^{\beta\beta} d\tau_1 d\tau_2 V_{pk_1}^{11} V_{k_1p}^{11} g^{01}(p,\tau-\tau_1) g^{01}(k_1,\tau_1-\tau_2) g^{01}(p,\tau_2)$$

$$+ \sum_{k_1} V_{pk_1}^{12} V_{k_1p}^{21} g^{01}(p,\tau-\tau_1) g^{02}(k_1,\tau_1-\tau_2) g^{01}(p,\tau_2)$$

$$(2.34)$$

where

$$g^{01}(p,\tau-\tau_2) = \langle T_{\tau}\alpha_{1,p}^{\dagger}(\tau)\alpha_{1,p}(\tau_2) \rangle$$
 (2.34a)

$$g^{01}(k_1, \tau_1 - \tau_2) = \langle T_{\tau} \alpha_{1, k_1}^{\dagger}(\tau_1) \alpha_{1, k_1}(\tau_2) \rangle$$
 (2.34b)

$$g^{02}(k_1, \tau_1 - \tau_2) = \langle T_{\tau} \alpha_{2,k_1}^{\dagger}(\tau_1) \alpha_{2,k_1}(\tau_2) \rangle$$
 (2.34c)

$$g^{01}(p,\tau_2) = \langle T_{\tau} \alpha_{1,p}^{\dagger}(\tau_2) \alpha_{1,p}(\tau_2) \rangle$$
 (2.35d)

Where g^{01} and g^{02} are the Green's function for single particle of particular spin.

Now, writing $G(p, ip_l)$ and $G(p, \tau - \tau')$ in momentum basis;

$$G(p, \tau - \tau') = \frac{1}{\beta} \sum_{ii\varepsilon_l} e^{-i\varepsilon_l(\tau - \tau')} G(p, i\varepsilon_l).$$
(2.35)

After some simplifications, $G(p, ip_l)$ can be written as

$$G(p, i\varepsilon_{l}) = \sum_{k_{1}} V_{pk^{1}}^{11} V_{k^{1}p}^{11} g^{01}(p, i\varepsilon_{l}) g^{01}(k_{1}, i\varepsilon_{l}) g^{01}(p, i\varepsilon_{l})$$

$$+ V_{pk^{1}}^{12} V_{k^{1}p}^{21} g^{01}(p, i\varepsilon_{l}) g^{02}(k_{1}, i\varepsilon_{l}) g^{01}(p, i\varepsilon_{l}) .$$

$$(2.36)$$

Changing the indices p by k in equation (2.36)

$$G(k, i\varepsilon_{l}) = \sum_{k_{1}} V_{kk^{1}}^{11} V_{k^{1}p}^{11} g^{01}(k, i\varepsilon_{l}) g^{01}(k_{1}, i\varepsilon_{l}) g^{01}(k, i\varepsilon_{l})$$

$$+ V_{kk^{1}}^{12} V_{k^{1}k}^{21} g^{01}(k, i\varepsilon_{l}) g^{02}(k_{1}, i\varepsilon_{l}) g^{01}(k, i\varepsilon_{l})$$

$$(2.37)$$

Impurities in our system are randomly distributed, therefore the average properties of impurities can be calculated by taking the average over all possible impurity configurations for a given quantity. Any macroscopic system of interest can be described by this impurity averaging, which is called self-averaging at temperatures that are experimentally feasible. In this way, the probability distribution of the impurity configuration can be viewed as the result of aggregating the probability distributions of individual impurities. The only factors which depend on the impurity position are V_{k,k_1} . Thus $\bar{G}(k,ip_l)$ is calculated by solving following expression $\overline{V_{kk_1}V_{k_1k_2}\dots V_{k_{l-1},k_l}}$. For example, for l=2, we need to calculate $\overline{V_{kk_1}V_{k_1k}}$.

$$\begin{split} \overline{V_{kk_1}V_{k_1k}} &= \prod_{i=1}^{\aleph} \left(\frac{1}{\mathbf{N}^2} \int d^2r_i\right) \frac{v^2}{4\mathbf{N}^2} \sum_{j_1=1}^{\aleph} e^{i(k-k_1).r_{j_1}} \sum_{j_2=1}^{\aleph} e^{i(k_1-k).r_{j_2}} \\ &\times \left[\left(1 + p_k p_{k_1}^*\right) \right] \left[\left(1 + p_{k_1} p_k^*\right) \right] \end{split}$$

$$= \frac{V^2}{4N^2} \sum_{j_1=1}^{N} \sum_{j_2=1}^{N} \prod_{i=1}^{N} \left(\frac{1}{N^2} \int d^2 r_i \right) e^{i(k-k_1) \cdot r_{j_1}} e^{i(k_1-k) \cdot r_{j_2}}$$

$$\times \left[\left(1 + p_k p_{k_1}^* \right) \right] \left[\left(1 + p_{k_1} p_k^* \right) \right]$$
(2.38)

which gives

$$\overline{V_{kk_1}V_{k_1k}} = \frac{v^2}{4N^2} \Big[[(\aleph^2 - \aleph)\delta_{kk_1}\delta_{k_1k} + \aleph] \, \Big[\big(1 + p_k p_{k_1}^*\big) \Big] \Big[\big(1 + p_{k_1} p_k^*\big) \Big] \Big], \tag{2.39}$$

and consequently, we obtain

$$G(k, i\varepsilon_{l}) = g^{01}(k, i\varepsilon_{l}) \sum_{k_{1}} \frac{v^{2}}{4N^{2}} [(\aleph^{2}) \delta_{kk_{1}} \delta_{k_{1}k} + \aleph] \times [(1 + p_{k} p_{k_{1}}^{*})] [(1 + p_{k_{1}} p_{k}^{*})] \times g^{01}(k_{1}, i\varepsilon_{l}) g^{01}(k_{1}, i\varepsilon_{l}) + g^{01}(k_{1}, i\varepsilon_{l}) \times \sum_{k_{1}} \frac{v^{2}}{4N^{2}} [(\aleph^{2}) \delta_{kk_{1}} \delta_{k_{1}k} + \aleph] \times [(p_{k} - p_{k_{1}})] [(p_{k}^{*} - p_{k_{1}}^{*})] g^{02}(k_{1}, i\varepsilon_{l}) g^{01}(k_{1}, i\varepsilon_{l})$$

$$(2.40)$$

Equation (2.40) can be represented by two set of diagrams one from \aleph^2 and another from \aleph . The contribution from \aleph^2 (Fig 1(a)) will cancel as it represents a reducible diagram.

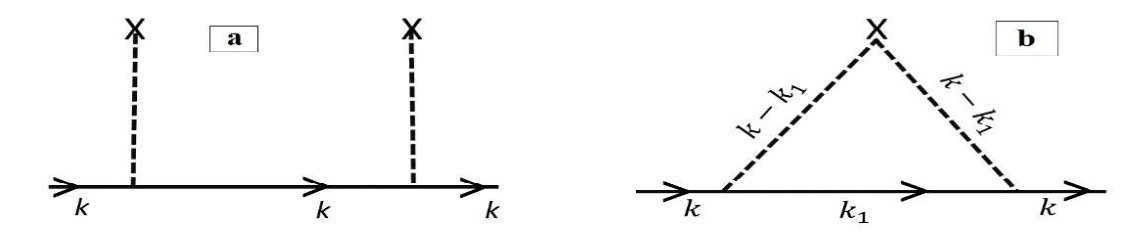


Fig 2.1: Feynman diagrams for $G(k, i\varepsilon_l)$ for orders n = 2

Thus we have

$$G(k, i\varepsilon_{l}) = g^{01}(k, i\varepsilon_{l}) \sum_{k_{1}} \frac{v^{2}}{4N} n \left(1 + p_{k} p_{k_{1}}^{*}\right) \left(1 + p_{k_{1}} p_{k}^{*}\right) g^{01}(k_{1}, i\varepsilon_{l})$$

$$\times g^{01}(k, i\varepsilon_{l}) + g^{01}(k, i\varepsilon_{l}) \sum_{k_{1}} \frac{v^{2}}{4N} n \left(p_{k} - p_{k_{1}}\right) \times \left(p_{k}^{*} - p_{k_{1}}^{*}\right)$$

$$\times g^{02}(k_{1}, i\varepsilon_{l}) g^{01}(k, i\varepsilon_{l}), \tag{2.41}$$

where

$$g^{01}(k_1, i\varepsilon_l) = \sum_{k_1} \frac{1}{ip_n - \epsilon_{1,k_1}} , g^{02}(k_1, i\varepsilon_l) = \sum_{k_1} \frac{1}{ip_n - \epsilon_{2,k_1}} .$$
 (2.42)

Equation (2.41) can be written as

$$G(k, i\varepsilon_l) = g^{01}(k, i\varepsilon_l) \Sigma(i\varepsilon_l) g^{01}(k, i\varepsilon_l)$$
 (2.43)

where $\Sigma(i\varepsilon_l)$ is the self-energy and is given by

$$\Sigma(i\varepsilon_{l}) = \frac{v^{2}}{4N} \sum_{k_{1}} \left[n \left[\left(1 + p_{k} p_{k_{1}}^{*} \right) \right] \left[\left(1 + p_{k_{1}} p_{k}^{*} \right) \right] \right] g^{01}(k_{1}, i\varepsilon_{l})$$

$$+ \frac{v^{2}}{4N} \sum_{k_{1}} \left[n \left[\left(p_{k} - p_{k_{1}} \right) \right] \left[\left(p_{k}^{*} - p_{k_{1}}^{*} \right) \right] \right] g^{02}(k_{1}, i\varepsilon_{l}).$$
 (2.44)

Now we perform analytical continuation for the upper half of the plane. We substitute $i\varepsilon_l \to \epsilon + i\eta$, when $\varepsilon_l > 0$ and for the lower half of the plane we substitute $\varepsilon_l < 0$ $i\varepsilon_l \to \epsilon - i\eta$, so that we get

$$\Sigma(i\varepsilon_{l}) = \frac{v^{2}}{4N} \sum_{k_{1}} \frac{\left[n\left[(1 + p_{k}p_{k_{1}}^{*})\right]\left[(1 + p_{k_{1}}p_{k}^{*})\right]\right]}{\epsilon - \epsilon_{1,k_{1}} + isgn(\varepsilon_{l})\eta} + \frac{v^{2}}{4N} \sum_{k_{1}} \frac{\left[n\left[(p_{k} - p_{k_{1}})\right]\left[(p_{k}^{*} - p_{k_{1}}^{*})\right]\right]}{\epsilon - \epsilon_{2,k_{1}} + isgn(\varepsilon_{l})\eta} .$$
(2.45)

Relaxation time is given by the imaginary part of self-energy. Hence the relaxation time for type (1) is given by

$$\frac{1}{\tau_k^1} = \frac{2\pi v^2 n}{\hbar 4N} \sum_{k_1} ([(1+|p_k|^2|p_k|^2)] \delta(\epsilon - \epsilon_{1,k_1}) + [|p_k|^2 + |p_k|^2] \delta(\epsilon - \epsilon_{2,k_1})).$$
(2.46)

Similarly, the relaxation time for type (2) electrons reads

$$\frac{1}{\tau_k^2} = \frac{2\pi}{\hbar} \frac{v^2 n}{4\mathbf{N}} \sum_{k_1} ([(1 + |p_k|^2 |p_k|^2)] \delta(\epsilon - \epsilon_{2,k_1}) + [|p_k|^2 + |p_k|^2] \delta(\epsilon - \epsilon_{1,k_1})).$$
(2.47)

Using the following dirac delta relation

$$\delta(g(x)) = \sum_{i} \frac{\delta(x - x_i)}{|g'(x_i)|},$$
(2.48)

Eq. (2.47) can be written as

$$\frac{1}{\tau_k^1} = \frac{v^2 n}{\pi \hbar} \int_0^{\pi} dk_y \left\{ \sum_{i=1,2} \frac{1}{\sqrt{4t^2 - y_i^2}} \left[\frac{1}{|1 + w(y_i)|} + \frac{1}{|1 - w(y_i)|} \right] \right\}, \tag{2.49}$$

where

$$w(y_i) = \frac{1}{2} \frac{\alpha_R y_i / t^2}{\sqrt{1 + \sin^2 k_y - \frac{y_i^2}{4t^2}}},$$
(2.50)

with

$$y_{1} = \frac{\mu - \epsilon_{0} - 2t\cos k_{x}}{1 + \frac{\alpha_{R}^{2}}{t^{2}}} - \frac{2\alpha_{R}}{1 + \frac{\alpha_{R}^{2}}{t^{2}}} \sqrt{1 + \sin^{2}k_{x}},$$
 (2.51(a))

$$y_2 = \frac{\mu - \epsilon_0 - 2t\cos k_x}{1 + \frac{\alpha_R^2}{t^2}} + \frac{2\alpha_R}{1 + \frac{\alpha_R^2}{t^2}} \sqrt{1 + \sin^2 k_x}.$$
 (2.51(a))

In a low scattering regime, the relaxation times for type 1 and type 2 particles have been considered the same i.e.,

$$\frac{1}{\tau_k^1} = \frac{1}{\tau_k^2} = \frac{1}{\tau} \quad . \tag{2.52}$$

2.2.4 Longitudinal Charge Conductivity

Using the Kubo formalism [16], we calculate the charge conductivity in the x-direction. We start by calculating the current-current correlation function.

$$\Pi(i\omega) = \frac{\hbar}{N} \int_0^\beta d\tau \, e^{i\omega_n \tau} \langle T_\tau J_c^x(\tau) J_c^x(0) \rangle, \tag{2.53}$$

where ω_n is the Matsubara frequency, T_{τ} defines time ordering operator, T denotes system-temperature, and the angular brackets refer to the thermal average. Conductivity is calculated using the imaginary part of $\Pi(i\omega)$:

$$\sigma_{xx} = \lim_{\omega \to 0} Im \left[\frac{\Pi_{ref}(i\omega)}{\omega} \right]. \tag{2.54}$$

From Eq. (2.28) we can write

$$\vec{J}_{x}^{c}(-\tau) = \sum_{k} f_{1}^{x}(k)\alpha_{1,k}^{\dagger}(-\tau)\alpha_{1,k}(-\tau) + \sum_{k} f_{2}^{x}(k)\alpha_{2,k}^{\dagger}(-\tau)\alpha_{2,k}(-\tau)
+ \sum_{k} f_{3}^{x}(k)\alpha_{1,k}^{\dagger}(-\tau)\alpha_{2,k}(-\tau) + \sum_{k} f_{3}^{*x}(k)\alpha_{2,k}^{\dagger}(-\tau)\alpha_{1,k}(-\tau)
(2.55)$$

so that $\langle T_{\tau}J_c^x(\tau)J_c^x(-\tau)\rangle$ becomes

$$\langle T_{\tau}J_{c}^{x}(\tau)J_{c}^{x}(-\tau)\rangle$$

$$= \langle \left[\sum_{k} f_{1}^{x}(k)^{2} \alpha_{1,k}^{\dagger}(\tau) \alpha_{1,k}(\tau) \alpha_{1,k}^{\dagger}(-\tau) \alpha_{1,k}(-\tau) + \sum_{k} f_{2}^{x}(k)^{2} \alpha_{2,k}^{\dagger}(\tau) \alpha_{2,k}(\tau) \alpha_{2,k}^{\dagger}(-\tau) \alpha_{2,k}(-\tau) + \sum_{k} f_{3}^{x}(k) f_{3}^{x*}(k) \alpha_{1,k}^{\dagger}(\tau) \alpha_{2,k}(\tau) \alpha_{2,k}^{\dagger}(-\tau) \alpha_{1,k}(-\tau) + \sum_{k} f_{3}^{x}(k) f_{3}^{x*}(k) \alpha_{2,k}^{\dagger}(\tau) \alpha_{1,k}(\tau) \alpha_{1,k}^{\dagger}(-\tau) \alpha_{2,k}(-\tau) \right] \rangle.$$

$$(2.56)$$

Thus $\Pi(i\omega_n)$ reads

$$\Pi(i\omega_{n}) = \frac{\hbar}{N} \int_{0}^{\beta} d\tau \, e^{i\omega\tau} \left\langle \left[\sum_{\mathbf{k}} f_{1}^{x}(k)^{2} \alpha_{1,\mathbf{k}}^{\dagger}(\tau) \alpha_{1,\mathbf{k}}(\tau) \alpha_{1,\mathbf{k}}^{\dagger}(-\tau) \alpha_{1,\mathbf{k}}(-\tau) \right. \right. \\
\left. + \sum_{\mathbf{k}} f_{2}^{x}(k)^{2} \alpha_{2,\mathbf{k}}^{\dagger}(\tau) \alpha_{2,\mathbf{k}}(\tau) \alpha_{2,\mathbf{k}}^{\dagger}(-\tau) \alpha_{2,\mathbf{k}}(-\tau) \\
\left. + \sum_{\mathbf{k}} f_{3}^{x}(k) f_{3}^{x*}(k) \alpha_{1,\mathbf{k}}^{\dagger}(\tau) \alpha_{2,\mathbf{k}}(\tau) \alpha_{2,\mathbf{k}}^{\dagger}(-\tau) \alpha_{1,\mathbf{k}}(-\tau) \\
\left. + \sum_{\mathbf{k}} f_{3}^{x}(k) f_{3}^{x*}(k) \alpha_{2,\mathbf{k}}^{\dagger}(\tau) \alpha_{1,\mathbf{k}}(\tau) \alpha_{1,\mathbf{k}}^{\dagger}(-\tau) \alpha_{2,\mathbf{k}}(-\tau) \right] \right\rangle \tag{2.57}$$

Parts of Eq. (2.57) are solved separately. We begin by calculating the correlation function for the first term of equation (2.57). The correlation function for the first term in the Fourier basis is calculated using Wick's theorem and is given by:

$$\prod_{c}'(i\omega_{n}) = \frac{\hbar}{N} \frac{1}{\beta} \sum_{k,ip_{n}} f_{1}^{x}(k)^{2} \int_{0}^{\beta} d\tau \, G(k,ip_{n}) G(k,ip_{n}+i\omega_{n}) , \qquad (2.58)$$

and can be represented by the following Feynman diagram.

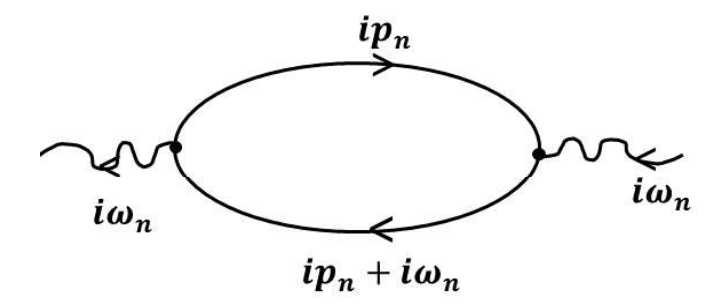


Fig 2.2 Bubble diagram for the current-current correlation function.

Here $G(k, ip_n + i\omega_n)$ and $G(k, ip_n)$ represents single-particle Green functions and corresponds to the upper and lower lines of the bubble diagram and have a frequency difference of $i\omega_n$. Also at each vertex momentum remains conserved. To calculate the longitudinal charge conductivity (LCC), we start by calculating the imaginary part of the current-current correlation function. Then we rewrite the expression in terms of spectral functions by performing analytic continuation $(i\omega_n \to \omega + i\delta)$. Finally, we divide the current-current correlation function by ω and in the limit $\omega \to 0$, LCC for the first part of current-current correlation function is given by

$$\sigma_{xx}^{c} = -\frac{\hbar}{N} \sum_{k} f_{1}^{x}(k)^{2} \int_{-\infty}^{\infty} d\epsilon \, A(k, \epsilon)^{2} \left\{ \frac{\partial n_{F}(\epsilon)}{\partial \epsilon} \right\}. \tag{2.59}$$

Similarly, we can calculate the correlation functions for the other terms of Eq. (2.57), and therefore, the expression for the total LCC is given by:

$$\sigma_{xx}^{c} = -\frac{\hbar}{N} \sum_{k} \int d\epsilon \left\{ \frac{\partial n_{F}(\epsilon)}{\partial \epsilon} \right\} \left[f_{1}^{x^{2}}(k) A^{1}(k,\epsilon)^{2} + f_{2}^{x^{2}}(k) A^{2}(k,\epsilon)^{2} + 2f_{3}^{x^{2}} A^{1}(k,\epsilon) A^{2}(k,\epsilon) \right], \tag{2.60}$$

where $A^1(k,\epsilon)$ and $A^2(k,\epsilon)$ represent the spectral functions for the electrons.

At low temperature and low impurity concentration, we can make the approximation: $\frac{\partial n_F(\epsilon)}{\partial \epsilon} = -\delta(\epsilon - \mu)$ and so the spectral function can be written as:

$$A^{1,2}(k,\epsilon) = 2\pi\delta(\mu - \epsilon_{1,2,k}) \quad and \quad (A^{1,2}(k,\epsilon))^2 = \frac{1}{\hbar} 4\pi\tau\delta(\mu - \epsilon_{1,2,k}). \quad (2.61)$$

Therefore, the expression for conductivity becomes

$$\sigma_{xx}^{c} = \frac{4\pi}{N} \sum_{k} \left[\left(f_1^{x}(k) \right)^2 \tau \delta\left(\mu - \epsilon_k^1\right) + \left(f_1^{x}(k) \right)^2 \tau \delta\left(\mu - \epsilon_k^2\right) \right]. \tag{2.62}$$

Using Eq. (2.58), we obtain the final expression for charge conductivity as:

$$\sigma_{xx}^{c} = \frac{2}{\pi} \tau \int_{-\pi}^{\pi} \sum_{i=1,2} \frac{dk_{x}}{\sqrt{4t^{2} - y_{i}^{2}}} \left[\frac{\left(f_{1}^{x}(k_{x}, y_{i})\right)^{2}}{[1 + w(y_{i})]} + \frac{\left(f_{2}^{x}(k_{x}, y_{i})\right)^{2}}{[1 - w(y_{i})]} \right] (2.63)$$

where $f_1^x(k_x, y)$ and $f_2^x(k_x, y)$ are given by

$$f_1^x(k_x, y_i) = 2tsink_x - \frac{2\alpha_R cosk_x sink_x}{\sqrt{1 + sin^2(k_x) - \left(\frac{y_i}{2t}\right)^2}}, \qquad (2.64(a))$$

$$f_2^x(k_x, y_i) = 2tsink_x + \frac{2\alpha_R cosk_x sink_x}{\sqrt{1 + sin^2(k_x) - \left(\frac{y_i}{2t}\right)^2}}, \qquad (2.64(b))$$

Similarly the charge conductivity σ_{yy}^c is given by

$$\sigma_{yy}^{c} = \frac{2}{\pi} \tau \int_{-\pi}^{\pi} \sum_{i=1,2} \frac{dk_{y}}{\sqrt{4t^{2} - x_{i}^{2}}} \left[\frac{\left(f_{1}^{y}(k_{x}, x_{i})\right)^{2}}{[1 + w(x_{i})]} + \frac{\left(f_{2}^{y}(k_{y}, x_{i})\right)^{2}}{[1 - w(x_{i})]} \right],$$

(2.65)

where

$$g(x_i) = \frac{\frac{1}{2}\alpha_R x_i/t^2}{\sqrt{1 + \sin^2(k_y) - \left(\frac{x_i}{2t}\right)^2}},$$
 (2.66)

$$f_1^y(k_y, x) = 2tsink_y - \frac{2\alpha_R cosk_y sink_y}{\sqrt{1 + sin^2 k_y - \left(\frac{x}{2t}\right)^2}},$$
 (2.67(a))

$$f_2^{y}(k_y, x) = 2tsink_y + \frac{2\alpha_R cosk_y sink_y}{\sqrt{1 + sin^2 k_y - \left(\frac{x}{2t}\right)^2}} . \tag{2.67(b)}$$

2.2.5 Longitudinal Spin Conductivity

Calculating the longitudinal spin conductivity involves using two expressions: the charge current density (2.24), and the spin current density (2.28), and applying the same formalism as calculated the charge conductivity. The expression for spin conductivity is thus given by

$$\sigma_{xx}^{s_z} = \frac{4\pi}{N} \sum_{k} \left[f_1^{(x)}(k) h_{1x}(k) A^1(k, \epsilon)^2 + f_2^{(x)}(k) h_{1x}(k) A^2(k, \epsilon)^2 \right], \quad (2.68)$$

which can be finally written as

$$\sigma_{xx}^{s_z} = \frac{2}{\pi} \tau \int_{-\pi}^{\pi} \sum_{i=1,2} \frac{dk_x h_x(k_x, y_i)}{\sqrt{4t^2 - y_i^2}} \left[\frac{\left(f_1^x(k_x, y_i)\right)^2}{\left[1 + w(y_i)\right]} + \frac{\left(f_2^x(k_x, y_i)\right)^2}{\left[1 - w(y_i)\right]} \right]$$
, (2.69)

where $h_x(k_x, y)$ is given by

$$h_{x}(k_{x},y) = \frac{2\alpha_{R}\left(1 - \left(\frac{y}{2t}\right)^{2}\right)}{\sqrt{1 + \sin^{2}(k_{x}) - \left(\frac{y}{2t}\right)^{2}}} cosk_{x} sink_{x}. \tag{2.70}$$

Similarly the spin conductivity $\sigma_{yy}^{s_z}$ is given by

$$\sigma_{yy}^{s_z} = \frac{2}{\pi} \tau \int_{-\pi}^{\pi} \sum_{i=1,2} \frac{dk_y h_y (k_y, x_i)}{\sqrt{4t^2 - x_i^2}} \left[\frac{\left(f_1^y (k_x, x_i)\right)^2}{\left[1 + w(x_i)\right]} + \frac{\left(f_2^y (k_y, x_i)\right)^2}{\left[1 - w(x_i)\right]} \right]$$

$$(2.71)$$

. where $h_y(k_y, y)$ is given by

$$h_{y}(k_{y},x) = \frac{2\alpha_{R}\left(1 - \left(\frac{x}{2t}\right)^{2}\right)}{\sqrt{1 + \sin^{2}(k_{y}) - \left(\frac{x}{2t}\right)^{2}}} cosk_{y} sink_{y}. \tag{2.72}$$

2.3 Numerical Results.

We present in this section our numerical results on the nature of longitudinal spin and charge conductivity along with relaxation time (τ) for various system parameters. These results have been obtained by computing Eqs. (2.49), (2.63) and (2.69). We measure all the energies in terms of t, and the relaxation time is determined in terms of $\tau_0 = \hbar/t$. Fig 2.1 shows the energy dissipation in k_x direction with and without spin-orbit interaction (SOI). When SOI is present, spin degeneracy is lifted, and we have two different bands for up-and down-spin electrons.

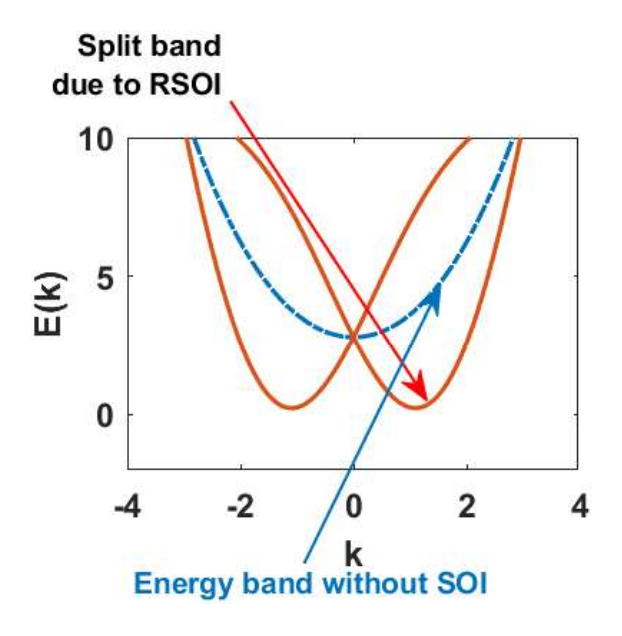


Fig 2.1 Energy dissipation along the x-direction in k space.

Fig 2.2, studied relaxation time (τ) for different system parameters. Fig 2.2(a) shows the plot of relaxation time (τ) vs chemical potential (μ) for various Rashba spin-orbit coefficient α_R value. For a small range of the chemical potential (μ), τ increases with increase in μ , and exhibits a peak at a specific value of $\mu(\mu_c)$. When the chemical potential is increased beyond that particular value, τ starts decreasing rapidly, but if μ is further increased, the decrease in τ slows down. This behavior can be observed for a particular value of α_R . As α_R is increased, τ also increases. In Fig 2.2(b), τ is plotted for various impurity strength values (v). The relaxation time behavior remains qualitatively the same, but the peak value decreases with increase in the impurity strength v. In Fig 2.2(c), τ is plotted with α_R for various μ value. The figure shows that as we increase α_R , τ increases and saturates to a constant value for a particular value of μ . As μ increases, the qualitative behaviour of τ remains the same, but it saturates to a lower value. Similar nature can be seen when τ is plotted with α_R for various v values, i.e., the relaxation time saturation value is lower for a higher value of imputiry strength.

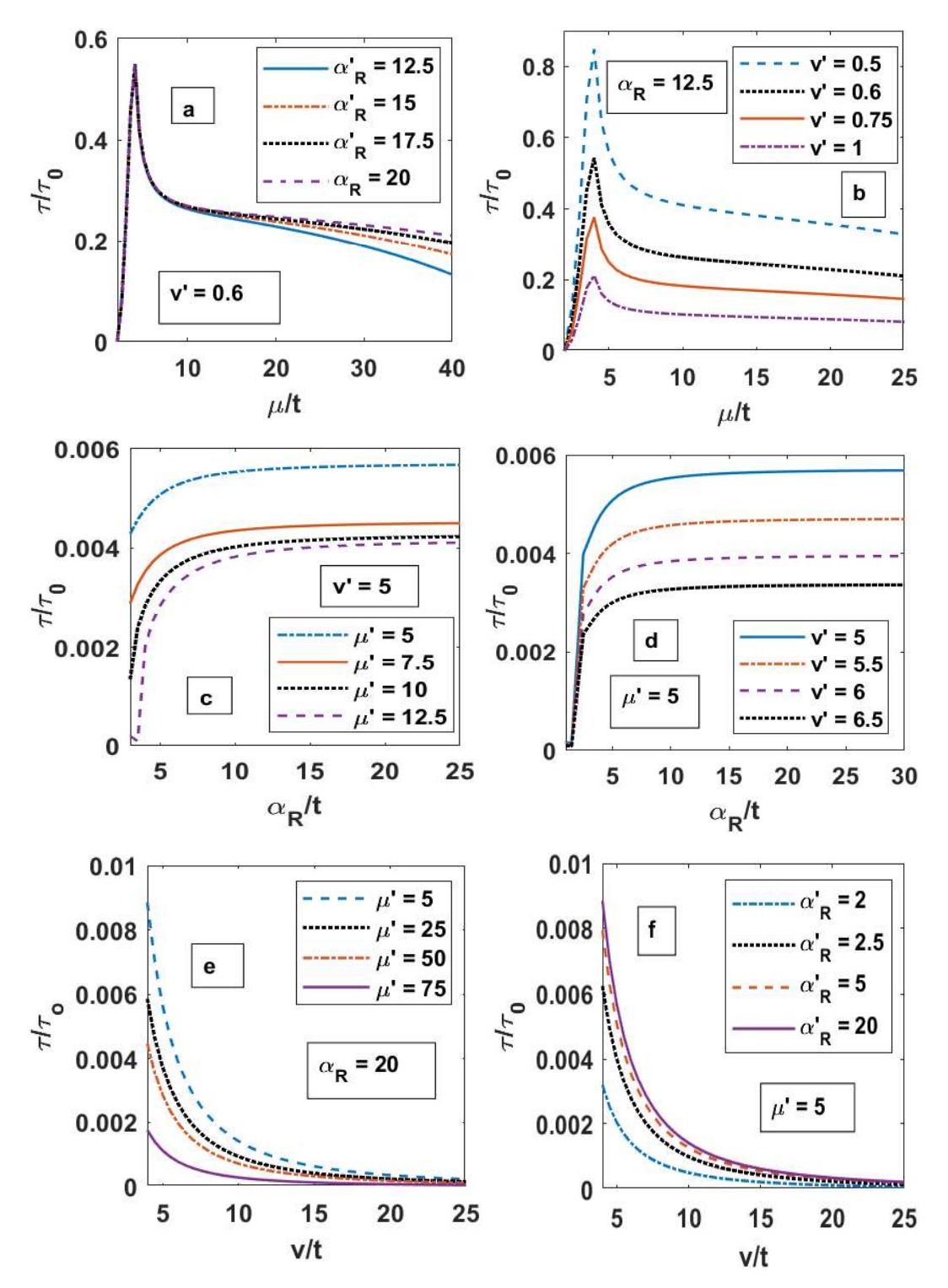


Fig. 2.2 Releaxation time (τ) : (a) Chemical potential μ for various RSOI coefficient α_R values; (b) μ for various impurity Strength ν values; (c) RSO coupling strength α_R for various μ values; (d) α_R various ν values; (e) ν for various μ values; (f) ν for various α_R values.

Fig 2.2 (d) shows plots of τ vs. α_R for different values of v. As we increase v, τ decreases. The behaviour of τ versus v for various values of μ and α_R is given in Figs. 2.2(e,f). As expected, τ decreases with increasing v, and the effect is more prominent at lower values of v. Also, the rate of decrease increases at lower values of μ and decreases at higher values of α_R .

The expressions for the longitudinal spin and charge conductivity are given by Equation. (2.69) and (2.63) and the relaxation time value appering in these equations is taken from equation (2.49). The behaviour of longitudinal charge conductivity (LCC) is presented in Fig 2.3. In Fig 2.3(a), LCC is plotted with μ for a few α_R values and a fixed value of v. Like τ , LCC also displays a sharp peak at $\mu = \mu_c$. Interestingly, however, the height of the LCC peak is much higher than that of τ . As μ exceeds μ_c , initially LCC decreases rapidly and then slowly and finally saturates to a constant value. Also, as α_R is increased, the peak height of LCC increases. When LCC is plotted with μ for various v values and for a specific value of α_R , one can see from Fig. 2.3(b) that the behaviour of LCC remains the same, though the peak value of CC decreases with increasing v. In Fig 2.3(c), LCC is plotted against α_R , for different μ values. One can observe that LCC increases smoothly and monotonically with μ . Similar behaviour is observed when LCC vs. α_R is plotted for different values of v. Fig 2.3 (d) shows plots of LCC vs. α_R for different values of v. Again LCC shows a monotonically increasing behaviour. Also, as we increase v, LCC decreases. The behaviour of LCC versus v for various values of μ and α_R is given in Figs. 2.3(e,f) . Fig. 2.3 (e) shows, as anticipated, that LCC decreases with increasing v. Furthermore, LCC dereases more rapidly around μ_c than at values of μ far away from μ_c . LCC vs v behaviour for various α_R value is given in Fig. 2.3(f) We can see that LCC responds more to v when v is small as well as when α_R is large.

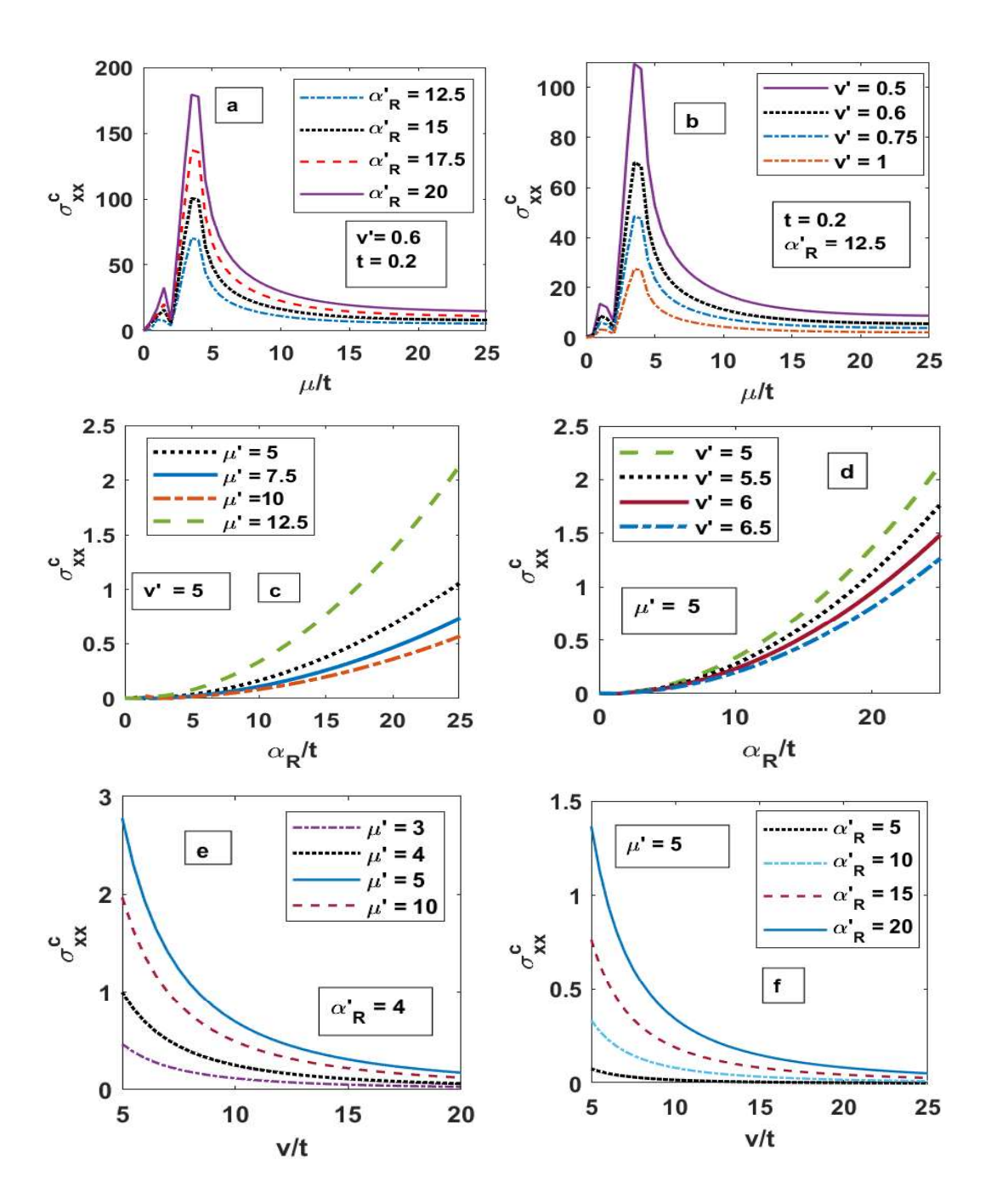


Fig. 2.3 Longitudinal charge conductivity (LCC): (a) Chemical potential μ for various RSOI coefficient α_R values; (b) μ for various impurity Strength v values; (c) RSO coupling strength α_R for various μ values; (d) α_R various v values; (e) v for various μ values; (f)) v for various α_R values.

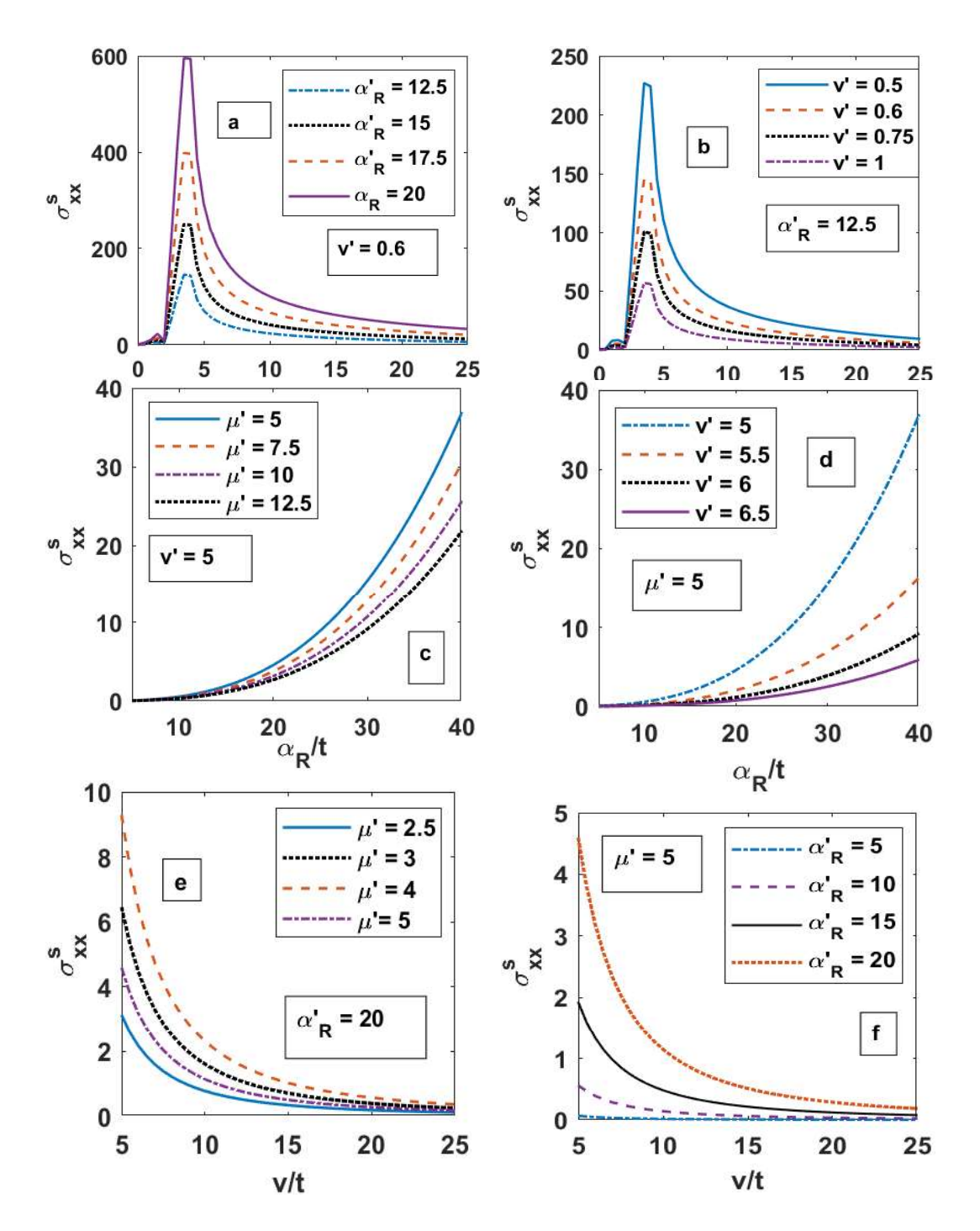


Fig 2.4 Longitudinal spin conductivity (LSC): (a) Chemical potential μ for various RSOI coefficient α_R values; (b) μ for various impurity Strength v values; (c) RSO coupling strength α_R for various μ values; (d) α_R various v values; (e) v for various μ values; (f) v for various α_R values.

Fig 2.4 gives the variation of spin conductivity (LSC) for various system parameters. Fig 2.4(a) shows the LSC vs. μ plot for various α_R values. LSC shows a similar dependence on μ as LCC and displays a peak for the same chemical potential value ($\mu = \mu_c$). When compared with LCC, LSC shows similar behaviour as of LCC, though the peak value in LSC is much higher than that in LCC for the same α_R .

Also, compared to LCC, LSC remains significant for higher value of μ . Fig. 2.4(b) shows LSC vs. μ plot for various v values. The nature of the curves is similar to that in Fig. 2.4(a). LSC is found to decreases with increasing v. Fig 2.4(c) illustrates the nature of LSC as a function of α_R for a few values of μ . Again we see that LSC is more prominent for higher values of α_R . In Fig 2.4(d), LSC versus α_R is shown for different values of v. The behaviour is similar to Fig 2.4(d).

However, the value of LSC is much higher than the corresponding LCC. In Fig 2.4(e), we plot LSC with respect to v directly for several vaues μ . Like LCC, LSC also decreases with increasing v. Finally, LSC versus v is plotted in Fig 2.4(f) for various α_R values. Again we find that LSC decreases rapidly with v and α_R – dependence is more vital for smaller values of v. As α_R rises, LSC goes to zero for higher values of v.

The variation of the ratio of LSC to LCC (θ) (= $\sigma_{xx}^s/\sigma_{xx}^c$) with respect to α_R is presented in Fig 2.5 for different values of μ . The figure shows that θ increases with θ almost linearly but decreases with increasing μ .

Finally, we calculate LCC and LSC for a realistic system namely for platinum. For Pt, $\alpha_R = 0.41 meV$ and the value of bulk μ is approximately 8 meV [18]. For a two-dimensional Platinium, the μ -value may be a little different from the bulk value. LCC and LSC also depend on hopping strength and impurity strength, for which we can only choose some plausible values. We obtain $\sigma_{xx}^c = 2.1 \times 10^{-6}$

 $10^6 \,\Omega^{-1} m^{-1}$ and $\sigma_{xx}^s = 2.5 \times 10^5 \,\Omega^{-1} m^{-1}$ and the ratio of LSC to LCC becomes: $\theta = (\sigma_{xx}^s/\sigma_{xx}^c) = 0.11$. The experimental value of $\theta = \sigma_{xx}^s/\sigma_{xx}^c$ lies in the range: 0.08 - 0.16 [19, 20]. Thus our calculation provides a reasonably accurate value θ .

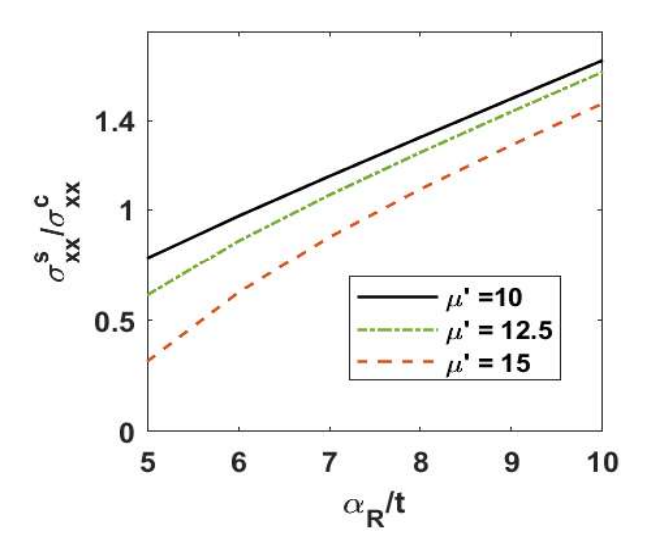


Fig. 2.5 Ratio of LCC to LSC i. e., $(\sigma_{xx}^s/\sigma_{xx}^c)$ (= θ) versus RSOI strength (α_R/t) for different values of μ .

2.4 Conclusion

We have studied the Rashba spin-orbit interaction effect on the charge and spin transport in a two-dimensional tight-binding electronic system that contains random impurities. This system is diagonalizable in the absence of the impurities and the system has two different bands for up and down-spin electrons. We have used the Matsubara Green function technique and computed the Feynman diagrammatic technique to calculate the relaxation time caused by impurity-electron scattering. To calculate the spin and charge conductivities, we have used the Kubo formalism. For the sake of simplicity and to understand our system better, we have worked in the dilute-impurity and the low-temperature regime.

Our findings predict that as a function of the chemical potential μ , both the longitudinal charge and spin conductivities and also the relaxation time display peak structures at some critical value of the chemical potential μ (μ_c). Beyond that critical value, the charge and spin conductivities fall off quite rapidly with increasing μ , though the corresponding drop in the relaxation time is relatively slow, Also, the longitudinal spin conductivity peaks are found to be much higher than the longitudinal charge conductivity peaks. These peaks increase with increasing RSOI strength and decrease as the impurity strength increases. However, in the case of relaxation time, the peak value is independent of RSOI. Furthermore, it is shown that both the charge and spin conductivities and also the relaxation time increase with RSOI and decrease with the electron-impurity interaction strength.

2.5 References

- G. A. Prinz, Science 282, 1660 (1998); S. A. Wolf et al., Science 294, 1488 (2001).
- 2. I. Z' utic', J. Fabian, and S. D. Sarma, Rev. Mod. Phys. **76**,323 (2004).
- 3. M. I. Dyakonov and V. I. Perel, JETP **33**, 1053 (1971).
- 4. J. E. Hirsch, Phys. Rev. Lett. **83**, 1834 (1999).
- 5. S. Zhang, Phys. Rev. Lett. **85**, 393 (2000).
- 6. S. Murakami, N. Nagaosa, and S. C. Zhang, Science **301**,1348 (2003).
- 7. J. Sinova *et al.*, Phys. Rev. Lett. **92**, 126603 (2004).
- 8. Y. K. Kato *et al.*, Science **306**, 1910 (2004).
- 9. J. Wunderlich, B. Kaestner, J. Sinova, and T. Jungwirth, Phys. Rev. Lett. 94, 047204 (2005).
- 10. P.-Q. Jin, Y.-Q. Li, and F.-C. Zhang, cond-mat/0502231.
- 11. S. Murakami, N. Nagaosa, and S.C. Zhang, Phys. Rev. B **69**, 235206 (2004).
- 12. E. I. Rashba, Phys. Rev. B **68**, 241315(R) (2003);

- 13. J. Shi, P. Zhang, D. Xiao and Q. Niu, Phys. Rev. Lett. 96, 076604 (2006).
- 14. D. Culcer et al., Phys. Rev. Lett. 93, 046602 (2004).
- 15. S. Zhang and Z. Yang, Phys. Rev. Lett. 94, 066602 (2005).
- 16. G. D. Mahan, Many Particle Physics (Plenum, New York) (1981).
- 17. Tanaka et al. Physical Review B 77,165117 (2008)
- 18. Dye, D.H., Ketterson, J.B. & Crabtree, G.W. J Low Temp Phys **30**, 813, (1978)
- 19. Zhang, W., Han, W., Jiang, X. et al. Nature Phys 11, 496–502 (2015)
- 20. Lijun Zhu , lujun Zhu , Manling Sui , Daniel C. Ralph , Robert A. Buhrman Science Advances: EAA8025 19 Jul 2019

CHAPTER 3

Torque-dependent Spin and charge conductivity in presence of Rashba and Dresselhaus spin-orbit interactions and static random disorder for a two-dimensional tight-binding system.

3.1 Introduction

In Chapter 2, we have discussed torque-dependent transport in a disordered system which lacks the inversion symmetry. In this chapter we will examine the effect of Dresselhaus [1] spin-orbit interaction (DSOI) as well as Rashba spin-orbit interaction (RSOI) [2] on our two-dimensional tight-binding system. As the Dresselhaus spin-orbit interaction (DSOI) effect is caused by bulk inversion asymmetry and can be found in almost every system, the present study is more realistic. We shall also study how the system behaves when one of the SOI effects dominates the other in the presence of impurity

3.2 The Model

We consider a two-dimensional tightly bound electronic system in the presence of RSOI, DSOI and random impurities. The Hamiltonian of the system is given by

$$H = H_0 + H_{imp}. (3.1)$$

where

$$H_{0} = \sum_{i} \epsilon_{0} c_{i}^{\dagger} c_{i} + t \left[\sum_{i_{x}, i_{y}} c_{i_{x}, i_{y}}^{\dagger} c_{i_{x+1}, i_{y}} + c_{i_{x}, i_{y}}^{\dagger} c_{i_{x}, i_{y+1}} + h.c \right]$$

$$-i\alpha_{R} \left[\sum_{i_{x}, i_{y}} c_{i_{x}, i_{y}}^{\dagger} \sigma_{y} c_{i_{x+1}, i_{y}} + h.c \right] + i\alpha_{R} \left[\sum_{i_{x}, i_{y}} c_{i_{x}, i_{y}}^{\dagger} \sigma_{x} c_{i_{x}, i_{y+1}} + h.c \right]$$

$$+i\beta_{D} \left[\sum_{i_{x}, i_{y}} c_{i_{x}, i_{y}}^{\dagger} \sigma_{x} c_{i_{x+1}, i_{y}} + h.c \right] - i\beta_{D} \left[\sum_{i_{x}, i_{y}} c_{i_{x}, i_{y}}^{\dagger} \sigma_{y} c_{i_{x}, i_{y+1}} + h.c \right], \quad (3.2)$$

and

$$H_{imp} = \sum_{i,l} v \delta(r_i - r_l) c_i^{\dagger} c_i.$$
 (3.3)

The first four terms appearing in Eq. (3.2) have already been introduced in the previous chapter. The last two terms represent DSOI. Eq. (3.3) has also been introduced in Chapter 2 and it is the electron-impurity interaction term.

In the k-space H_0 is given by

$$H_{0} = \sum_{\mathbf{k}_{x}, \mathbf{k}_{y}} c_{\mathbf{k}_{x}, \mathbf{k}_{y}}^{\dagger} \left[\epsilon_{\mathbf{k}} + 2\alpha_{R} \left(sink_{x} \sigma_{y} - sink_{y} \sigma_{x} \right) + 2\beta_{D} \left(sink_{y} \sigma_{y} - sink_{x} \sigma_{x} \right) \right] c_{\mathbf{k}_{x}, \mathbf{k}_{y}}.$$

$$(3.4)$$

To diagonalize the Hamiltonian (3.4), we consider the following unitary transformations:

$$\begin{pmatrix} \alpha_{1,k} \\ \alpha_{2,k} \end{pmatrix} = U_k \begin{pmatrix} c_{k\uparrow} \\ c_{k\downarrow} \end{pmatrix} \quad , \quad (\alpha_{1,k}^{\dagger} \quad \alpha_{2,k}^{\dagger}) = (c_{k\uparrow}^{\dagger} \quad c_{k\downarrow}^{\dagger}) U_k^{\dagger}$$
 (3.5)

where U_k is given by

$$U_k = \frac{1}{\sqrt{2}} \begin{bmatrix} 1 & p_{k_x, k_y} \\ -p_{k_x, k_y}^* & 1 \end{bmatrix}. \tag{3.6}$$

The non-diagonal elements p_{k_x,k_y} and p_{k_x,k_y}^* are given by

$$p_{k_x,k_y} = \frac{\left(\alpha_R sink_y + \beta_D sink_x\right) + i\left(\alpha_R sink_y + \beta_D sink_x\right)}{\sqrt{\left(\alpha_R sink_y + \beta_D sink_x\right)^2 + \left(\alpha_R sink_x + \beta_D sink_y\right)^2}}.$$
 (3.7)

$$p_{k_x,k_y}^* = \frac{\left(\alpha_R sink_y + \beta_D sink_x\right) - i\left(\alpha_R sink_y + \beta_D sink_x\right)}{\sqrt{\left(\alpha_R sink_y + \beta_D sink_x\right)^2 + \left(\alpha_R sink_x + \beta_D sink_y\right)^2}}.$$
 (3.8)

Therefore, the Hamiltonian (3.2) in term of transformed operator can be written as

$$\begin{split} &H_{0}\\ &=\sum_{\mathbf{k}_{x},\mathbf{k}_{y}}\left[\left(\epsilon_{k}-2\sqrt{\left(\alpha_{R}sink_{y}+\beta_{D}sink_{x}\right)^{2}+\left(\alpha_{R}sink_{x}+\beta_{D}sink_{y}\right)^{2}}\right)\alpha_{\mathbf{1},k}^{\dagger}\alpha_{\mathbf{1},k}\\ &+\left(\epsilon_{k}+2\sqrt{\left(\alpha_{R}sink_{y}+\beta_{D}sink_{x}\right)^{2}+\left(\alpha_{R}sink_{x}+\beta_{D}sink_{y}\right)^{2}}\right)\alpha_{\mathbf{1},k}^{\dagger}\alpha_{\mathbf{1},k}\right]. \end{split}$$

With further simplifications, we can write H_0 as:

$$H_0 = \sum_{\mathbf{k}_{\mathbf{x}}, \mathbf{k}_{\mathbf{y}}} \left[\epsilon_{1,k} \alpha_{1,k}^{\dagger} \alpha_{1,k} + \epsilon_{2,k} \alpha_{1,k}^{\dagger} \alpha_{1,k} \right], \tag{3.9}$$

where $\epsilon_{1,2,k}$ is

$$\epsilon_{1,2,k} = \left(\epsilon_k \mp 2\sqrt{\left(\alpha_R sink_y + \beta_D sink_x\right)^2 + \left(\alpha_R sink_x + \beta_D sink_y\right)^2}\right).$$

3.2.1 Spin Current

As before, to get the spin current operator, we start from the spin polarization operator [3, 4] which is defined as:

$$\vec{P}^{s_z} = \sum_{i_x, i_y} \vec{R}_{i_x, i_y} c_{i_x, i_y}^{\dagger} s_z c_{i_x, i_y}.$$
(3.10)

As pointed out already, the time derivative of Spin polarization should give the spin current density \vec{J}^{S_z} and is given by

$$\vec{J}^{s_z} = \frac{\partial \vec{P}^{s_z}}{\partial t} = i \left[H_0 , \sum_{\mathbf{j}_x, \mathbf{j}_y} \vec{R}_{\mathbf{j}_x, \mathbf{j}_y} c_{\mathbf{j}_x, \mathbf{j}_y}^{\dagger} \sigma_z c_{\mathbf{j}_x, \mathbf{j}_y} \right]. \tag{3.11}$$

We write $H_0 = H_0^1 + H_0^R + H_D^0$, where

$$H_0^1 = \sum_{i_x, i_y} \epsilon_0 c_i^{\dagger} c_i + t \left[\sum_{i_x, i_y} (c_{i_x, i_y}^{\dagger} c_{i_{x+1}, i_y} + c_{i_x, i_y}^{\dagger} c_{i_x, i_{y+1}} + h.c) \right], \tag{3.12}$$

$$H_0^R = i\alpha_R \left[\sum_{i_x, i_y} c_{i_x, i_y}^{\dagger} \, \sigma_x c_{i_x, i_{y+1}} + \text{h.c.} \right] - i\alpha_R \left[\sum_{i_x, i_y} c_{i_x, i_y}^{\dagger} \, \sigma_y \, c_{i_{x+1}, i_y} + \text{h.c.} \right], \quad (3.13)$$

$$H_0^D = i\beta_D \left[\sum_{i_x, i_y} c_{i_x, i_y}^{\dagger} \sigma_x c_{i_{x+1}, i_y} + h.c \right] - i\beta_D \left[\sum_{i_x, i_y} c_{i_x, i_y}^{\dagger} \sigma_y c_{i_x, i_{y+1}} + h.c \right]. (3.14)$$

Substituting Eqns. (3.12), (3.13), and (3.14) in (3.11), we get the expression for Spin Current Density as:

$$\begin{split} \vec{J}^{s_{z}} &= \frac{\partial \vec{P}^{s_{z}}}{\partial t} = & \quad \text{it} \sum_{i_{x},i_{y}} (\vec{R}_{i_{x+1},i_{y}} - \vec{R}_{i_{x},i_{y}}) \left[c^{\dagger}_{i_{x},i_{y}} \sigma_{z} c_{i_{x+1},i_{y}} - c^{\dagger}_{i_{x+1},i_{y}} \sigma_{z} c_{i_{x},i_{y}} \right] \\ &+ it \sum_{i_{x},i_{y}} (\vec{R}_{i_{x},i_{y+1}} - \vec{R}_{i_{x},i_{y}}) \left[c^{\dagger}_{i_{x},i_{y}} \sigma_{y} c_{i_{x},i_{y+1}} - c^{\dagger}_{i_{x},i_{y+1}} \sigma_{y} c_{i_{x},i_{y}} \right] \\ &+ i\alpha_{R} \sum_{i_{x},i_{y}} (\vec{R}_{i_{x+1},i_{y}} + \vec{R}_{i_{x},i_{y}}) \left[c^{\dagger}_{i_{x},i_{y}} \sigma_{x} c_{i_{x+1},i_{y}} - c^{\dagger}_{i_{x+1},i_{y}} \sigma_{x} c_{i_{x},i_{y}} \right] \\ &+ i\alpha_{R} \sum_{i_{x},i_{y}} (\vec{R}_{i_{x},i_{y+1}} + \vec{R}_{i_{x},i_{y}}) \left[c^{\dagger}_{i_{x},i_{y}} \sigma_{y} c_{i_{x},i_{y+1}} - c^{\dagger}_{i_{x},i_{y+1}} \sigma_{y} c_{i_{x},i_{y}} \right] \\ &+ i\beta_{D} \sum_{i_{x},i_{y}} (\vec{R}_{i_{x+1},i_{y}} + \vec{R}_{i_{x},i_{y}}) \left[c^{\dagger}_{i_{x},i_{y}} \sigma_{y} c_{i_{x+1},i_{y}} - c^{\dagger}_{i_{x+1},i_{y}} \sigma_{y} c_{i_{x},i_{y}} \right] \\ &+ i\beta_{D} \sum_{i_{x},i_{y}} (\vec{R}_{i_{x},i_{y+1}} + \vec{R}_{i_{x},i_{y}}) \left[c^{\dagger}_{i_{x},i_{y}} \sigma_{x} c_{i_{x},i_{y+1}} - c^{\dagger}_{i_{x},i_{y+1}} \sigma_{x} c_{i_{x},i_{y}} \right]. \end{split}$$

(3.15)

In x direction spin current density is given by

$$J_{x}^{s_{z}} = \operatorname{it} \sum_{i_{x}, i_{y}} \left[c_{i_{x}, i_{y}}^{\dagger} \sigma_{z} c_{i_{x+1}, i_{y}} - c_{i_{x+1}, i_{y}}^{\dagger} \sigma_{z} c_{i_{x}, i_{y}} \right]$$

$$+ i\alpha_{R} \sum_{i_{x}, i_{y}} (2i_{x} + 1) \left[c_{i_{x}, i_{y}}^{\dagger} \sigma_{x} c_{i_{x+1}, i_{y}} - c_{i_{x+1}, i_{y}}^{\dagger} \sigma_{x} c_{i_{x}, i_{y}} \right]$$

$$+ i\alpha_{R} \sum_{i_{x}, i_{y}} (2i_{x}) \left[c_{i_{x}, i_{y}}^{\dagger} \sigma_{y} c_{i_{x}, i_{y+1}} - c_{i_{x}, i_{y+1}}^{\dagger} \sigma_{y} c_{i_{x}, i_{y}} \right]$$

$$+ i\beta_{D} \sum_{i_{x}, i_{y}} (2i_{x} + 1) \left[c_{i_{x}, i_{y}}^{\dagger} \sigma_{y} c_{i_{x+1}, i_{y}} - c_{i_{x+1}, i_{y}}^{\dagger} \sigma_{y} c_{i_{x}, i_{y}} \right]$$

$$+ i\beta_{D} \sum_{i_{x}, i_{y}} (2i_{x}) \left[c_{i_{x}, i_{y}}^{\dagger} \sigma_{x} c_{i_{x}, i_{y+1}} - c_{i_{x}, i_{y+1}}^{\dagger} \sigma_{x} c_{i_{x}, i_{y}} \right].$$

$$(3.16)$$

Similarly the Spin current density along y-direction

$$J_{y}^{S_{z}} = \operatorname{it} \sum_{i_{x}, i_{y}} \left[c_{i_{x}, i_{y}}^{\dagger} \sigma_{z} c_{i_{x}, i_{y+1}} - c_{i_{x}, i_{y+1}}^{\dagger} \sigma_{z} c_{i_{x}, i_{y}} \right]$$

$$+ i \alpha_{R} \sum_{i_{x}, i_{y}} (2i_{y}) \left[c_{i_{x}, i_{y}}^{\dagger} \sigma_{x} c_{i_{x+1}, i_{y}} - c_{i_{x+1}, i_{y}}^{\dagger} \sigma_{x} c_{i_{x}, i_{y}} \right]$$

$$+ i \alpha_{R} \sum_{i_{x}, i_{y}} (2i_{y} + 1) \left[c_{i_{x}, i_{y}}^{\dagger} \sigma_{y} c_{i_{x}, i_{y+1}} - c_{i_{x}, i_{y+1}}^{\dagger} \sigma_{y} c_{i_{x}, i_{y}} \right]$$

$$+ i \beta_{D} \sum_{i_{x}, i_{y}} (2i_{y}) \left[c_{i_{x}, i_{y}}^{\dagger} \sigma_{y} c_{i_{x+1}, i_{y}} - c_{i_{x+1}, i_{y}}^{\dagger} \sigma_{y} c_{i_{x}, i_{y}} \right]$$

$$+ i \beta_{D} \sum_{i_{x}, i_{y}} (2i_{x} + 1) \left[c_{i_{x}, i_{y}}^{\dagger} \sigma_{x} c_{i_{x}, i_{y+1}} - c_{i_{x}, i_{y+1}}^{\dagger} \sigma_{x} c_{i_{x}, i_{y}} \right]. \quad (3.17)$$

In the eigen space, the expression of Spin current reads

$$J_{x}^{S_{z}} = 2t \sum_{\mathbf{k}_{x}, \mathbf{k}_{y}} \sin \mathbf{k}_{x} c_{\mathbf{k}_{x}, \mathbf{k}_{y}}^{\dagger} \sigma_{z} c_{\mathbf{k}_{x}, \mathbf{k}_{y}}$$

$$+ 2 \sum_{k_{x}, k_{y}} \frac{2[\beta_{D}^{2} - \alpha_{R}^{2}] \cos k_{x} \sin^{2} k_{y} p_{k_{x} k_{y}}^{*}}{\left(\alpha_{R} \sin k_{y} + \beta_{D} \sin k_{x}\right)^{2} + \left(\alpha_{R} \sin k_{x} + \beta_{D} \sin k_{y}\right)^{2}}$$

$$\times \alpha_{k}^{\dagger} \begin{bmatrix} (\beta_{D} - i\alpha_{R}) p_{k_{x}, k_{y}}^{*} & (\beta_{D} + i\alpha_{R}) p_{k_{x}, k_{y}}^{2} \\ -(\beta_{D} - i\alpha_{R}) p_{k_{x}, k_{y}}^{*2} & (\beta_{D} + i\alpha_{R}) p_{k_{x}, k_{y}}^{*2} \end{bmatrix} \alpha_{k}. \tag{3.18}$$

3. 2.2 Charge current

The charge current operator is obtained through charge polarizing operator which is defined as:

$$\vec{P}^c = \sum_{i_x, i_y} \vec{R}_{i_x, i_y} c_{i_x, i_y}^{\dagger} I c_{i_x, i_y}.$$
 (3.19)

The time derivative of the above polarization operator gives the charge current. So we can write

$$\vec{J}^c = \frac{\partial \vec{P}^c}{\partial t} = i \left[H_0 , \sum_{j_x, j_y} \vec{R}_{j_x, j_y} c_{j_x, j_y}^{\dagger} I c_{j_x, j_y} \right]. \tag{3.20}$$

We write $H_0 = H_0^1 + H_0^R + H_0^D$ and calculate the following commutators.

$$\begin{split} \left[H_{0}^{1},\vec{P}^{c}\right] &= t \sum_{\mathbf{i}_{x},\mathbf{i}_{y}} (\vec{R}_{\mathbf{i}_{x+1},\mathbf{i}_{y}} - \vec{R}_{\mathbf{i}_{x},\mathbf{i}_{y}}) \left[c_{\mathbf{i}_{x},\mathbf{i}_{y}}^{\dagger} c_{\mathbf{i}_{x+1},\mathbf{i}_{y}} - c_{\mathbf{i}_{x+1},\mathbf{i}_{y}}^{\dagger} c_{\mathbf{i}_{x},\mathbf{i}_{y}}\right] \\ &+ t \sum_{\mathbf{i}_{x},\mathbf{i}_{y}} (\vec{R}_{\mathbf{i}_{x},\mathbf{i}_{y+1}} - \vec{R}_{\mathbf{i}_{x},\mathbf{i}_{y}}) \left[c_{\mathbf{i}_{x},\mathbf{i}_{y}}^{\dagger} c_{\mathbf{i}_{x},\mathbf{i}_{y+1}} - c_{\mathbf{i}_{x},\mathbf{i}_{y+1}}^{\dagger} c_{\mathbf{i}_{x},\mathbf{i}_{y}}\right]. \end{split}$$
(3.21)

$$\begin{split} \left[H_{0}^{R},\vec{P}^{c}\right] &= \alpha_{R} \sum_{\mathbf{i}_{x},\mathbf{i}_{y}} (\vec{R}_{\mathbf{i}_{x+1},\mathbf{i}_{y}} - \vec{R}_{\mathbf{i}_{x},\mathbf{i}_{y}}) \left[c_{\mathbf{i}_{x},\mathbf{i}_{y}}^{\dagger} \sigma_{y} c_{\mathbf{i}_{x+1},\mathbf{i}_{y}} + c_{\mathbf{i}_{x+1},\mathbf{i}_{y}}^{\dagger} \sigma_{y} c_{\mathbf{i}_{x},\mathbf{i}_{y}}\right] \\ &- \alpha_{R} \sum_{\mathbf{i}_{x},\mathbf{i}_{y}} \left(\vec{R}_{\mathbf{i}_{x},\mathbf{i}_{y+1}} - \vec{R}_{\mathbf{i}_{x},\mathbf{i}_{y}}\right) \left[c_{\mathbf{i}_{x},\mathbf{i}_{y}}^{\dagger} \sigma_{x} c_{\mathbf{i}_{x},\mathbf{i}_{y+1}} + c_{\mathbf{i}_{x},\mathbf{i}_{y+1}}^{\dagger} \sigma_{x} c_{\mathbf{i}_{x},\mathbf{i}_{y}}\right]. \end{split}$$
(3.22)

$$[H_0^D, \vec{P}^c] = \beta_D \sum_{i_x, i_y} (\vec{R}_{i_{x+1}, i_y} - \vec{R}_{i_x, i_y}) \left[c_{i_x, i_y}^{\dagger} \sigma_x c_{i_{x+1}, i_y} + c_{i_{x+1}, i_y}^{\dagger} \sigma_x c_{i_x, i_y} \right]$$

$$-\beta_D \sum_{i_x, i_y} \left(\vec{R}_{i_x, i_{y+1}} - \vec{R}_{i_x, i_y} \right) \left[c_{i_x, i_y}^{\dagger} \sigma_y c_{i_x, i_{y+1}} + c_{i_x, i_{y+1}}^{\dagger} \sigma_y c_{i_x, i_y} \right]. \quad (3.23)$$

Substituting Eqns. (3.21) - (3.23) in Eq. (3.20), we obtain

$$\vec{J}^{c} = \frac{\partial \vec{P}^{c}}{\partial t} = i \left[H_{0}^{1} + H_{0}^{R} + H_{0}^{D}, \sum_{j_{x}, j_{y}} \vec{R}_{j_{x}, j_{y}} c_{j_{x}, j_{y}}^{\dagger} I c_{j_{x}, j_{y}} \right]$$

which on further simplification leads to

$$\begin{split} \vec{J}^{c} &= i t \sum_{i_{x},i_{y}} (\vec{R}_{i_{x+1},i_{y}} - \vec{R}_{i_{x},i_{y}}) \left[c^{\dagger}_{i_{x},i_{y}} c_{i_{x+1},i_{y}} - c^{\dagger}_{i_{x+1},i_{y}} c_{i_{x},i_{y}} \right] \\ &+ i t \sum_{i_{x},i_{y}} (\vec{R}_{i_{x},i_{y+1}} - \vec{R}_{i_{x},i_{y}}) \left[c^{\dagger}_{i_{x},i_{y}} c_{i_{x},i_{y+1}} - c^{\dagger}_{i_{x},i_{y+1}} c_{i_{x},i_{y}} \right] \\ &+ i \alpha_{R} \sum_{i_{x},i_{y}} (\vec{R}_{i_{x+1},i_{y}} - \vec{R}_{i_{x},i_{y}}) \left[c^{\dagger}_{i_{x},i_{y}} \sigma_{y} c_{i_{x+1},i_{y}} + c^{\dagger}_{i_{x+1},i_{y}} \sigma_{y} c_{i_{x},i_{y}} \right] \\ &- i \alpha_{R} \sum_{i_{x},i_{y}} \left(\vec{R}_{i_{x},i_{y+1}} - \vec{R}_{i_{x},i_{y}} \right) \left[c^{\dagger}_{i_{x},i_{y}} \sigma_{x} c_{i_{x},i_{y+1}} + c^{\dagger}_{i_{x},i_{y+1}} \sigma_{x} c_{i_{x},i_{y}} \right] \\ &- \beta_{D} \sum_{i_{x},i_{y}} \left(\vec{R}_{i_{x+1},i_{y}} - \vec{R}_{i_{x},i_{y}} \right) \left[c^{\dagger}_{i_{x},i_{y}} \sigma_{x} c_{i_{x+1},i_{y}} + c^{\dagger}_{i_{x+1},i_{y}} \sigma_{x} c_{i_{x},i_{y}} \right] \\ &+ \beta_{D} \sum_{i_{x},i_{y}} \left(\vec{R}_{i_{x},i_{y+1}} - \vec{R}_{i_{x},i_{y}} \right) \left[c^{\dagger}_{i_{x},i_{y}} \sigma_{y} c_{i_{x},i_{y+1}} + c^{\dagger}_{i_{x+1},i_{y}} \sigma_{y} c_{i_{x},i_{y}} \right]. \end{split}$$

In x-direction the contribution of charge current is given by

$$J_{x}^{c} = it \sum_{i_{x}, i_{y}} \left[c_{i_{x}, i_{y}}^{\dagger} c_{i_{x+1}, i_{y}} - c_{i_{x+1}, i_{y}}^{\dagger} c_{i_{x}, i_{y}} \right]$$

$$+ \alpha_{R} \sum_{i_{x}, i_{y}} \left[c_{i_{x}, i_{y}}^{\dagger} \sigma_{y} c_{i_{x+1}, i_{y}} + c_{i_{x+1}, i_{y}}^{\dagger} \sigma_{y} c_{i_{x}, i_{y}} \right]$$

$$- \beta_{D} \sum_{i_{x}, i_{y}} \left[c_{i_{x}, i_{y}}^{\dagger} \sigma_{x} c_{i_{x+1}, i_{y}} + c_{i_{x+1}, i_{y}}^{\dagger} \sigma_{x} c_{i_{x}, i_{y}} \right].$$

$$(3.24)$$

Similarity In y-direction, we have charge current

$$J_{y}^{c} = \sum_{i_{x},i_{y}} it \left[c_{i_{x},i_{y}}^{\dagger} c_{i_{x},i_{y+1}} - c_{i_{x},i_{y+1}}^{\dagger} c_{i_{x},i_{y}} \right]$$

$$- i\alpha_{R} \sum_{i_{x},i_{y}} \left[c_{i_{x},i_{y}}^{\dagger} \sigma_{x} c_{i_{x},i_{y+1}} + c_{i_{x},i_{y+1}}^{\dagger} \sigma_{x} c_{i_{x},i_{y}} \right]$$

$$+ \beta_{D} \sum_{i_{x},i_{y}} \left[c_{i_{x},i_{y}}^{\dagger} \sigma_{y} c_{i_{x},i_{y+1}} + c_{i_{x},i_{y+1}}^{\dagger} \sigma_{y} c_{i_{x},i_{y}} \right].$$

$$(3.25)$$

In terms of the α —operators, the charge currents in x and y directions are calculated using Eqs. (3.5-3.8). We obtain

$$J_{x}^{c} = 2t \sum_{k} (sink_{x}) \alpha_{k}^{\dagger} \alpha_{k} - i\alpha_{k} \sum_{k} (cosk_{x}) \alpha_{k}^{\dagger} \begin{bmatrix} p_{k}^{*} - p_{k} & 1 + p_{k}^{2} \\ -(1 + p_{k}^{*2}) & -(p_{k}^{*} - p_{k}) \end{bmatrix} \alpha_{k}$$
$$-i\beta_{D} \sum_{k} (cosk_{x}) \alpha_{k}^{\dagger} \begin{bmatrix} (p_{k}^{*} + p_{k}) & 1 - p_{k}^{2} \\ (1 - p_{k}^{*2}) & -(p_{k}^{*} + p_{k}) \end{bmatrix} \alpha_{k}. \tag{3.26}$$

On further simplification, we can write

$$J_{x}^{c} = \sum_{k} (2tsink_{x} - i\alpha_{R}(cosk_{x})(p_{k}^{*} - p_{k}) - i\beta_{D}(cosk_{x})(p_{k}^{*} + p_{k})) \alpha_{1,k}^{\dagger} \alpha_{1,k}$$

$$+ \sum_{k} (2tsink_{x} - i\alpha_{R}(cosk_{x})(p_{k} - p_{k}^{*}) - i\beta_{D}(cosk_{x})(p_{k}^{*} + p_{k})) \alpha_{2,k}^{\dagger} \alpha_{2,k}$$

$$+ \sum_{k} (-i\alpha_{R}(cosk_{x})(1 + p_{k}^{2}) - i\beta_{D}(cosk_{x})(1 - p_{k}^{2})) \alpha_{1,k}^{\dagger} \alpha_{2,k}$$

$$+ \sum_{k} (-i\alpha_{R}(cosk_{x})(1 + p_{k}^{*2}) - i\beta_{D}(cosk_{x})(1 - p_{k}^{*2})) \alpha_{2,k}^{\dagger} \alpha_{1,k}.$$

$$(3.27)$$

Now using

$$f_1^x(\mathbf{k}) = 2t\sin k_x - \cos k_x \left(i\alpha_{\rm R}(p_{k_x,k_y}^* - p_{k_x,k_y}) + \beta_{\rm D}(p_{k_x,k_y}^* + p_{k_x,k_y}) \right).$$

$$f_2^x(\mathbf{k}) = 2t\sin k_x + \cos k_x \Big(i\alpha_{\rm R}(p_{k_x,k_y}^* - p_{k_x,k_y}) + \beta_{\rm D}(p_{k_x,k_y}^* + p_{k_x,k_y}) \Big).$$

$$f_3^{x}(\mathbf{k}) = -\cos k_x \left(i\alpha_{R} \left(1 + p_{k_x, k_y}^2 \right) + \beta_{D} \left(1 - p_{k_x, k_y}^2 \right) \right). \tag{3.28}$$

The charge current along x direction reads

$$J_x^c = e/\hbar \sum_{k} \left(f_1^x(\mathbf{k}) \alpha_{1,k}^{\dagger} \alpha_{1,k} + f_2^x(\mathbf{k}) \alpha_{2,k}^{\dagger} \alpha_{2,k} + f_3^x(\mathbf{k}) \alpha_{1,k}^{\dagger} \alpha_{2,k} + f_3^x(\mathbf{k}) \alpha_{1,k}^{\dagger} \alpha_{2,k} \right). \tag{3.29}$$

Calculating in a similar fashion, we obtain the charge current in y direction as

$$J_{y}^{c} = e/\hbar \sum_{k} \left(f_{1}^{y}(\mathbf{k}) \alpha_{1,k}^{\dagger} \alpha_{1,k} + f_{2}^{y}(\mathbf{k}) \alpha_{2,k}^{\dagger} \alpha_{2,k} + f_{3}^{y}(\mathbf{k}) \alpha_{1,k}^{\dagger} \alpha_{2,k} + f_{3}^{y}(\mathbf{k}) \alpha_{1,k}^{\dagger} \alpha_{2,k} \right).$$

$$(3.30)$$

where $f_1^{y}(\mathbf{k})$, $f_2^{y}(\mathbf{k})$, $f_3^{y}(\mathbf{k})$ and $f_3^{*y}(\mathbf{k})$ are given by

$$f_1^{y}(\mathbf{k}) = 2t\sin k_y - \cos k_y \left(i\alpha_{R}(p_{k_x,k_y}^* - p_{k_x,k_y}) + \beta_{D}(p_{k_x,k_y}^* + p_{k_x,k_y}) \right).$$
(3.30a)

$$f_2^{y}(\mathbf{k}) = 2t\sin k_y + \cos k_y \left(i\alpha_{R}(p_{k_x,k_y}^* - p_{k_x,k_y}) + \beta_{D}(p_{k_x,k_y}^* + p_{k_x,k_y}) \right).$$
(3.30b)

$$f_3^{y}(\mathbf{k}) = -\cos k_y \left(i\alpha_{R} \left(1 + p_{k_x, k_y}^2 \right) + \beta_{D} \left(1 - p_{k_x, k_y}^2 \right) \right). \tag{3.30c}$$

$$f_3^{*y}(\mathbf{k}) = (-\cos k_y) \left(i\alpha_R (1 + p_k^{*2}) + i\beta_D (1 - p_k^{*2}) \right). \tag{3.30d}$$

3.2.3 Relaxation Time

Relaxation time is given by the imaginary part of the self -energy. We have already discussed its calculation in Chapter 2. The expression for relaxation time of an electron of type (1) in the presence of RSOI and DSOI and impurities is given by:

$$\frac{1}{\tau_k^1} = \frac{2\pi v^2 n}{\hbar 4N} \sum_{k_1} \left([(1 + |p_k|^2 |p_k|^2)] \delta(\epsilon - \epsilon_{1,k}) + [|p_k|^2 + |p_k|^2] \delta(\epsilon - \epsilon_{2,k}) \right).$$
(3.31)

Similarly the relaxation time for an electron of type (2) reads

$$\frac{1}{\tau_k^2} = \frac{2\pi}{\hbar} \frac{v^2 n}{4N} \sum_{k_1} \left(\left[\left(1 + |p_p|^2 |p_k|^2 \right) \right] \delta(\epsilon - \epsilon_{2,k}) \right) + \left[|p_p|^2 + |p_k|^2 \right] \delta(\epsilon - \epsilon_{1,k}).$$
(3.32)

Using the relation

$$\delta(g(x)) = \sum_{i} \frac{\delta(x - x_i)}{|g'(x_i)|}, \qquad (3.33)$$

in Eq. (3.30), the relaxation time τ_k^1 can be written as

$$\frac{1}{\tau_k^1} = \frac{v^2 n}{\pi \hbar} \int_0^{\pi} dk_y \sum_{i=1,2} \left\{ \frac{1}{\sqrt{4t^2 - x_1^2}} [1/|1 + w(x_i)|] + \frac{1}{\sqrt{4t^2 - x_1^2}} [1/|1 - w(x_i)|] \right\},$$
(3.34)

where

$$w(x_{i}) = \frac{x_{i}}{2t^{2}\sqrt{1 - \frac{x_{i}^{2}}{4t^{2}}}} \times \frac{2\alpha_{R}\beta_{D}sink_{y} + (\alpha_{R}^{2} + \beta_{D}^{2})\sqrt{1 - \frac{x_{i}^{2}}{4t^{2}}}}{\sqrt{\left(\alpha_{R}sink_{y} + \beta_{D}\sqrt{1 - \frac{x_{i}^{2}}{4t^{2}}}\right)^{2} + \left(\beta_{D}sink_{y} + \alpha_{R}\sqrt{1 - \frac{x_{i}^{2}}{4t^{2}}}\right)^{2}}},$$
 (3.35)

and

$$x_{1} = \frac{\mu - 2tcosk_{y} + 2\sqrt{(\alpha_{R}^{2} + \beta_{D}^{2})sin^{2}k_{y} + \alpha_{R}^{2} + \beta_{D}^{2} + 4\alpha_{R}\beta_{D}}}{1 + \alpha_{R}^{2} + \beta_{D}^{2} + 2\alpha_{R}\beta_{D}sink_{y}},$$
(3.36)

$$x_{2} = \frac{\mu - 2tcosk_{y} - 2\sqrt{(\alpha_{R}^{2} + \beta_{D}^{2})sin^{2}k_{y} + \alpha_{R}^{2} + \beta_{D}^{2} + 4\alpha_{R}\beta_{D}}}{1 + \alpha_{R}^{2} + \beta_{D}^{2} + 2\alpha_{R}\beta_{D}sink_{y}},$$
(3.37)

In the case when the impurity concentration is low, the relaxation time for type

(1) and type (2) electrons will be same and we have

$$\frac{1}{\tau_k^1} = \frac{1}{\tau_k^2}. (3.38)$$

3.2.4 Longitudinal Charge Conductivity (LCC)

To calculate longitudinal charge conductivity, we used Kubo formalism [5], as we have obtained in chapter 2, using equations (2.53-2.60), the expression for longitudinal charge conductivity is given by

$$\sigma_{xx}^{c} = -\frac{e^{2}}{N\hbar} \sum_{\mathbf{k}} [(f_{1}^{x})^{2}(\mathbf{k})A_{1}^{2}(\mathbf{k},\mu) + (f_{2}^{x})^{2}(\mathbf{k})A_{2}^{2}(\mathbf{k},\mu) + 2f_{3}^{x}(\mathbf{k})f_{3}^{*x}(\mathbf{k})A_{1}(\mathbf{k},\mu)A_{2}(\mathbf{k},\mu)].$$
(3.39)

In the low-impurity and low-temperature regime, the spectral functions can be written as

$$(A_1(k,\epsilon))^2 = \frac{1}{\hbar} 4\pi \tau(\mu) \delta(\mu - \epsilon_{1,k}), \qquad (A_2(k,\epsilon))^2 = \frac{1}{\hbar} 4\pi \tau \delta(\mu - \epsilon_{2,k}).$$
(3.40)

so that Eq. (3.39) becomes

$$\sigma_{xx}^{c} = \frac{e^{2}}{N\hbar} \sum_{k} \left[(f_{1}^{(x)})^{2}(k)\tau\delta(\mu - \epsilon_{1,k}) + (f_{2}^{(x)})^{2}(k)\tau\delta(\mu - \epsilon_{1,k}) \right],$$
(3.41)

which on using Eq. (3.32) reads

$$\sigma_{xx}^{c} = \frac{2}{\pi} \tau \int_{-\pi}^{\pi} \sum_{i=1,2} \frac{dk_{x}}{\sqrt{4t^{2} - y_{i}^{2}}} \left[\frac{\left(f_{1}^{x}(k_{x}, y_{i})\right)^{2}}{\left[1 + w(y_{i})\right]} + \frac{\left(f_{2}^{x}(k_{x}, y_{i})\right)^{2}}{\left[1 - w(y_{i})\right]} \right]$$
(3.42)

where f_1^x , f_2^x and $g(y_{1,2})$ is given by

$$f_{1}^{x}(k_{x},y) = 2tsink_{x} - \frac{2cosk_{x} \left[\left(2\alpha_{R}\beta_{D}\sqrt{1 - \frac{y^{2}}{4t^{2}}} + (\alpha_{R}^{2} + \beta_{D}^{2})sink_{x} \right) \right]}{\sqrt{\left(\alpha_{R}sink_{x} + \beta_{D}\sqrt{1 - \frac{y^{2}}{4t^{2}}} \right)^{2} + \left(\beta_{D}sink_{x} + \alpha_{R}\sqrt{1 - \frac{y^{2}}{4t^{2}}} \right)^{2}}},$$
(3.43)

$$f_{2}^{x}(k_{x},y) = 2tsink_{x} + \frac{2cosk_{x}\left[\left(2\alpha_{R}\beta_{D}\sqrt{1 - \frac{y^{2}}{4t^{2}}} + (\alpha_{R}^{2} + \beta_{D}^{2})sink_{x}\right)\right]}{\sqrt{\left(\alpha_{R}sink_{x} + \beta_{D}\sqrt{1 - \frac{y^{2}}{4t^{2}}}\right)^{2} + \left(\beta_{D}sink_{y} + \alpha_{R}\sqrt{1 - \frac{y^{2}}{4t^{2}}}\right)^{2}}},$$
(3.44)

$$g(y_{1,2}) = \frac{y_1}{2t^2 \sqrt{1 - \frac{y_{1,2}^2}{4t^2}}} \frac{2\alpha_R \beta_D sink_x + (\alpha_R^2 + \beta_D^2) \sqrt{1 - \frac{y_{1,2}^2}{4t^2}}}{\sqrt{\left(\alpha_R sink_x + \beta_D \sqrt{1 - \frac{y_{1,2}^2}{4t^2}}\right)^2 + \left(\beta_D sink_x + \alpha_R \sqrt{1 - \frac{y_{1,2}^2}{4t^2}}\right)^2}}.$$
(3.45)

Similarly, LCC is given by

$$\sigma_{yy}^{c} = \frac{2}{\pi} \tau \int_{-\pi}^{\pi} \sum_{i=1,2} \frac{dk_{y}}{\sqrt{4t^{2} - x_{i}^{2}}} \left[\frac{\left(f_{1}^{y}(k_{x}, x_{i})\right)^{2}}{[1 + w(x_{i})]} + \frac{\left(f_{2}^{y}(k_{y}, x_{i})\right)^{2}}{[1 - w(x_{i})]} \right]$$
(3.46)

where f_1^y , f_2^y and $g(x_{1,2})$ are given by

$$f_{1}^{y}(k_{y},x) = 2tsink_{y} - \frac{2cosk_{y}\left[\left(2\alpha_{R}\beta_{D}\sqrt{1 - \frac{x^{2}}{4t^{2}}} + (\alpha_{R}^{2} + \beta_{D}^{2})sink_{y}\right)\right]}{\sqrt{\left(\alpha_{R}sink_{y} + \beta_{D}\sqrt{1 - \frac{x^{2}}{4t^{2}}}\right)^{2} + \left(\beta_{D}sink_{y} + \alpha_{R}\sqrt{1 - \frac{x^{2}}{4t^{2}}}\right)^{2}}},$$
(3.47)

$$f_{2}^{y}(k_{y},x) = 2tsink_{y} + \frac{2cosk_{y}\left[\left(2\alpha_{R}\beta_{D}\sqrt{1-\frac{x^{2}}{4t^{2}}} + (\alpha_{R}^{2} + \beta_{D}^{2})sink_{y}\right)\right]}{\sqrt{\left(\alpha_{R}sink_{y} + \beta_{D}\sqrt{1-\frac{x^{2}}{4t^{2}}}\right)^{2} + \left(\beta_{D}sink_{y} + \alpha_{R}\sqrt{1-\frac{x^{2}}{4t^{2}}}\right)^{2}}},$$
(3.48)

$$g(x_{1,2}) = \frac{x_1}{2t^2 \sqrt{1 - \frac{x_1^2}{4t^2}}} \frac{2\alpha_R \beta_D sink_y + (\alpha_R^2 + \beta_D^2) \sqrt{1 - \frac{x_1^2}{4t^2}}}{\sqrt{\left(\alpha_R sink_y + \beta_D \sqrt{1 - \frac{x_1^2}{4t^2}}\right)^2 + \left(\beta_D sink_y + \alpha_R \sqrt{1 - \frac{x_1^2}{4t^2}}\right)^2}}.$$
(3.49)

3.2.5 Longitudinal Spin Conductivity (LSC)

Calculating the longitudinal spin conductivity involves using two expressions: the charge (3.28), and the spin current density (3.18), and employ the similar formalism as we have used for the calculation for LCC. The expression for spin conductivity is thus given by

$$\sigma_{xx}^{s_z} = \frac{4\pi}{N} \sum_{k} [f_1^x(k) h_{1x}(k) A^1(k, \epsilon)^2 + f_2^x(k) h_{1x}(k) A^2(k, \epsilon)^2]. \quad (3.50)$$

which on using Eqns. (3.39) and (3.49) becomes

$$\sigma_{xx}^{s_z} = \frac{4\pi}{N} \sum_{k} \left[f_1^x(k) h_{1x}(k) \tau(\mu) \delta(\mu - \epsilon_k^1) + f_2^x(k) h_{1x}(k) \tau(\mu) \delta(\mu - \epsilon_k^2) \right].$$
(3.51)

On further simplification and by using the relation (3.32), the expression for LSC reduces to

$$\sigma_{xx}^{s_z} = \frac{2}{\pi} \tau \int_{-\pi}^{\pi} \sum_{i=1,2} \frac{dk_x h_x (k_x, y_i)}{\sqrt{4t^2 - y_i^2}} \left[\frac{\left(f_1^x (k_x, y_i)\right)^2}{\left[1 + w(y_i)\right]} + \frac{\left(f_2^x (k_x, y_i)\right)^2}{\left[1 - w(y_i)\right]} \right]$$
(3.52)

where $h_{ix}(k)$ is given by

$$h_{ix}(k) = \sum_{k} \frac{2(\beta_D^2 - \alpha_R^2)^2 sin^2 k_y cosk_x sink_x}{\left[\left(\alpha_R sink_x + \beta_D \sqrt{1 - \frac{y^2}{4t^2}} \right)^2 + \left(\beta_D sink_x + \alpha_R \sqrt{1 - \frac{y^2}{4t^2}} \right)^2 \right]^{3/2}}.$$
(3.53)

Similarly, LSC $(\sigma_{yy}^{s_z})$ is given by

$$\sigma_{yy}^{s_z} = \frac{2}{\pi} \tau \int_{-\pi}^{\pi} \sum_{i=1,2} \frac{dk_y h_y (k_y, x_i)}{\sqrt{4t^2 - x_i^2}} \left[\frac{\left(f_1^y (k_x, x_i)\right)^2}{\left[1 + w(x_i)\right]} + \frac{\left(f_2^y (k_y, x_i)\right)^2}{\left[1 - w(x_i)\right]} \right] (3.54)$$

where $h_y(k)$ is given by

$$h_{y}(k) = \sum_{k} \frac{2(\beta_{D}^{2} - \alpha_{R}^{2})^{2} sin^{2} k_{x} cosk_{y} sink_{y}}{\left(\left(\alpha_{R} sink_{y} + \beta_{D} \sqrt{1 - \frac{x^{2}}{4t^{2}}}\right)^{2} + \left(\beta_{D} sink_{x} + \alpha_{R} \sqrt{1 - \frac{x^{2}}{4t^{2}}}\right)^{2}\right)^{3/2}}.$$
(3.55)

3.3 Numerical Results and discussion

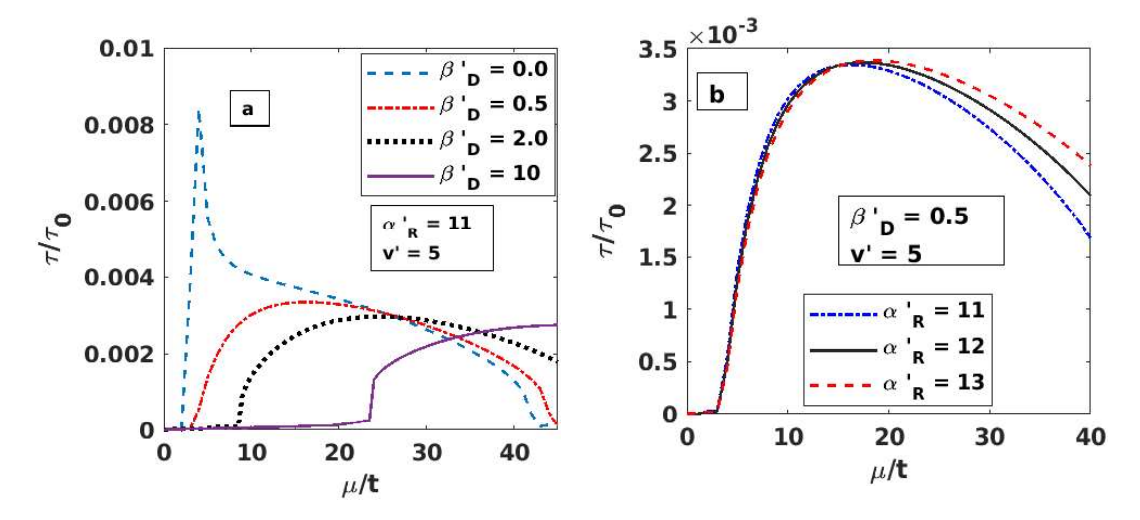


Fig. 3.1 Relaxation time τ versus: (a) Chemical potential μ for various DSOI coefficient β_D values; (b) μ for various RSOI Strength α_R values.

In Fig 3.1, the relaxation time τ is plotted with respect to the chemical potential μ (or more precisely with respect to μ' which is given by: $\mu' = \mu/t$). Fig. 3.1(a), show τ versus μ plot for various β_D values with a fixed value of α_R . In the absence of DSOI, τ remains independent of μ up to a certain value of μ (μ_1) after which it increases with μ and attains a peak. As μ increases further, initially τ falls off very rapidly giving rise to a sharp peak, but above a certain μ , τ reduces rather slowly with increasing μ and eventually becomes zero at some critical μ (μ_2). A decrease in τ implies more and more scattering events. When the effect

of Dresselhaus coupling is included, we observe a broad maximum in τ instead of a sharp peak. Also the maximum and the critical chemical potentials μ_1 and μ_2 shift towards right as β_D increases. The increase in DSOI strength leads to a decrease in bulk inversion symmetry, causing more scattering events which leads to decrease in relaxation time. When β_D is kept constant, Fig 3.1(b) τ remains independent of α_R up to a specific μ value after which α_R — dependence of τ is evident. It should be noted that the results remain same if the strength of either of RSOI or DSOI is interchanged.

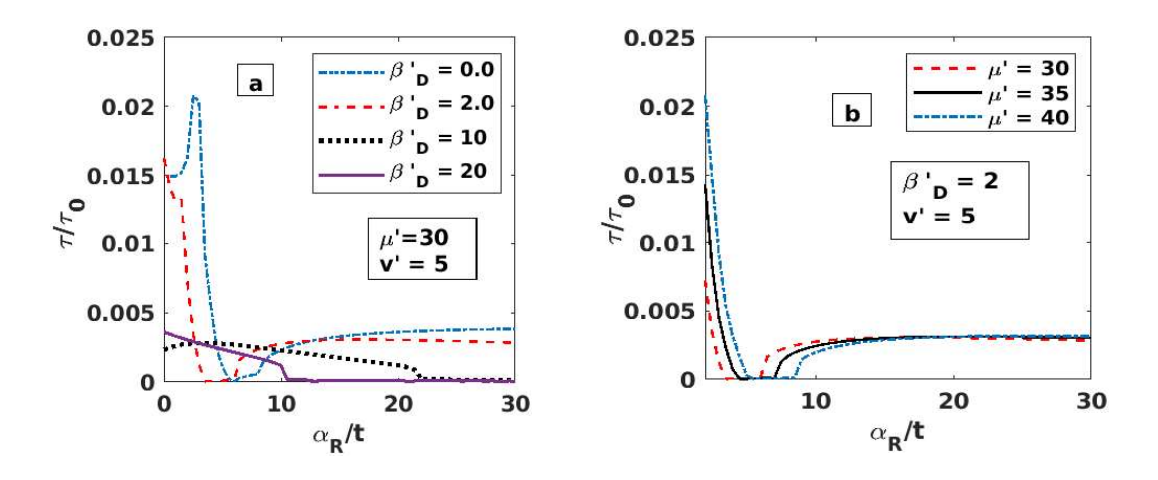


Fig. 3.2 Relaxation time τ versus: (a) RSOI strength for various DSOI coefficient β_D ; (b) α_R for various chemical potential μ values.

In Fig 3.2, τ is plotted with α_R for various β_D value. In the absence of the DSOI effect, τ , with α_R , initially increases, and develops a peak and then sharply falls off to zero. Then again it increases with the further increase in α_R , though slowly, and eventually saturates to a fixed value. In the presence of DSOI, the initial peak that appears in τ for $\beta_D=0$, disappears, but the rest of the behaviour remains the same. For intermediate values of β_D , τ decreases monotonically with increasing α_R and eventually becomes zero. When β_D is large, and α_R is small, τ is small compared to the $\beta_D=0$ - case. As α_R increases further, τ decreases and slowly

become zero. This behavior is due to bulk symmetry breaking which increases with increasing β_D and reduces τ . In Fig 3.2(b), τ versus α_R for a certain value of β_D is plotted for different values of μ . The qualitative behaviour of τ does not change even as μ increases.

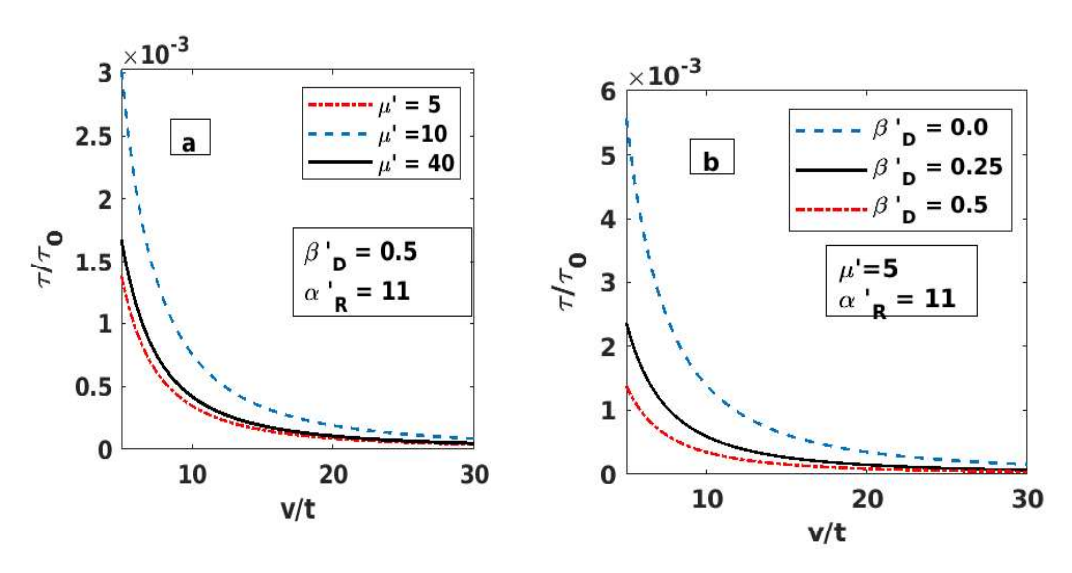


Fig. 3.3 Relaxation time τ versus: (a) Impurity strength v for various μ values; (b) Impurity srength v for various α_R values.

In Fig 3.3(a), we plot τ versus v. As v increases, τ decreases monotonically, which is understandable. We also observe that the τ decreases more rapidly with at small v values. Furthermore, τ increases with μ up to a critical value after which it decreases with increasing μ . Also one can see that, effect of μ is more prominent for lower impurity strength. In Fig. 3.3(b), τ is plotted with v for different β_D values. Again the figure shows a rapid decrease in τ with increasing v. Again effect of DSOI strength is more prominent for lower impurity strength.

We compute the charge and spin conductivities using Eqns. (3.42) and (3.52). Fig. 3.4 shows the nature of LCC with various system parameters. In Fig 3.4 (a), LCC is plotted with μ for a certain value of α_R and for a few small values of β_D . In the absence of Dresselhaus effect, LCC displays a sharp peak at a critical value of μ . For weak DSOI also, LCC shows a peak structure but the peak has a shorter

height. Furthermore, for weak DSOI, as μ increases, LCC eventually saturates to a constant value. For strong DSOI. Fig 3.4(b), LCC remains small at low values of μ and shows a hump-like structure as μ is increased. These humps increase in height with the increase in β_D and shift towards right. In Fig 3.4 (c), we show the variation of LCC with μ for various α_R value but with a low value of β_D namely, $\beta_D' = 0.5$. Again we see a peak structure is observed with respect to μ . Also, as α_R is increased, the peak increases.

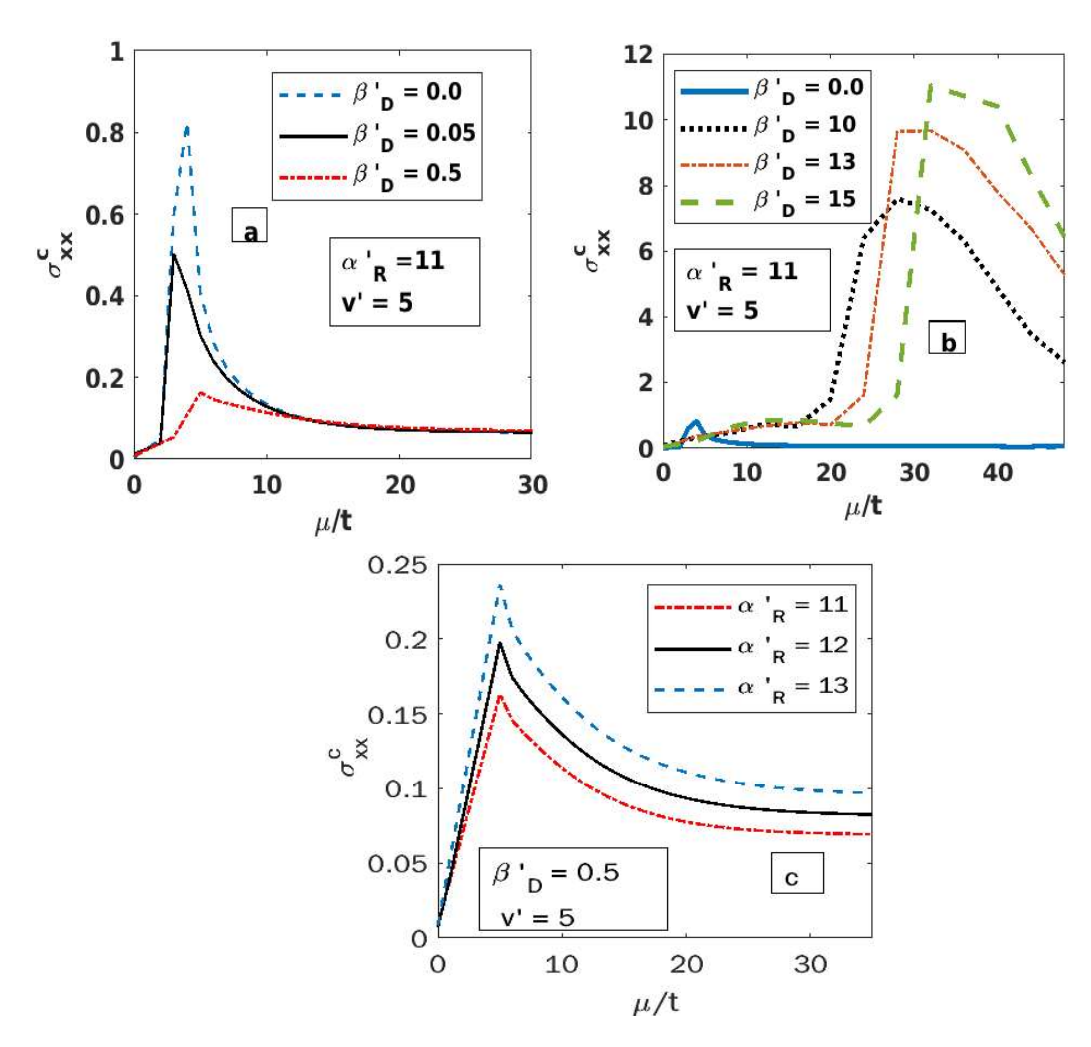


Fig. 3.4 LCC versus: (a, b) μ for various β_D values; (c) μ for various α_R values.

Fig 3.5 presents LCC versus α_R plot for various μ values. We see a non-monotonic nature of LCC. The inset shows the plot for small values of α_R explicitly. As α_R increases, initially LCC increases and reaches a peak at a critical value of α_R . As α_R is further increased, LCC goes through a dip and then it increases continuously and monotonically with α_R . This behaviour is consistent with that observed in Fig 3.3 and Fig 3.4. The variation of LCC with α_R for various β_D is presented in Fig. 3.5(b). In the absence of DSOI, LCC increases monotonically with α_R , though the increase is much higher when DSOI is present.

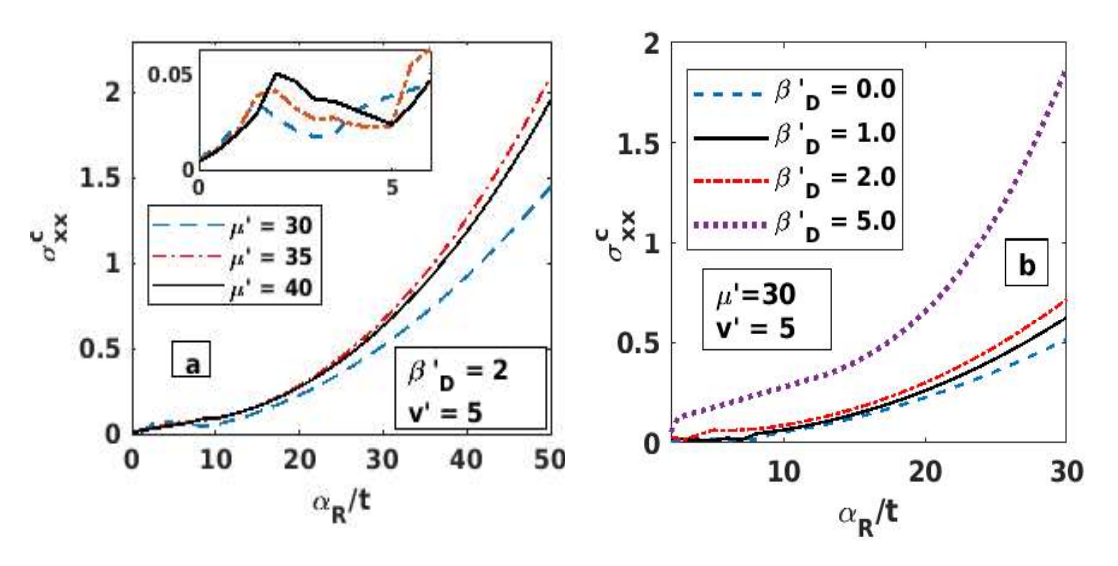


Fig. 3.5 LCC versus: (a) α_R for various μ values; (b) α_R for various β_D values.

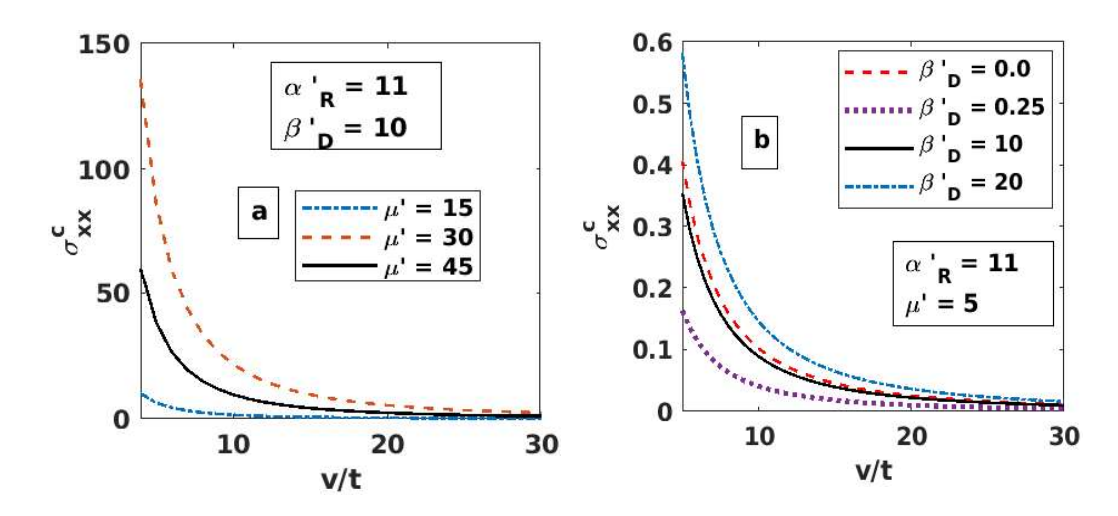


Fig. 3.6 LCC versus: (a) v for various μ values, (b) v for various β_D values.

In Fig 3.6, the dependence of LCC on v is presented. Fig 3.6(a) presents results for various values of μ while Fig. 3.6(b) gives results for various values of β_D . With increase in v, we see a decrease in LCC which is of course an expected behaviour. Again one can see that the dependence of both chemical potential and DSOI strength is more prominent for lower impurity strength.

In Fig 3.7, LSC is plotted with respect to μ . Fig. 3.7(a, b) gives results for various β_D and α_R values. One can see from Fig. 3.7(a) that LSC exhibits a peak at specific μ value in the absence of DSOI. For weak Dresselhaus interaction, the peak becomes shorter. For large β_D , SC remains zero up to a certain value of μ after which LSC develops a peak. Furthermore, the peak shifts towards a higher μ values with increase in β_D . Fig 3.7(b) shows a simple peak structure in LSC with chemical potential for various α_R values. Peaks become higher with increasing α_R . Furthermore, as μ become large LSC apparently goes to zero. Also one can observe, that LSC is zero whenever $\alpha_R = \beta_D$. In this case, the effects from RSOI and DSOI cancel each other (Eq.(3.52)).

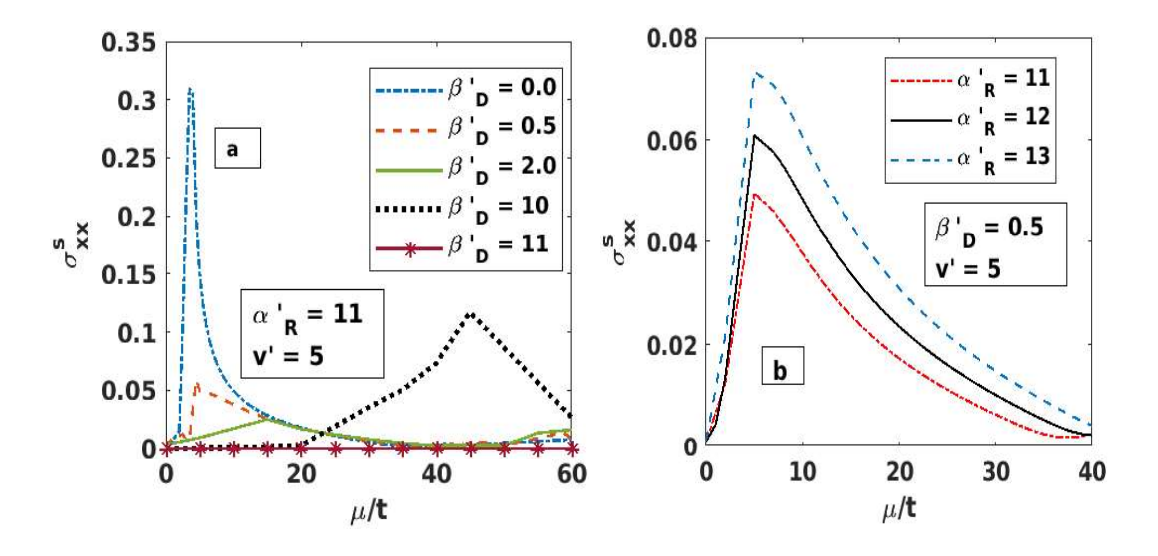


Fig. 3.7 LSC versus: (a) μ for various β_D values; (b) μ for various α_R values.

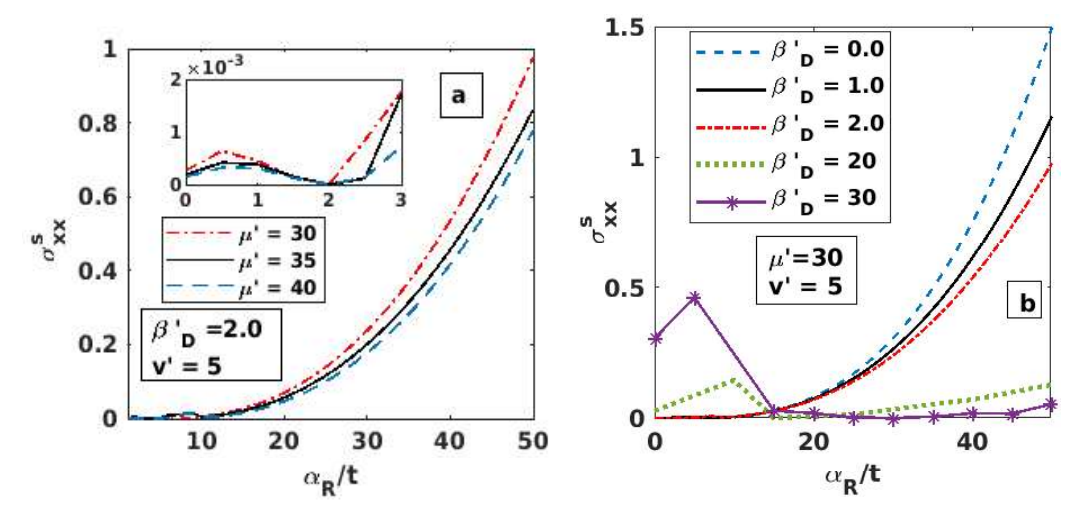


Fig. 3.8 LSC versus: (a) α_R for various μ values; (b) α_R for β_D values.

In Fig 3.8, the nature of LSC with α_R is given. The plot of spin conductivity versus RSOI strength for a set of values of μ is given in Fig 8(a). Initially, when RSOI strength is small, we observe an increase in LSC. For the fixed μ value, as RSOI strength increases and reaches close to DSOI strength, LSC decreases and becomes zero when RSOI and DSOI become equal. Beyond that, LSC increases smoothly with increase in α_R . Now if we increase the value of chemical potential μ , we observe decrease in LSC. Fig 3.8(b) shows the LSC versus α_R - plots for different values of β_D . As β_D increases Rashba and Dresselhaus effects counter each other due to which LSC increases at a lower rate, as explained earlier. It was also observed that, the effects of DSOI on LSC will remain the same, if we interchange RSOI with DSOI on LSC. So the DSOI effect caused by the bulk inversion asymmetry can easily be countered by the RSOI effect which we can be tuned by manipulating the external electric field. Also, Fig (3.8) also shows that martial with higher Dresselhaus strength require high chemical potential. Therefore to generate high LSC in materials with high DSOI strength, we have to consider those materials which also have high chemical potential.

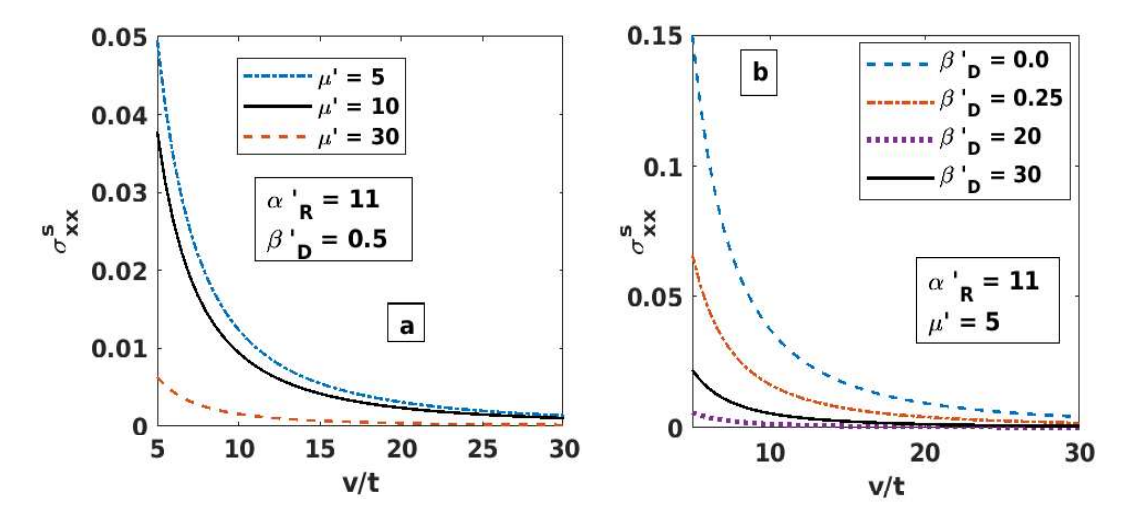


Fig. 3.9 LSC versus:(a) v for various chemical potential μ values; (b) v for various RSOI strength α_R values.

In Fig 3.9, the dependence of LSC on v is given. Fig 3.9(a) presents results for various μ value while Fig 3.9 (b) gives results for different values of β_D . Both the figures show that SC decreases as v increases. The effect is highly prominent at small v. Fig 3.9 (a) suggests that LSC is reduced more as μ is increased. Fig 3.9 (b) shows that the rate of increase of LSC is larger at larger values of β_D .

Fig 3.10(a) shows Longitudinal spin-to-charge conductivity ratio $\sigma_{xx}^S/\sigma_{xx}^C$ plot with α_R for various μ values. We see that with the increase in α_R , the ratio $\sigma_{xx}^S/\sigma_{xx}^C$ increases. And as we increase chemical potential the ratio $\sigma_{xx}^S/\sigma_{xx}^C$ increases. Fig 3.10 (b) shows the spin-to-charge ratio with α_R for various β_D values. The spin-to-charge conductivity ratio has finite value when $\beta_D \neq 0$ and $\alpha_R = 0$. As α_R increases, spin-to-charge ratio decreases and become zero at $\alpha_R = \beta_D$ as is clear from Eq. (3.42) and (3.52). With further increase in α_R the LSC/LCC ratio increases monotonically.

Form experimental data we know that Rashba strength for a material can be modified to 50% by gate voltage [6,7] and the ratio of the Rashba and Dresselhaus constants is of the order 1.5 to 2.5 [8]. For Indium Arsenide $\mu =$

 $-0.22 \, meV$, $\alpha_R = 1.6 \, meV$, $\beta_D = 1 \, meV$ [9, 10]. Thus the value of the LSC/LCC ratio comes out to be around 0.05.

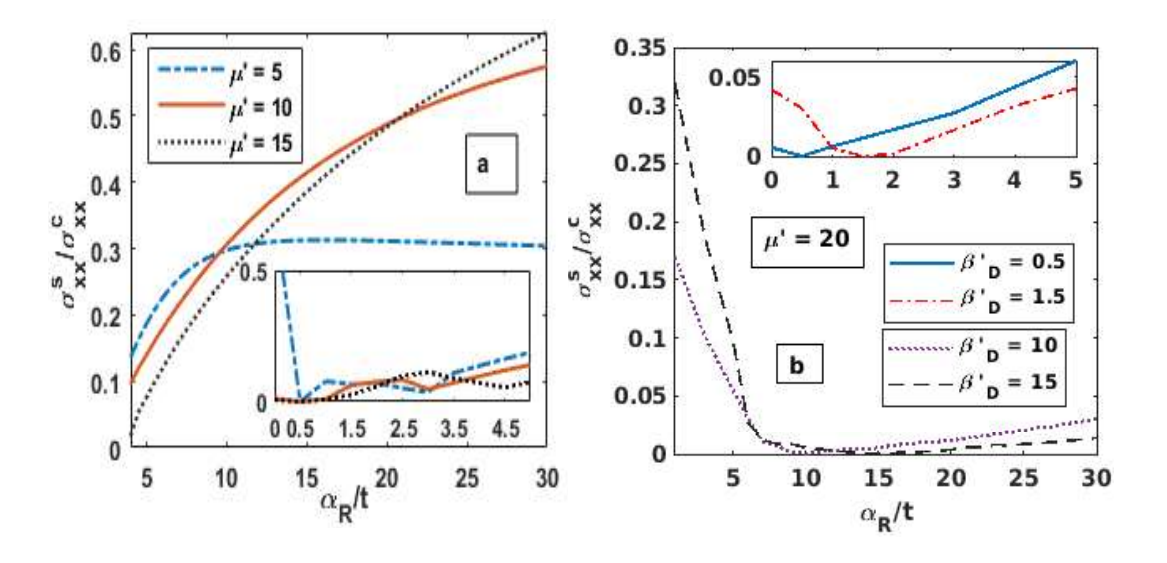


Fig. 3.10 [LSC/LCC] versus: (a) α_R for various values of μ ; (b) α_R for various values of β_D .

3.4 Conclusion

We have studied the Rashba and Dresselhaus spin-orbit interaction effect on the charge and spin transport for a two-dimensional tight-binding electronic system when randomized impurities are present. We used the Matsubara Green function technique and computed the lowest-order non-vanishing Feynman diagrams to calculate the relaxation time caused by the impurity-electron scattering. To calculate the spin and charge conductivities, we have used the Kubo formalism. We observe that for all values of the Rashba and Dresselhaus strength, the longitudinal charge and spin conductivities along with relaxation time exhibit peaks when studied as a function of chemical potential. Also, the longitudinal spin and charge conductivities increases with an increase in RSOI, but when along with RSOI, DSOI is also present, we observe a decrease in longitudinal

spin conductivity and an increase in longitudinal charge conductivity. Furthermore, the spin conductivity is zero whenever Rashba and Dresselhaus strengths become equal. Finally, we have shown that longitudinal spin to charge conductivity ratio with Rashba strength decreases till RSOI strength becomes equal to the DSOI strength. After this, it increases with the increase in Rashba strength

3.5 Reference

- 1.G. Dresselhaus, Phys. Rev. 100, 580 (1955).
- 2.E I Rashba Sov. Phys. Solid State 1, 368 (1959).
- 3. J. Shi, P Zhang, D. Xiao and Q. Niu, Phys. Rev. Lett **96**, 076604(2006).
- 4. H. Sharma, S. Sil, and A. Chatterjee, JMMM, **500**, 166329, (2020).
- 5. G. D. Mahan, Many Particle Physics (Plenum, New York) (1981).
- 6. J. Nitta, T. Akazaki, Hideaki Takayanagi, and T. Enoki, Phys. Rev. Lett. **78**, 1335 (2003).
- 7. S. D. Ganichev et al, cond-mat/0306521(2003).
- 8. V. Kulish, W. Liu and S. Manzhos, MRS Advances. 1 (2017).
- 9. N. A. Sinitsyn, E. M. Hankiewicz, W. Teizer, and J Sinova Phys. Rev. B 70, 081312 (2004)
- 10. J. B. Miller, et al, Phys. Rev. Lett. 90, 076807 (2003).

CHAPTER 4

Torque-dependent Spin-Hall conductivity and Hall angle in presence of Rashba and Dresselhaus spin-orbit interactions and static random disorder for a two-dimensional tight-binding system

4.1 Introduction

Chapters 2 and 3 are concerned with spin and charge transport in the presence of Dresselhaus and Rashba spin-orbit couplings and static random disorder. Were we observed that for all Rashba and Dresselhaus strength values, the longitudinal charge and spin conductivity and relaxation time display peaks with chemical potential. Also, longitudinal spin and charge conductivity increases with an increase in RSOI, but when along with RSOI, DSOI is present longitudinal spin conductivity decreases while longitudinal charge conductivity increases. Furthermore, whenever Rashba and Dresselhaus strengths become equal longitudinal spin conductivity becomes zero. We have also studied the longitudinal spin to charge conductivity ratio has higher value whenever Rashba is much larger than Dresselhaus.

In the present chapter, we shall explore the effect of spin-orbit coupling (SOI) and impurity on the torque-dependent spin-Hall conductivity (SHC) at zero temperature. And studied the effect of SOI on the spin-Hall angle. We shall employ the Feynman diagrammatic technique and the Kubo formalism.

4.2 Formalism

The term responsible for longitudinal charge conductivity (LCC) is given by (3.39) and (3.40) and

$$\sigma_{xx}^{c} = -\frac{\hbar}{N} \sum_{k} \int d\epsilon \left\{ \frac{\partial n_{F}(\epsilon)}{\partial \epsilon} \right\} \left[f_{1}^{x^{2}}(k) A^{1}(k,\epsilon)^{2} + f_{2}^{x^{2}}(k) A^{2}(k,\epsilon)^{2} + 2f_{3}^{x^{2}} A^{1}(k,\epsilon) A^{2}(k,\epsilon) \right], \tag{4.1}$$

In the low-impurity and low-temperature regime, the spectral functions can be written as

$$\left(A^{1,2}(k,\epsilon)\right)^2 = (4\pi/\hbar)\tau\delta(\mu - \epsilon_{k_{1,2}}). \tag{4.2}$$

Using Eq. (4.2) in Eq. (4.1), the expression for longitudinal CC reduces to

$$\sigma_{xx}^{c} = \frac{4\pi e^{2}\tau}{\hbar\tau_{0}kT'} \iint_{-\pi}^{\pi} dk_{x} dk_{y} \sum_{i=1,2} \left((f'_{i,x}(k_{x}, y_{i}))^{2} \right.$$

$$\times \exp\left((\epsilon'_{i,k} - \mu')/kT' \right) / kT' \left(1 + \exp\left((\epsilon'_{i,k} - \mu')/kT' \right) \right)^{2}$$

$$(4.3)$$

Similarly, using the Kubo formalism, we obtain the spin Hall conductivity (SHC) as

$$\sigma_{xy}^{s_z} = -\frac{1}{\pi} \sum \frac{Im[\langle |J_x^{s_z}| \rangle \langle |J_y^c| \rangle]}{(\epsilon_{1,k} - \epsilon_{2,k})^2 + (\frac{1}{\tau})^2} (f_F(\epsilon_{1,k}) - f_F(\epsilon_{2,k}))$$
(4.4)

where $J_x^{s_z}$ and J_y^c are the x and y-components of the longitudinal spin and charge currents. Using the expressions for $J_x^{s_z}$, J_y^c and τ from Eqns. (3.18), (3.30) and (3.34), in Eqns. (4.4), we get the final expression for SHC as

$$\sigma_{xy}^{s_{z}} = \frac{(\alpha'_{R}^{2} - \beta'_{D}^{2})}{\pi} \times \iint_{0}^{\pi} dk_{x} dk_{y} \frac{(f_{E}(\epsilon_{1,k}) - f_{E}(\epsilon_{2,k})) \cos k_{y} \sin^{2}k_{x}}{((|\zeta'(\mathbf{k})|)^{2} + (\tau_{0}/\tau)^{2})(|\zeta'(\mathbf{k})|)}, \quad (4.5)$$

where $f_E(\epsilon_{1,2,k})$ is the Fermi level, which at zero temperature is given by;

$$f_E(\epsilon_{1,k}) - f_E(\epsilon_{2,k}) = \text{heaviside}(\epsilon_{1,k} - \mu) - \text{heaviside}(\epsilon_{2,k} - \mu)$$
 (4.6)

4.3 Results

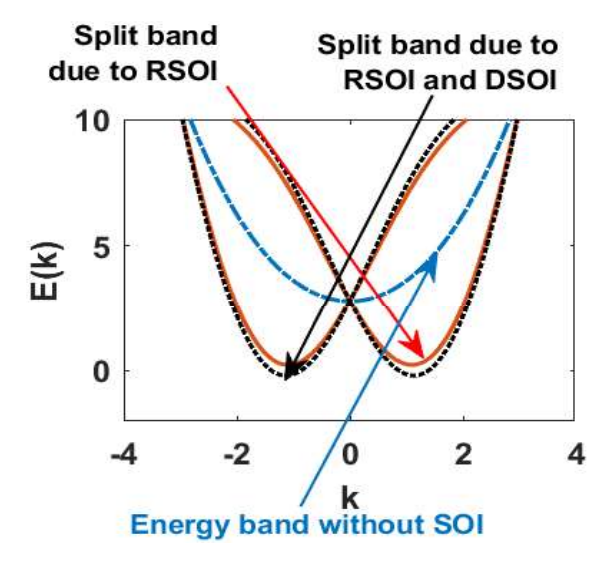


Fig. 4.1 Energy dispersion along the x-direction in k space.

Spin-Hall conductivity at zero temperature is given by Eqn. (4.5), which we have computed numerically to investigate the nature of SHC with different parameters. As earlier, here also we measure all energies in the unit of the hopping parameter. Fig 4.1 shows the energy dispersion in the k_x direction with and without spinorbit interaction (SOI). When SOI is present, spin degeneracy is lifted, and we have two different bands for up and down-spin electrons. Fig 4.2, illustrates the effect of renormalization and splitting where SHC is plotted with chemical potential μ . SHC remains zero up to a certain (small) value of the chemical potential and as the chemical potential increases beyond this value, SHC increases rapidly and attains a peak. This peak shows the availability of conducting states, which decreases with a further increase in μ leading to a decrease in SHC. In the presence of the DSOI effect, the conducting bands become deeper and narrower (Fig 4.1) and have fewer conducting states available, causing a decrease in SHC (Fig 4.2(a)). Also, as the Electron -impurity interaction strength v increases, SHC decreases (Fig 4.2(b)) which is an expected behaviour. When plotted with respect to α_R (Fig 4.3), the nature of SHC remains more or less qualitatively the same as it is with respect to μ .

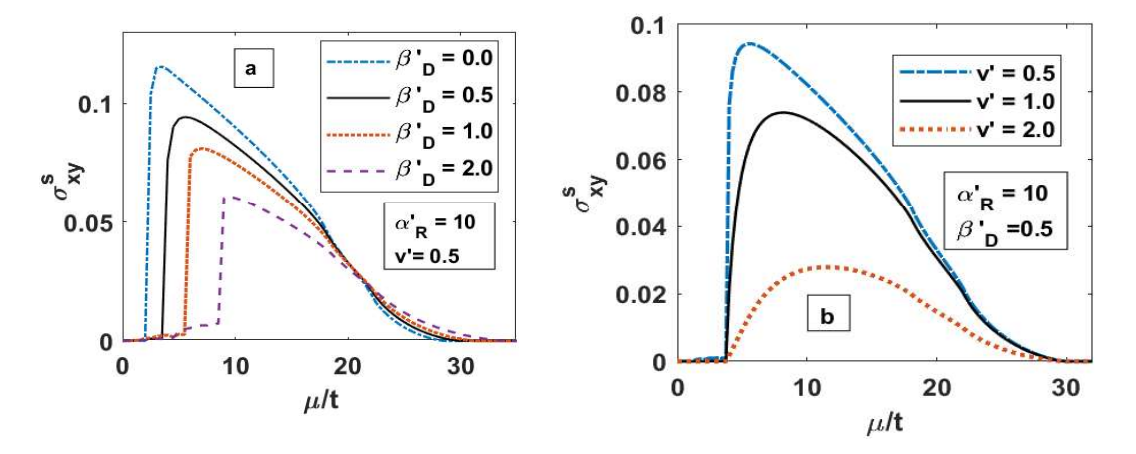


Fig. 4.2 Spin-Hall Conductivity versus Chemical potential μ for various values of: (a) β_D ; (b) v.

SHC remains small up to a particular value of α_R , after which, SHC increases and develops a peak. This peak predicts the maximum value for spin-Hall conductivity. With further increase in RSOI strength, peaks start decreasing and attain a constant minimum value. This is because, with an increase in RSOI strength, bands get broader and shifts lower Fig (4.1) creating a lower charge concentration near the Fermi level. This reduction in charge concentration becomes more when we include DSOI, as it causes additional broadening in bands. Also, whenever α_R and β_D become equal, SHC becomes zero.

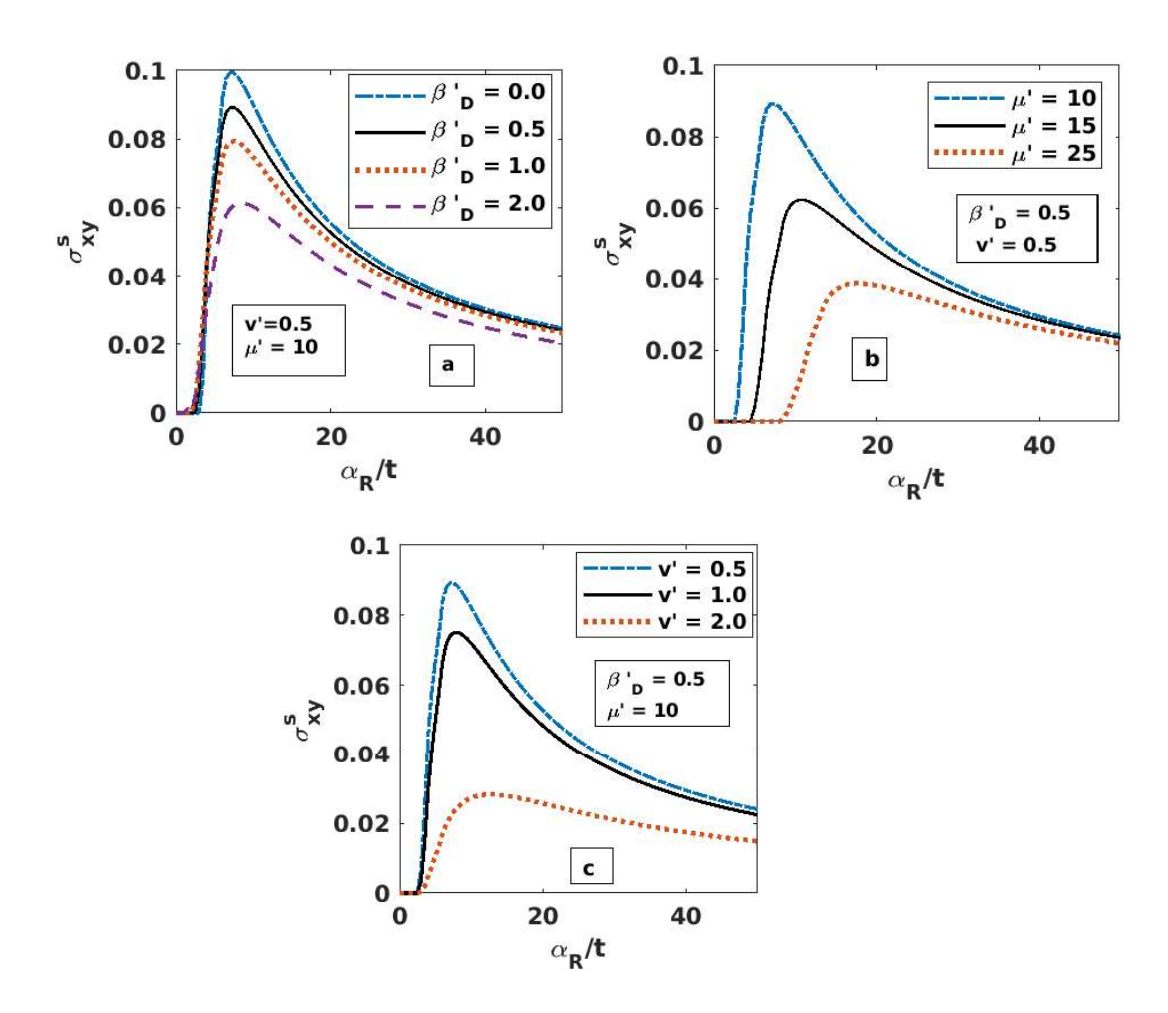


Fig. 4.3 SHC versus α_R for various: (a) β_D ; (b) μ ; (c) v values.

Fig. 4.3 (b) shows that with α_R , SHC decreases with an increase in μ , if μ lies in a certain range. This nature can be easily understood from Fig 4.2(a). Again we can observe from Fig. 4.3(c) that SHC decreases with an increase in v.

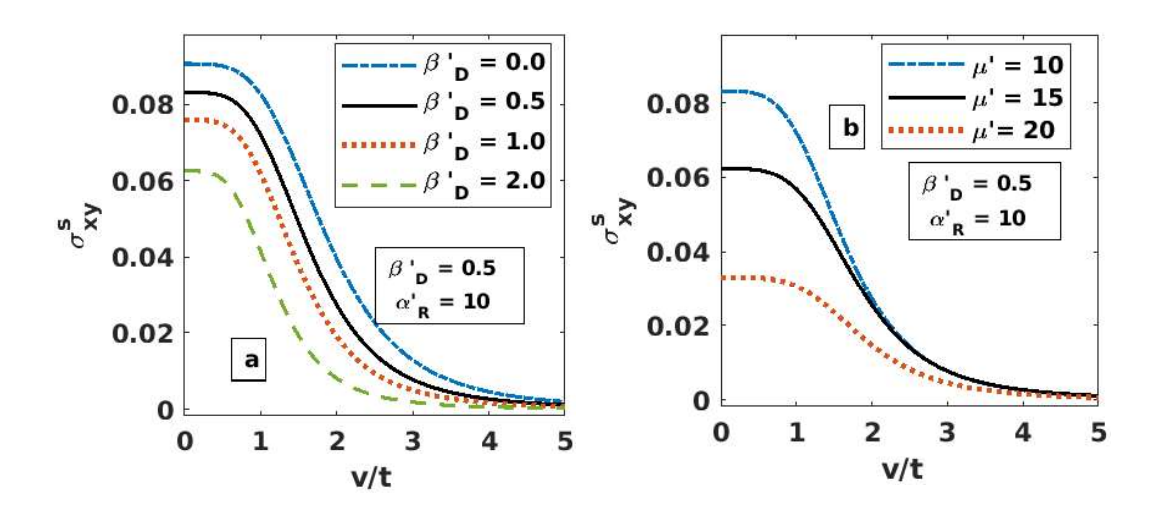


Fig. 4.4 SHC versus v for various values of: (a) β_D ; (b) μ .

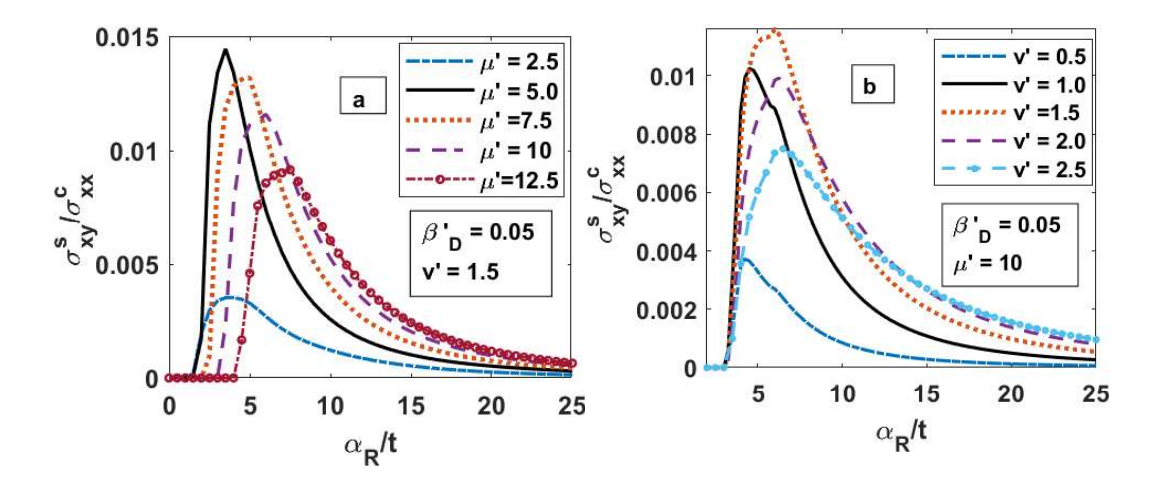


Fig. 4.5 SHC/LCC versus α_R for various values of: (a) μ ; (c) v.

In Fig 4.4, a plot of SHC with impurity strength v is given for different parameters. SHC remains unaffected when v is small. With the increase in impurity strength, scattering events increase, and we observe a decrease in SHC.

SHC also decreases when we increase the DSOI strength and the chemical potential.

Finally, we calculate the spin-Hall angle (SHA), which is described by the ratio of the spin-Hall conductivity to longitudinal charge conductivity. In Fig 4.5 (a), SHA is plotted with α_R for several μ values. SHA has a peak at some value of μ . Also, SHC remains essentially zero at low values of α_R . The peak height however depends on μ and ν .

In Fig 4.6, we present the three-dimensional and contour plots for the spin to charge conductivity ratio with respect to α_R and β_D . As expected, when α_R and β_D are small, the ratio SHC/LCC is almost zero. As we increase α_R keeping β_D constant, a

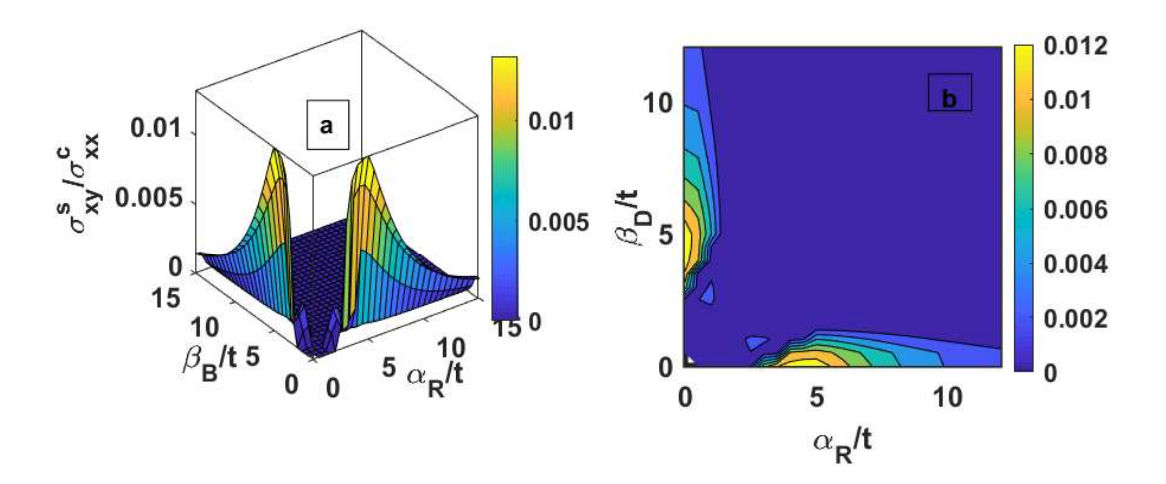


Fig. 4.6 (a) Three-dimensional plot of [LSC/LCC] in $(\alpha_R - \beta_D)$ -plane. (b). Contour plot of ratio of [LSC/LCC] in $(\alpha_R - \beta_D)$ -plane.

peak can be observed at some critical value. Afterwords the ratio decreases. A similar situation appears if β_D is increased, keeping α_R constant. When both α_R and β_D are increased simultaneously at an equal rate, the ratio remains zero, and as one is made more significant than the other, we observe a finite value for

SC/CC. Using the values of α_R , β_D and μ from previous chapters we find that the value of the SHC/LCC ratio can be in the range : 0.001-0.01 which, of course, has to be experimentally verified.

4.3 Conclusion

In this chapter, we have calculated spin-Hall conductivity and spin-Hall angle using the Kubo formalism and have examined their dependence on some of the system parameters. We observe that the spin-Hall conductance shows peak structure when studied with chemical potential, and the values of these peaks decrease with increasing DSOI strength, as DSOI broadens the energy bands. A similar observation has been seen when SHC is investigated as a function of RSOI.

We have also shown that in the presence of both SOI effects, SHC almost remains unaffected at low impurity strength and decreases when the impurity strength is high. Also, SHC increases with the increase in the difference between the RSOI and DSOI strength.

Finally, we have calculated longitudinal spin to charge conductivity ratio. We have shown that if any one of the SOIs (RSOI or DSOI) dominates, this ratio increases, and as the two SOI couplings become equal in strength, the ratio goes to zero.

CHAPTER 5

Torque-dependent Spin-Hall conductivity and Hall angle in presence of Rashba and Dresselhaus spin-orbit interactions and static random disorder for a two-dimensional tight-binding system at finite temperature

5.1 Introduction

So far, we have focused our attention on zero temperature calculation. However, experiments are performed mainly at finite temperatures. So to make contact with reality, we shall study in the present chapter longitudinal and transverse spin and charge conductivities at finite temperatures. We shall also be interested in studying the effect of SOI interactions on spin hall angle at finite temperature, which is defined as the ratio of spin hall conductivity to longitudinal charge conductivity (at finite temperature).

5.2 Formalism

To calculate the longitudinal and transverse charge and spin conductivity at finite temperature, we start from the definition of charge current in the x and y directions given by J_x^c (Eq. (3.29)) and J_y^c (Eq. (3.30)) and the spin current in the x-direction given by $J_x^{s_z}$ (Eq. (3.18)).

$$J_x^c = e/\hbar \sum_{k} \left(f_1^x(\mathbf{k}) \alpha_{1,k}^{\dagger} \alpha_{1,k} + f_2^x(\mathbf{k}) \alpha_{2,k}^{\dagger} \alpha_{2,k} + f_3^x(\mathbf{k}) \alpha_{1,k}^{\dagger} \alpha_{2,k} + f_3^x(\mathbf{k}) \alpha_{1,k}^{\dagger} \alpha_{2,k} \right)$$

$$+ f_3^{*x}(\mathbf{k}) \alpha_{1,k}^{\dagger} \alpha_{2,k} , \qquad (5.1)$$

$$J_{y}^{c} = e/\hbar \sum_{k} \left(f_{1}^{y}(\mathbf{k}) \alpha_{1,k}^{\dagger} \alpha_{1,k} + f_{2}^{y}(\mathbf{k}) \alpha_{2,k}^{\dagger} \alpha_{2,k} + f_{3}^{y}(\mathbf{k}) \alpha_{1,k}^{\dagger} \alpha_{2,k} + f_{3}^{y}(\mathbf{k}) \alpha_{1,k}^{\dagger} \alpha_{2,k} \right)$$

$$+ f_{3}^{*y}(\mathbf{k}) \alpha_{1,k}^{\dagger} \alpha_{2,k} , \qquad (5.2)$$

$$J_{x}^{s_{z}} = 2t \sum_{\mathbf{k}_{x}, \mathbf{k}_{y}} \sin \mathbf{k}_{x} c_{\mathbf{k}_{x}, \mathbf{k}_{y}}^{\dagger} \sigma_{z} c_{\mathbf{k}_{x}, \mathbf{k}_{y}}$$

$$+ 2 \sum_{k_{x}, k_{y}} \frac{2[\beta_{D}^{2} - \alpha_{R}^{2}] \cos k_{x} \sin^{2} k_{y} p_{k_{x} k_{y}}^{*}}{\left(\alpha_{R} \sin k_{y} + \beta_{D} \sin k_{x}\right)^{2} + \left(\alpha_{R} \sin k_{x} + \beta_{D} \sin k_{y}\right)^{2}}$$

$$\times \alpha_{k}^{\dagger} \begin{bmatrix} (\beta_{D} - i\alpha_{R}) p_{k_{x}, k_{y}}^{*} & (\beta_{D} + i\alpha_{R}) p_{k_{x}, k_{y}}^{2} \\ -(\beta_{D} - i\alpha_{R}) p_{k_{x}, k_{y}}^{*} & (\beta_{D} + i\alpha_{R}) p_{k_{x}, k_{y}}^{*} \end{bmatrix} \alpha_{k}$$
(5.3)

where the values of $f_i^x(\mathbf{k})$ and $f_i^y(\mathbf{k})$ are given in Eqns. (3.28, 3.30). Using the Kubo formalism as described in the earlier chapters, the expressions for LCC, LSC and SHC at finite temperature are given by

 σ_{xx}^c

$$= \frac{4\pi e^{2}\tau}{N\hbar\tau_{0}kT'} \iint_{-\pi}^{\pi} dk_{x}dk_{y} \sum_{i=1,2} \left((f'_{i,x}(k_{x}, y_{i}))^{2} \exp\left((\epsilon'_{i,k} - \mu')/kT' \right) / kT' \left(1 + \exp\left((\epsilon'_{i,k} - \mu')/kT' \right) \right)^{2} \right), \tag{5.4}$$

$$\sigma_{xx}^{s_{z}} = \frac{4\pi e \tau}{N \tau_{0} k T'} \iint_{-\pi}^{\pi} dk_{x} dk_{y} \sum_{i=1,2} (f'_{i,x}(k_{x}, y_{i}) g'_{x}(k_{x}, y_{i}) \exp((\epsilon'_{i,k} - \mu')/kT'))^{2}.$$

$$(5.5)$$

$$\sigma_{xy}^{s_{z}} = \frac{e(\alpha'_{R}^{2} - \beta'_{D}^{2})}{\pi} \int_{-\pi}^{\pi} dk_{x} dk_{y} \frac{\left(f_{E}(\epsilon_{1,k}) - f_{E}(\epsilon_{2,k})\right) \cos k_{y} \sin^{2}k_{x}}{\left(\left(\epsilon_{1,k} - \epsilon_{2,k}\right)^{2} + (\tau_{0}/\tau)^{2}\right) \left(|\zeta'(\mathbf{k})|\right)} (5.6)$$

where

$$g'^{x}(k_{x},k_{y}) = \frac{\left[2\hbar(\beta'_{D}^{2} - \alpha'_{R}^{2})^{2} \sin k_{x} \sin^{2}k_{y} \cos(k_{x})\right]}{|\zeta'(\mathbf{k})|^{3}},$$
(5.7)

$$\zeta(\mathbf{k}) = (\alpha_R \sin k_y + \beta_D \sin k_x) + i(\alpha_R \sin k_x + \beta_D \sin k_y)$$
 (5.8)

$$\zeta'(\mathbf{k}) = \zeta(\mathbf{k})/t. \tag{5.9}$$

5.3 Result and Discussion

5.3.1 Longitudinal Charge Conductivity (LCC)

We study the variation of the longitudinal charge conductivity (LCC) with respect to chemical potential μ in Fig 5.1. The zero-temperature behaviour is given in Fig. 5. 1(a). This has already been shown in Chapter 3. The temperature effect is shown in Fig. 5.1(b) where LCC is plotted with μ for various β_D values. One important difference at finite temperature is that now LCC has higher value as compared to zero temperature case when $\mu=0$. One can see that at small μ , LCC decreases with an increase in μ , and its value is essentially independent of DSOI and impurity strength. As μ increases further, LCC, in general, develops an inverted cusp-like structure or V-like and then with a further rise in μ , it develops a broad maximum, which is somewhat similar to T=0 case. For $\beta_D=0$, however, a sharp peak occurs in contrast to a broad maximum). Also, as β_D increases, the V-structure shifts to the right and also increases in depth. The broad maximum also shifts to the right with increasing β_D . Fig. 5.1(c) shows the LCC

versus μ plot for distinct temperature values. Initially as μ increases, LCC decreases up to a specific μ value which appears to be the same for all values of T. As μ is increased beyond that point, LCC increases and develops a broad maximum. The maximum of LCC shifts towards a lower value of μ as temperature rises. Generally, LCC varies with μ differently in different windows of μ at different values of temperature giving rise to numerous crossing behavior.

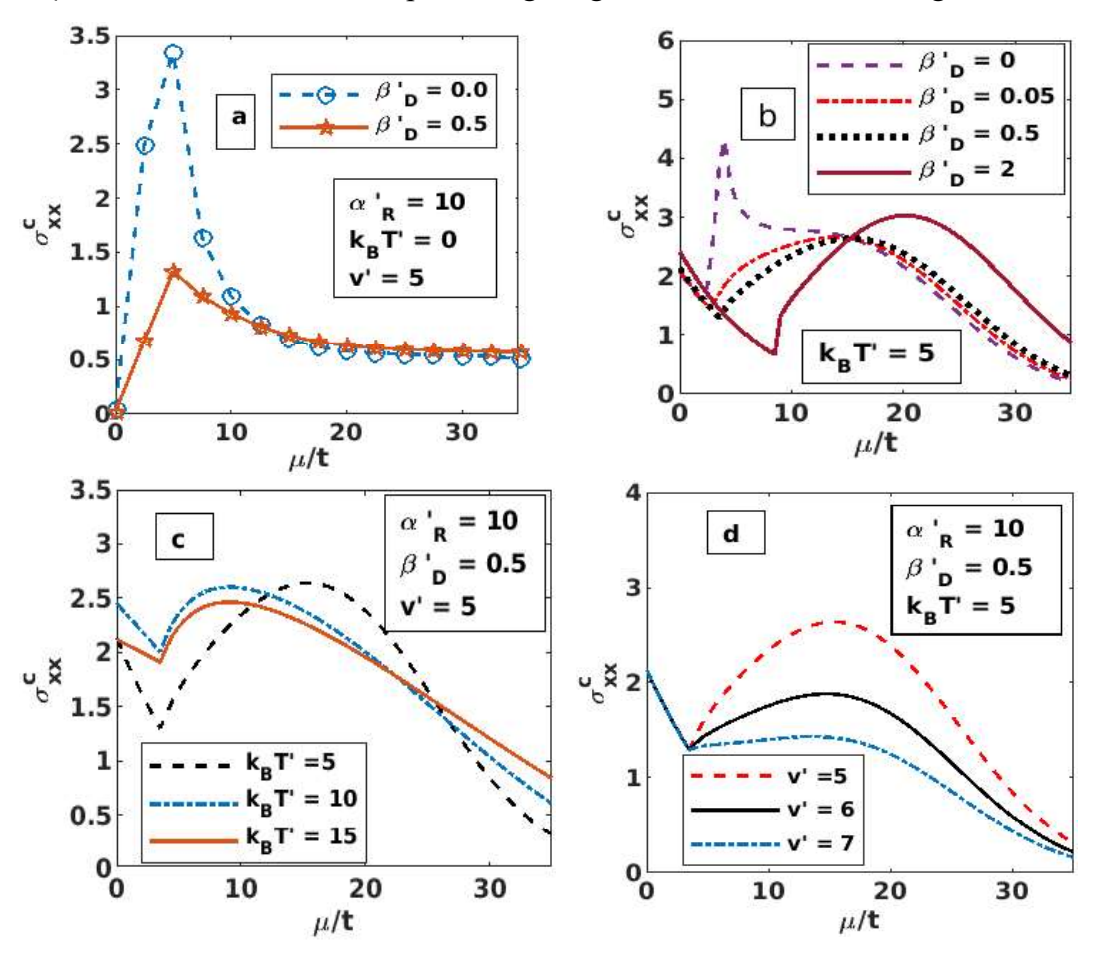


Fig. 5.1 Longitudinal Charge Conductivity (LCC) (σ_{xx}^c) versus Chemical potential μ for various values of : (a, b) DSOI coefficient β_D ; (c) k_BT ; (d) Impurity strength v.

In Fig 5.1(d), we show the plot of LCC with μ for three distinct values of the impurity-electron coupling strength v. Interestingly, up to a specific μ value, the V- structure of LCC remains independent of v. Beyond this μ , LCC decreases

with an increase in v. As the impurity coupling increases, the LCC peak decreases substantially and becomes broader.

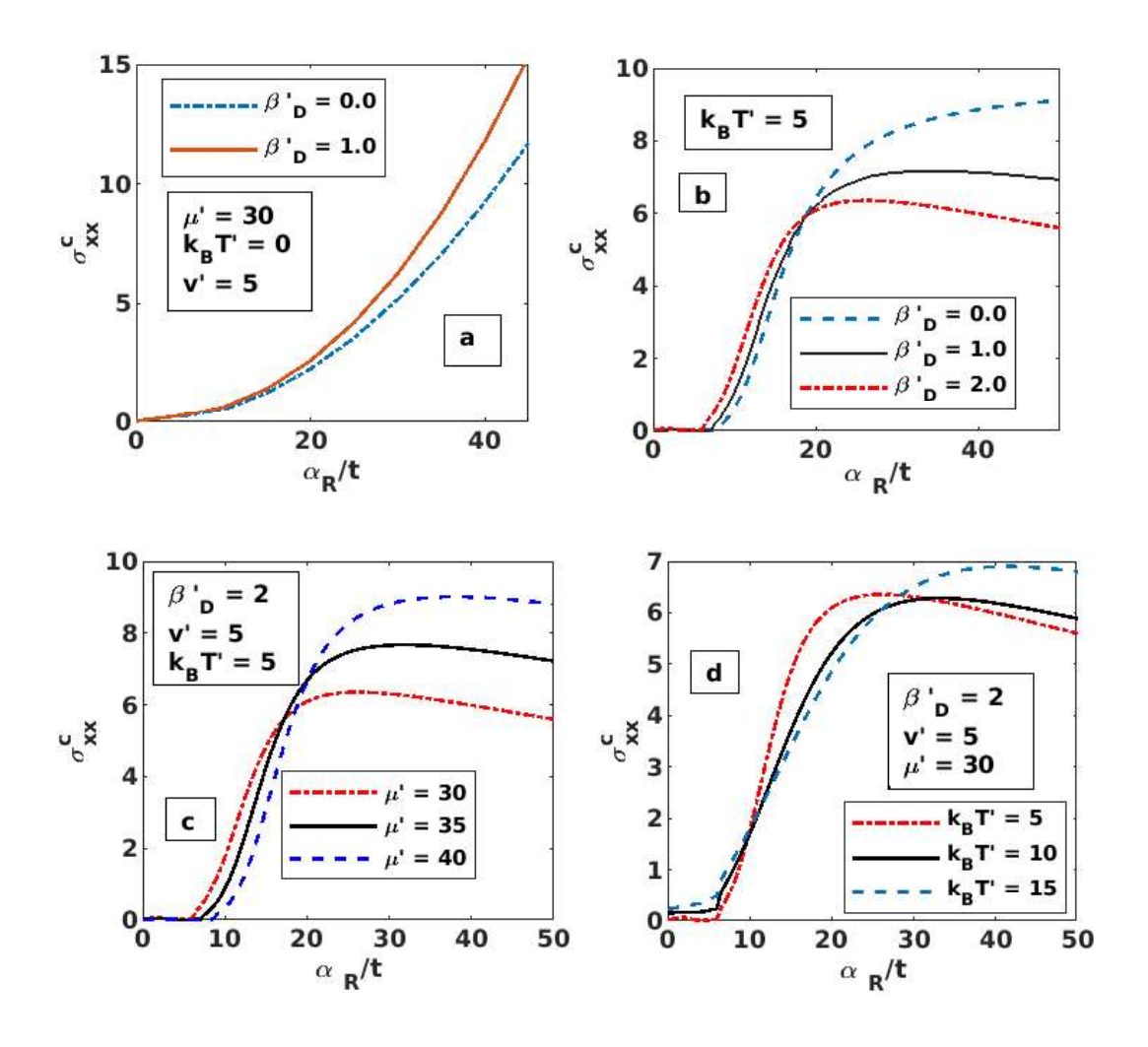


Fig. 5.2 LCC versus α_R for various : (a, b) β_D ; (c) μ ; (d) k_BT values.

Fig 5.2 describes the nature of LCC with RSOI strength α_R . In Fig 5.2(a), LCC is plotted with α_R for various β_D values at zero temperature for the sake of completeness. (We have already discussed this case in Chapters 2 and 3). Finite temperature plots are given in Fig 5.2(b). When α_R is small, LCC turns out to be zero and also remains independent of DSOI. As α_R is increased beyond a certain value, LCC starts increasing with the increase in α_R . In the case of $\beta_D = 0$, it

eventually shows a saturation effect, while in the presence of DSOI, it shows a down-turn behaviour. This down-turn effect increases with the increase in β_D . This can be understood as follows. With an increase in DSOI, the bulk inversion asymmetry increases which causes an increase in the scattering events leading to depletion in relaxation time and a consequent decrease in LCC. Fig. 5.2(c) shows LCC versus α_R plot for distinct μ value at $k_BT=5$. Again we see that for any value of μ , LCC remains zero up to a specific α_R value, after which as α_R increases, LCC increases rather rapidly. Beyond a certain value of α_R , LCC shows a slow decrease. As μ increases, we see a rise in LCC.

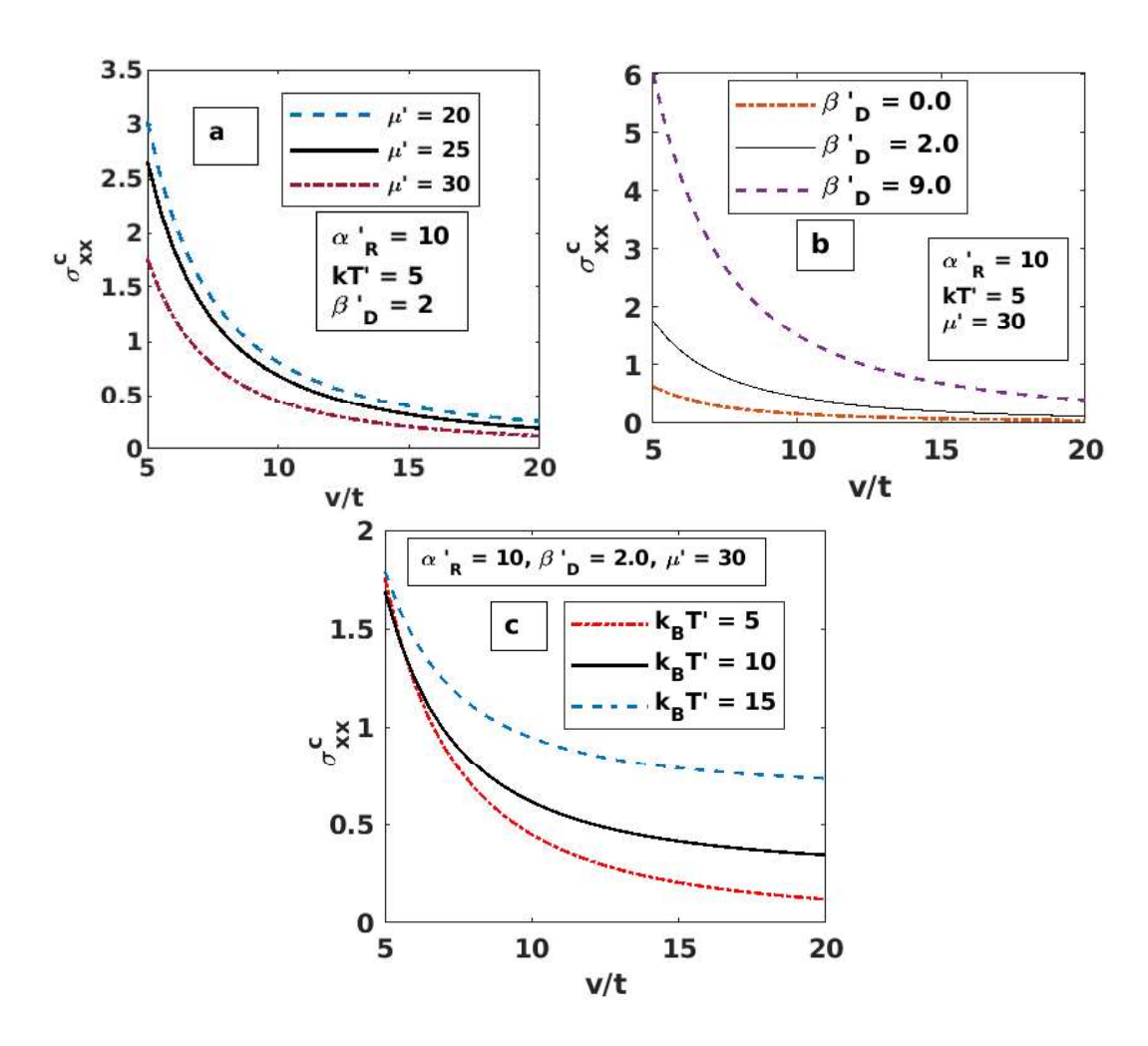


Fig. 5.3 LCC versus v for various values of: (a) μ ; (b) β_D ; (d) k_BT .

The behavior is quite complicated when LCC is plotted with α_R for various temperature values (Fig. 5.2(d)). In different windows of α_R , the the behaviour of LCC with α_R is different at different temperature. This gives rise to multiple crossing behavior. As α_R becomes large, LCC increases with an increase in temperature. In Fig 5.3, we plot LCC with respect to the electron-impurity interaction strength v. In general, LCC decreases quite rapidly as v increases. Fig 5.3(a) gives the nature for different μ values. Again we observe that the effect of chemical potential is more prominent for low impurity strength. A similar behaviour is observed when LCC is studied for different DSOI values (Fig 5.3(b)). The effect of DSOI is maximum when impurity strength is minimum. In Fig 5.3(c), LCC is plotted with v for various T values. We see that as T increases, LCC decreases at lower rate.

5.3.2 Longitudinal Spin Conductivity (LSC)

In Fig 5.4, the longitudinal spin conductivity (LSC) is plotted with respect to chemical potential μ . Figs. 5.4 (a) and (b) give the behavior for various of β_D value. In Fig 5.4(a), the results for T = 0 are plotted. A sharp peak structure is visible at $\beta_D = 0$. After the peak, LSC falls off to zero at some specific μ value. At a finite value of β_D , the qualitative behaviour is essentially the same but the peak height decreases, as explained in Chapter 2. Fig 5.4(b) describes the nature of LSC with respect to μ at finite temperature. One can see that in the absence of DSOI, LSC's behavior at nonzero T is significantly different from that at T = 0. LSC remains zero up to some specific value of μ and then develops a sharp peak. In addition to the sharp peak, LSC also exhibits a broad secondary maximum at a higher value of μ . In the presence of DSOI, both the first peak and the secondary maximum decrease in height and the secondary maximum shifts towards right. Above a certain value of β_D , the first peak changes into a shoulder and the secondary maximum becomes still shorter in height and shifts further towards

right. With further increase in β_D , the first peak completely disappears and LSC remains zero up to a larger value of μ and exhibits a broad maximum which is again right-shifted and shorter in height.

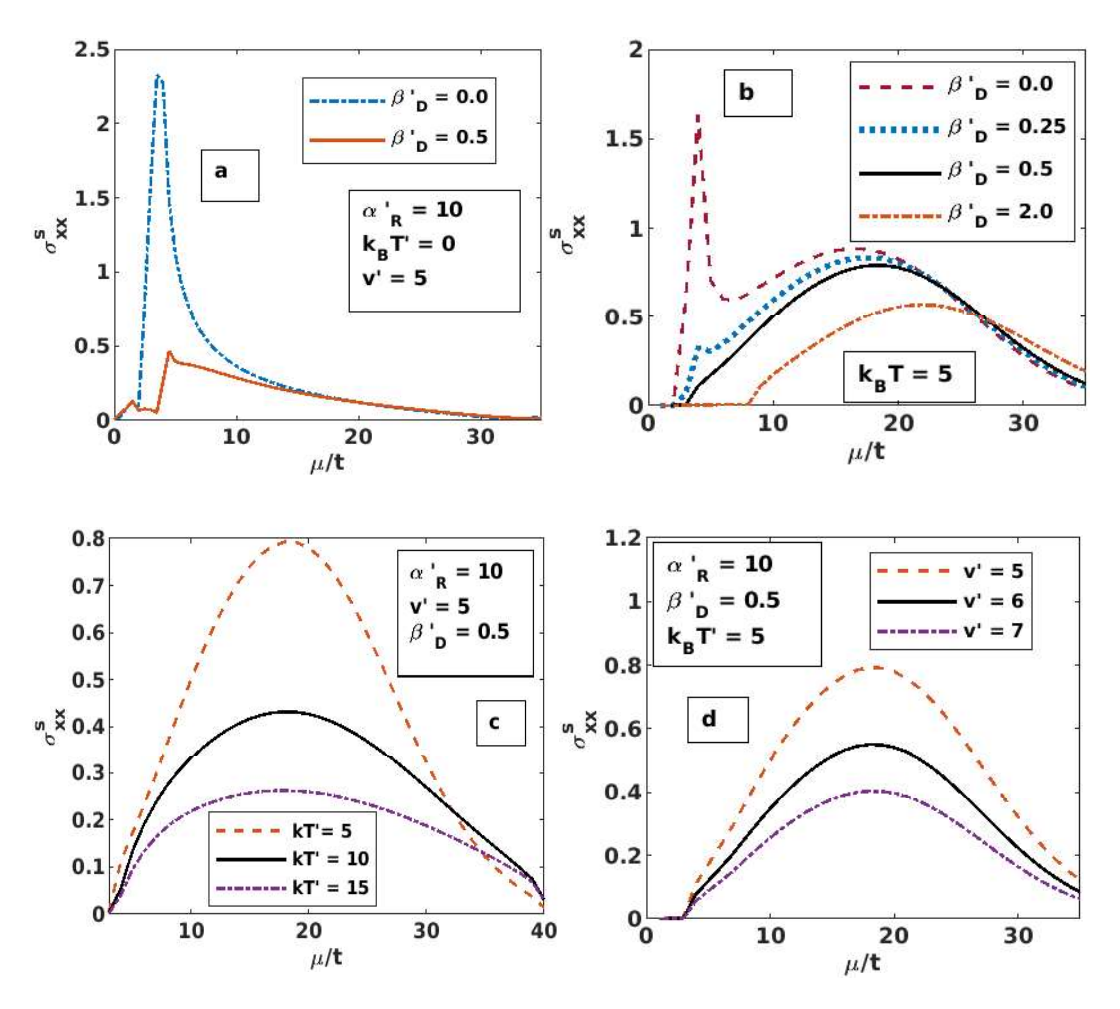


Fig. 5.4 LSC versus Chemical potential μ for various values of : (a, b) β_D ; (c) k_BT ; (d) v.

In Fig 5.4(c), LSC versus μ is plotted at different values of T for a fixed set of α_R and β_D such that only the secondary maximum occurs. One can see that as T increases, the peaks get broadened, and their heights decrease. Finally in Fig. 5.4(d), we plot LCC versus μ for various v value. The maximum structure is again visible and LSC is again found to decrease with increasing v.

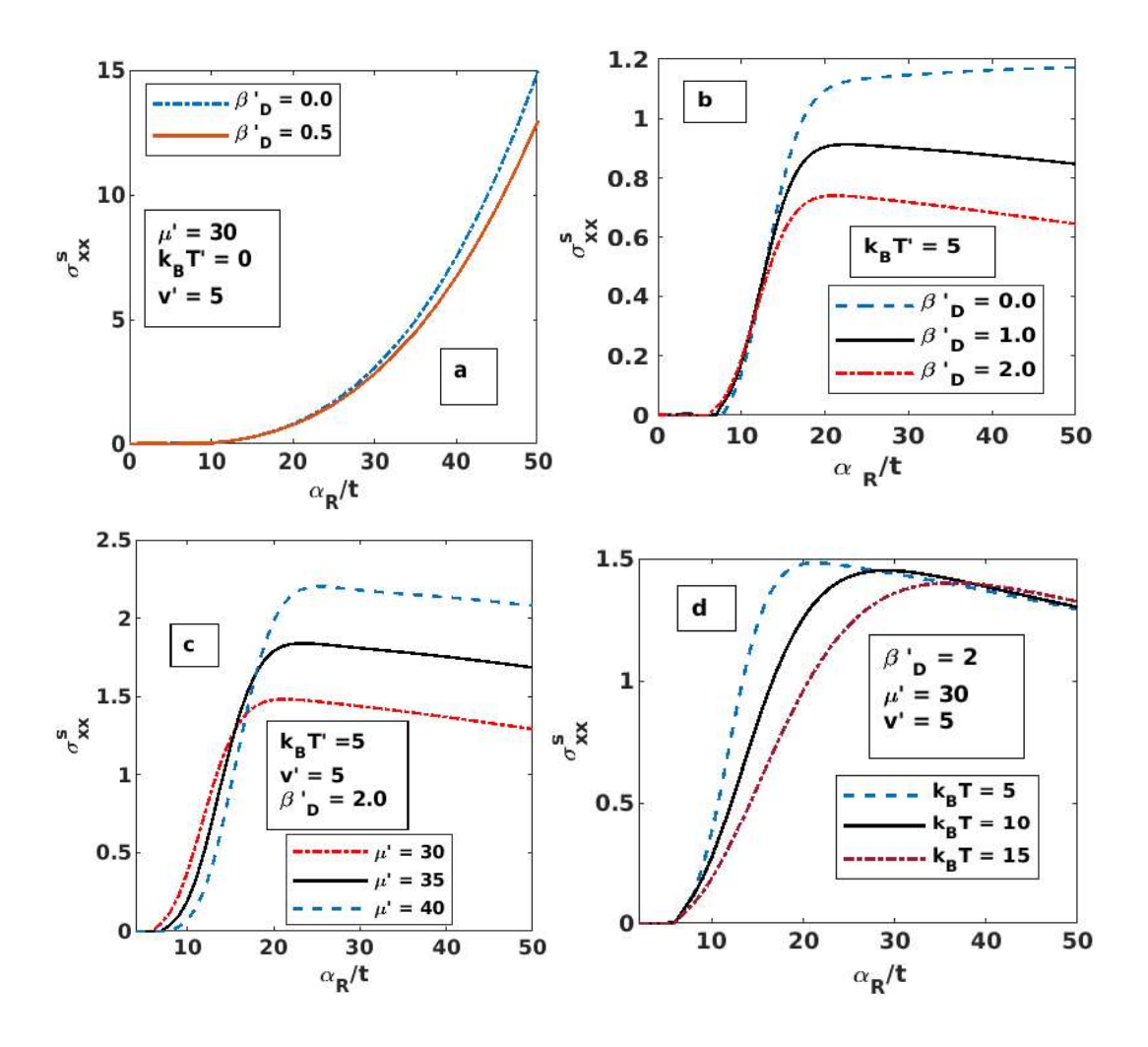


Fig. 5.5 LSC versus α_R for various : (a, b) β_D ; (c) μ ; (d) k_BT values.

In Fig 5.5, LSC is plotted with respect to α_R . In Fig 5.5(a) we show, for the sake of completeness, LSC's dependence on α_R for various value of β_D at T = 0 (which has already been studied in Chapters 2 and 3). Fig. 5.5(b) shows the data at finite temperature. At $T \neq 0$, and $\beta_D = 0$, LSC remains constant up to a critical value of α_R beyond which LSC increases monotonically up to a certain value of α_R after which LSC appears to saturate asymptotically for $\beta_D = 0$, while for $\beta_D \neq 0$, LSC shows a down-turn. This downturn behavior is more prominent for the higher values of β_D . Fig 5.5(c) show LSC with α_R plot for various μ values. The behaviour looks qualitatively more or less similar to LCC. Of course, the values

are much smaller than LCC. Fig 5.5(d) gives a plot of LSC versus α_R for various temperature values. Here we observe that only for an intermediate range of RSOI, LSC has significant temperature dependence.

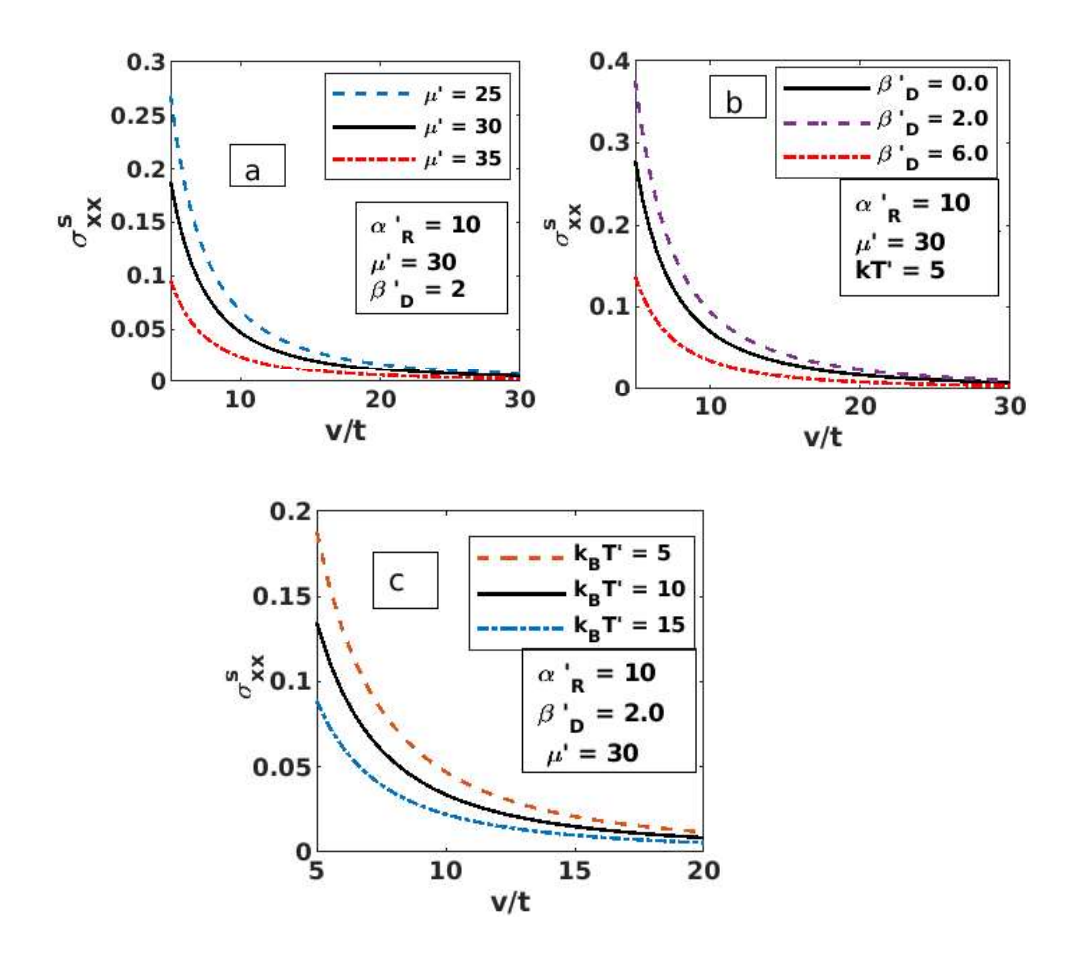


Fig. 5. 6 LSC versus v different values of: (a) μ ; (b) β_D ; (d) k_BT .

LSC is plotted with electron-impurity interaction strength v for various μ , β_D and k_BT values in Fig. 5.6. Fig. 5.6(a) shows that, in general, LSC decreases with increasing v and eventually appears to approach zero. LSC also decreases with increasing chemical potential (Fig. 5.6a) and temperature (Fig. 5.6c). LSC decreases when the difference between the RSOI and DSOI strengths decreases (Fig 5.6(b)).

5.3.3 Spin Hall Conductivity (SHC)

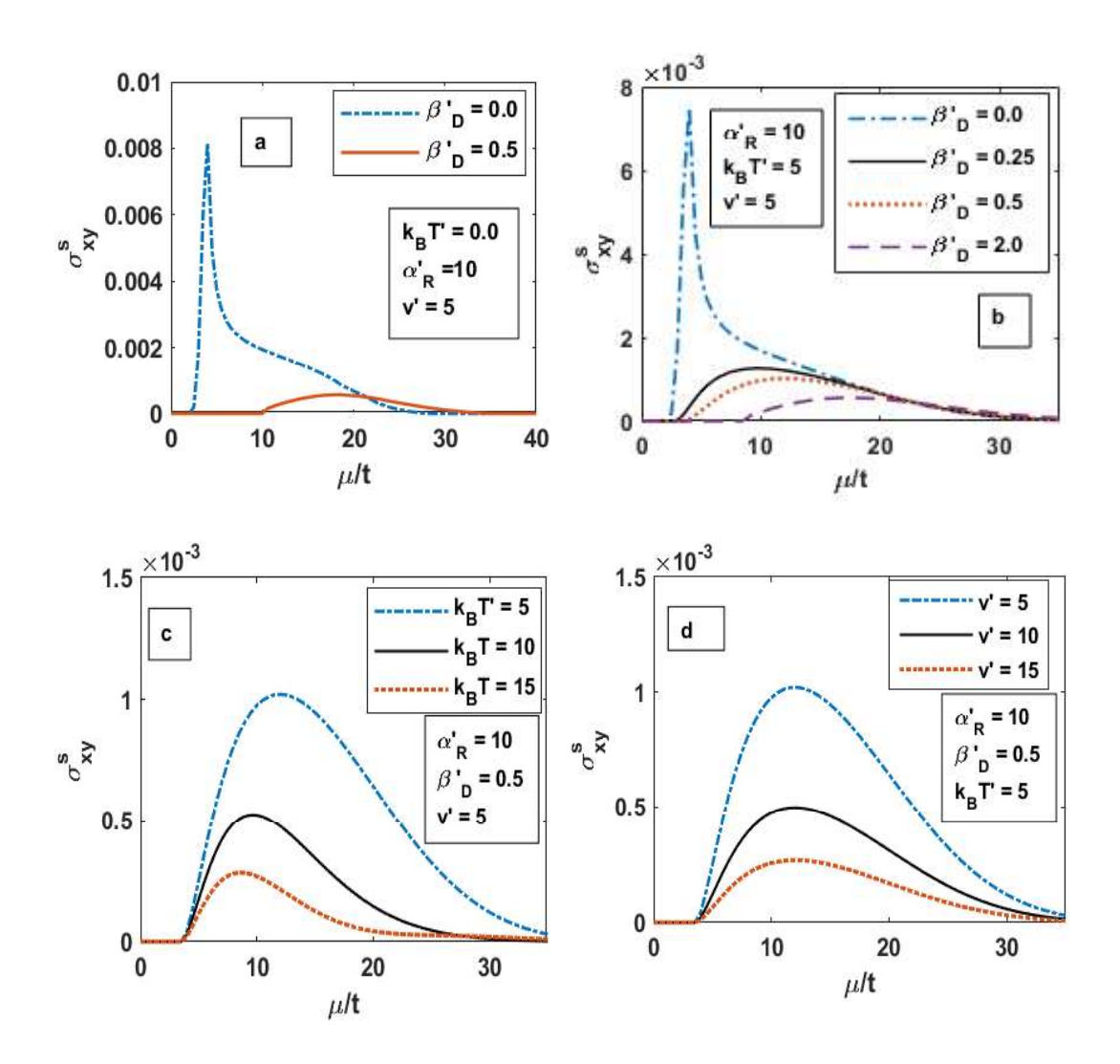


Fig. 5.7 SHC versus μ for various values of: (a, b) β_D ; (c) k_BT ; (d) v.

SHC is studied with chemical potential (μ) in Fig 5.7. Figs. 5.7(a, b) present the nature of SHC for various values of DSOI strength β_D . For T=0 and $\beta_D=0$, SHC exhibits peak structure similar to LCC and LSC. However, compared to LCC and LSC, the peak are much smaller and fall sharply when chemical potential is increased Fig 5.7(a). For finite DSOI strength, SHC is finite for a small chemical potential window. Fig 5.7(b) show the results for $T \neq 0$. When $\beta_D=0$, the plots are qualitatively similar to LSC for the lower value of chemical

potential. In general, the peak values of SHC are much smaller than those of LSC for the same parameter values.

In Fig 5.7(c) SHC vs chemical potential is plotted for various value of T. SHC has a similar behavior as of LSC. But the peak values are much smaller, and their height decreases much faster with increasing T. As plotted for different values of v, SHC exhibits similar behavior to LSC, except peak values that are smaller in magnitude than LSC Fig 5.7(d).

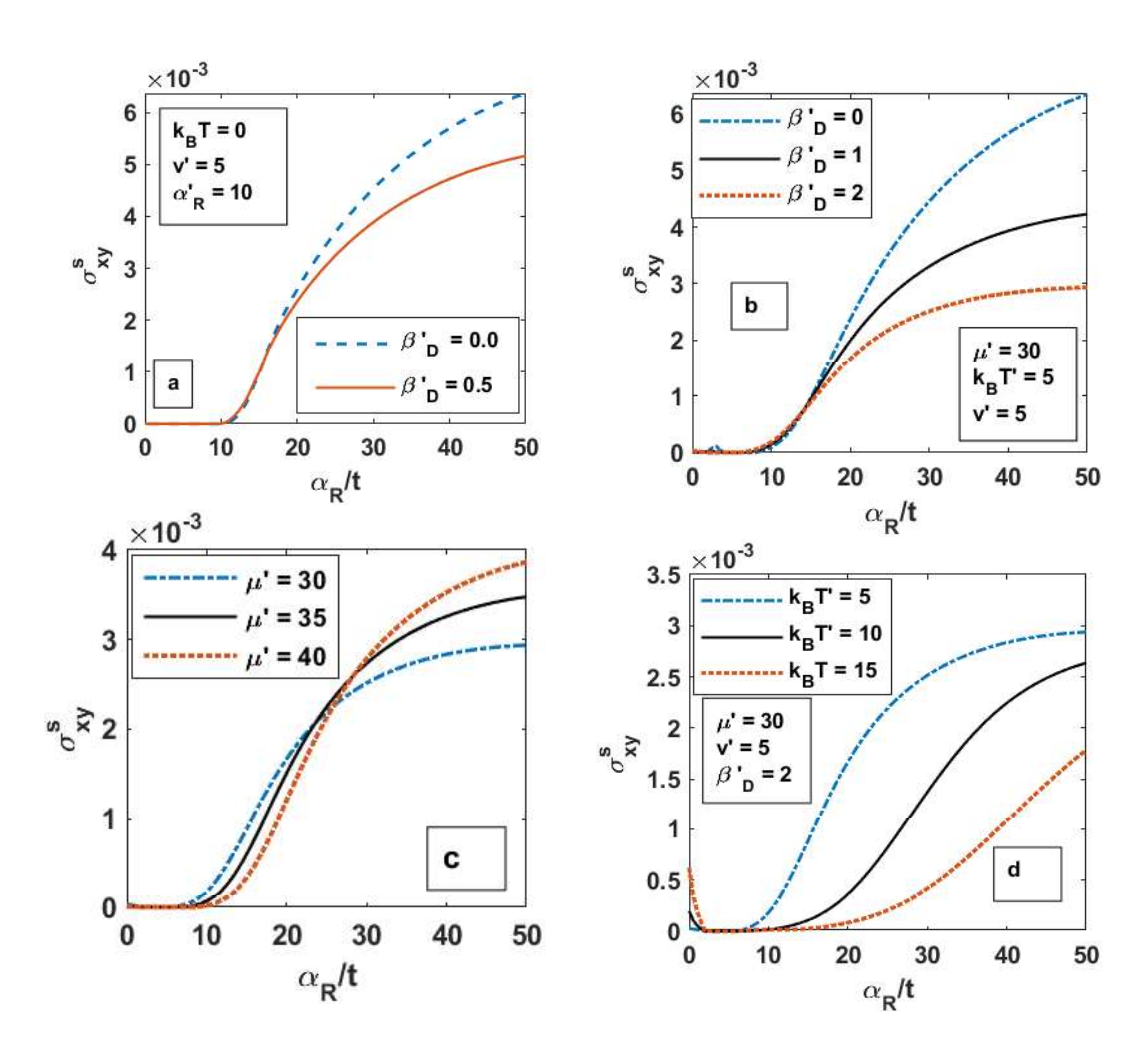


Fig. 5.8 SHC versus α_R for various(a, b) β_D ; (c) μ ; (d) k_BT values.

In Fig 5.8, we study spin-Hall conductivity (SHC) with RSOI strength α_R . Fig 5.8(a, b), shows SHC vs α_R plot for various β_D values. Fig 5.8(a) gives the nature of SHC at zero temperature. For weak RSOI, SHC almost remains zero irrespective of the value of β_D . As α_R increases, SHC also increases but, for α_R less than a certain value, SHC hardly depends on β_D . Beyond this value of α_R , the increase on SHC depends on β_D . In fact, for the same value of α_R , SHC decreases with the increase in β_D . As a function of α_R , SHC appears to saturate eventually.

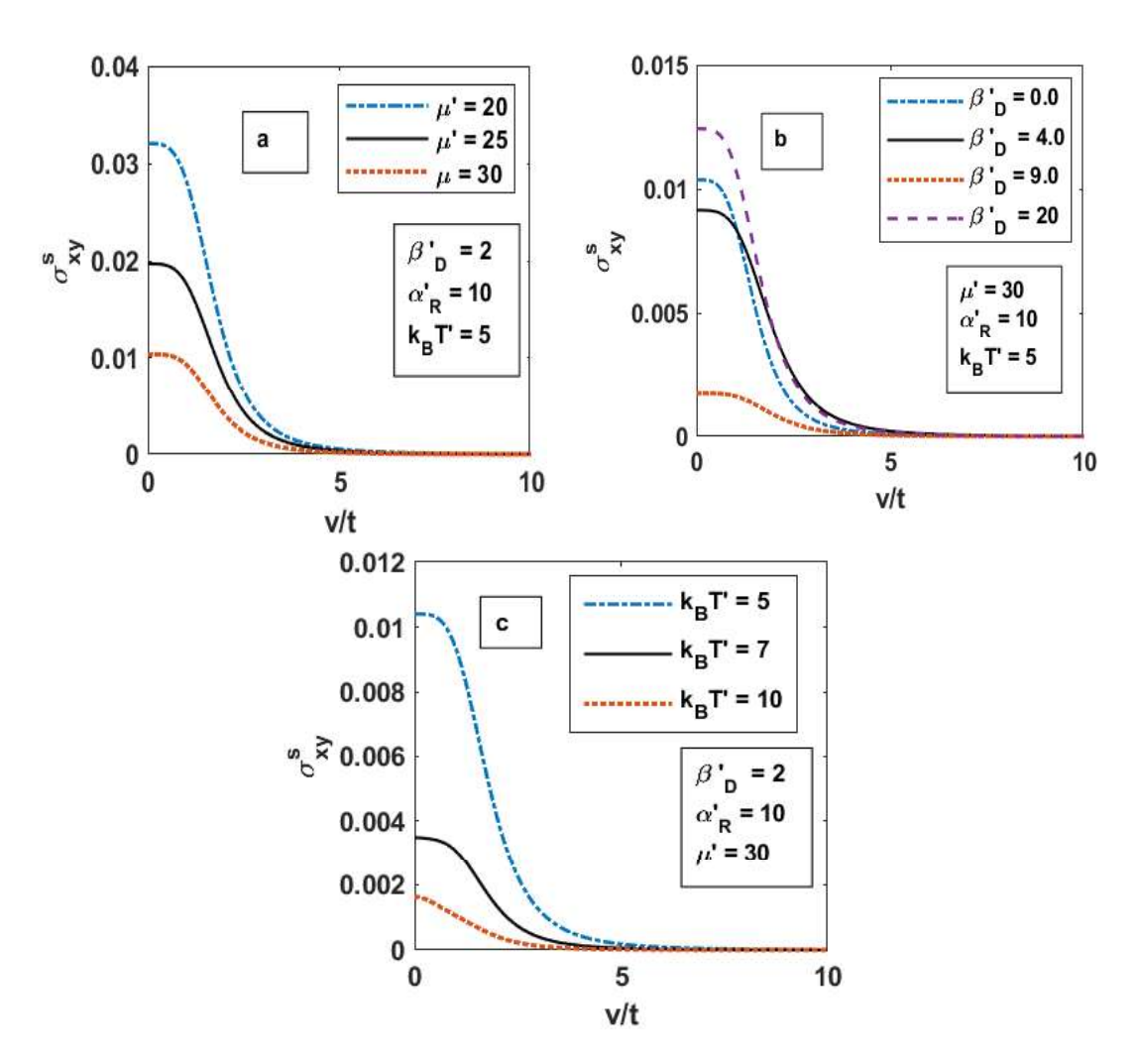


Fig. 5.9 SHC versus v for various: (a) μ ; (b) β_D ; (c) k_BT values.

Fig. 5.8(b) describes the behavior at non-zero temperature. The nature of SHC remains essentially the same at finite temperature. We observe that SHC saturates faster for higher values of β_D . Fig. 5.8(c) gives the results for various chemical potential μ value. The nature is a little similar to LSC and we see a crossing behaviour. Fig 5.8(d) shows the nature of SHC with α_R at different values of T. The temperature dependence of SHC vs. α_R curves looks stronger than that of the LSC vs. α_R curves increases, SHC also increases but, for α_R less than a certain value, SHC hardly depends on β_D . Beyond this value of α_R , the increase on SHC depends on β_D . In fact, for the same value of α_R , SHC decreases with the increase in β_D . As a function of α_R , SHC appears to saturate eventually. In Fig 5.9, we plot SHC with Impurity strength v for different system parameters. SHC exhibits a flat maximum around v= 0 and then falls off to zero much faster than LCC or LSC. SHC also decreases with increasing μ . When plotted for different values of DSOI, it shows a similar bahaviour as LSC

In Figs. 5.10 and 5.11, we present the three-dimensional and contour plots for the spin to charge conductivity ratio with respect to α_R and β_D . When α_R and β_D are both small, LCC becomes larger than both LSC and SHC and consequently the ratio SHC/LCC remains small. As we increase α_R , keeping β_D constant, the spin current increases much faster than the charge current; hence the ratio increases and shows a peak. The same happens when β_D is increased, keeping α_R constant. The ratio decreases as α_R approaches β_D and become zero, when α_R and β_D become equal. From experimental point of view, we can control RSOI strength up to 50% by tuning the gate field [5, 6] and therefore the ratio can be varied typically from 1.5 to 2.5 [7]. For Indium Arsenide, using the values of α_R , β_D and μ from previous chapters. we find that the value of the SHC/LCC ratio at finite temperature can be in the range : 0.001- 0.08, which has to be experimentally verified.

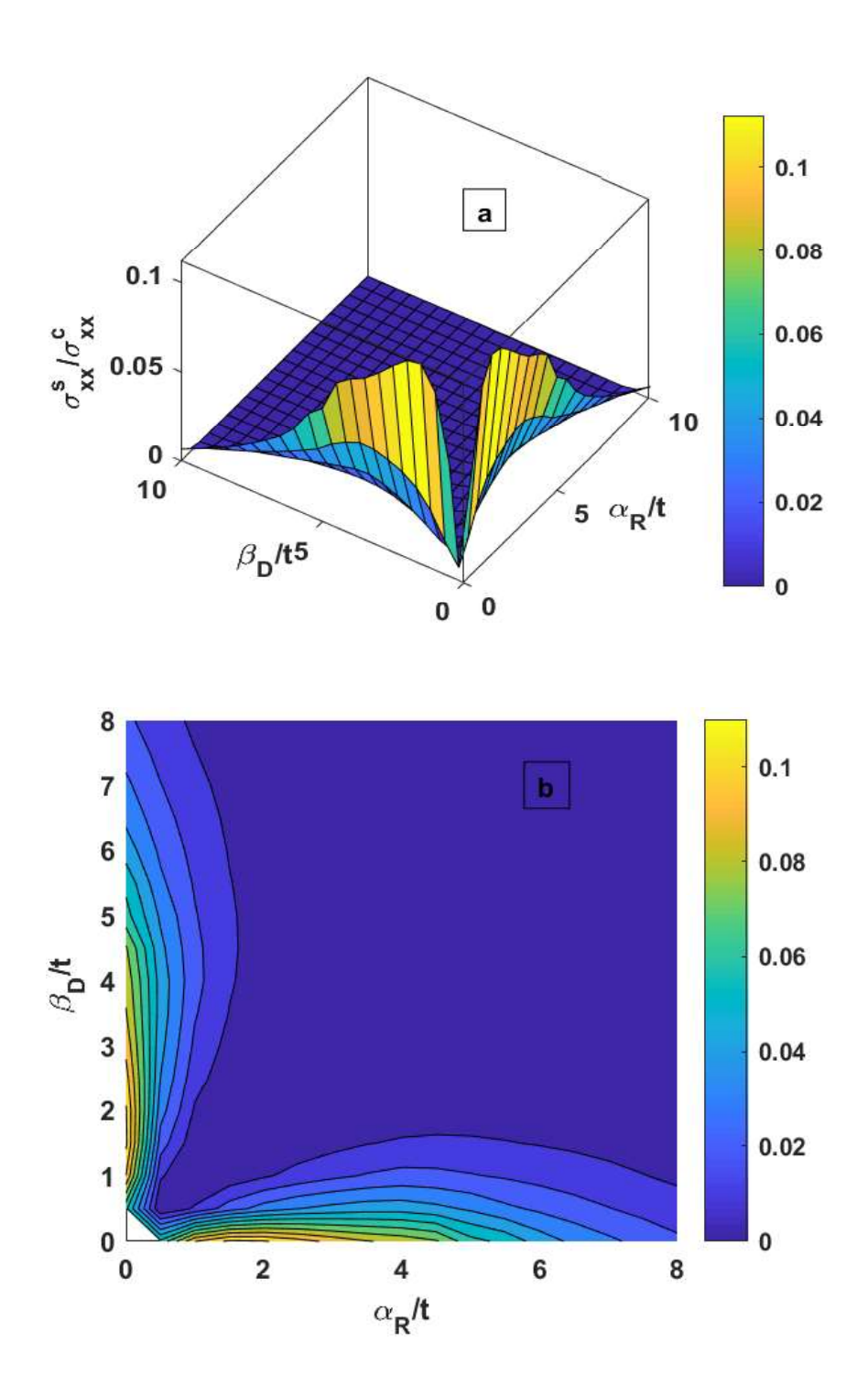


Fig. 5. 10 (a) Three-dimensional plot of [LSC/LCC] in $(\alpha_R - \beta_D)$ – plane; (b) Contour plot of [LSC/LCC] in $(\alpha_R - \beta_D)$ – plane .

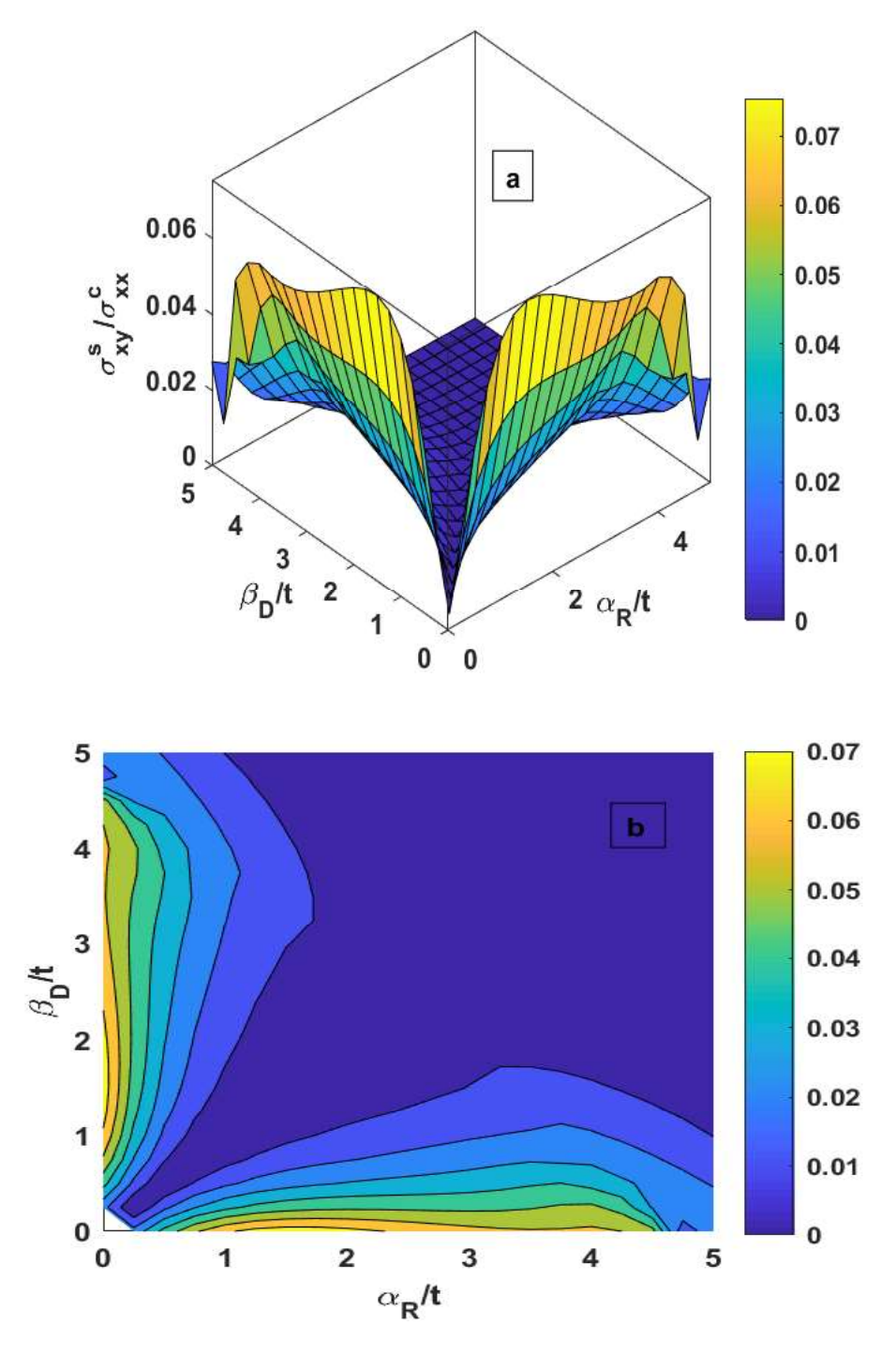


Figure. 5.11 (a) Three-dimensional plot of [SHC/LCC] versus RSOI and DSOI strengths; (b). Contour plot of [SHC/LCC] versus RSOI and DSOI strengths.

5.4 Conclusion

We have shown in this chapter that LCC, LSC, and SHC all display peak structure as a function of chemical potential. These peaks shift towards the larger value of chemical potential as DSOI strength increases and the peak height increases for LCC as DSOI strength increases and decreases for LSC and SHC. LSC and LCC increase monotonically with the RSOI strength at T = 0 K. However, at finite temperature, they seem to saturate to some constant value when the DSOI effect is absent. In the presence of DSOI, we see a downturn nature, i.e., conductivities start decreasing after a certain point. This downturn effect increases with rise in the DSOI strength. In SHC case, the downturn effect can be seen either in the presence or absence of T and DSOI. The conductivities in general decrease with increase in the electron-impurity interaction strength, though the rate of decrease is different for different conductivities. LCC and LSC decrease rapidly, while SHC remains essentially same at low impurity strength and decrease rapidly when impurity strength increases. Finally, we have calculated the spin to charge conductivity ratio and have shown that the ratio increases when the difference between the Rashba and Dresselhaus strength increases. We have also shown that the ratio is zero whenever Rashba strength becomes equal to Dresselhaus strength.

5.5 References.

- 1. H. Sharma, S. Sil, and A. Chatterjee, JMMM, **500**, 166329, (2020).
- 2. H. Sharma, S. Sil, and A. Chatterjee, JMMM, **529**, 167711, (2021).
- 3. E. I. Rashba, Phys. Rev. B **68** 241315 (R) (2003).
- 4. G. Dresselhaus, Phys. Rev. 100, 580 (1955).
- 5. J. B. Miller, et al, Phys. Rev. Lett. 90, 076807 (2003).
- 6. J. Nitta, T. Akazaki, Hideaki Takayanagi, and T. Enoki, Phys. Rev. Lett. **78**, 1335 (2003).
- 7. S. D. Ganichev et al, cond-mat/0306521(2003).

CHAPTER 6

Magneto-transport through a Quantum Dot Dimer in presence of quantum dissipation, electron-electron and electron-phonon interaction.

6.1 Introduction

The subject of transport through a single molecular transistor has attracted tremendous interest in the past few decades for various applications [1-7] in nanotechnology. A single molecular transistor (SMT) consists of a central part (which could be a quantum dot (QD) or molecules), a source, and a drain. The main characteristic feature required for the central part is that it should have discrete energy levels, and the gate voltage must be adjustable to control the current flowing through it [8-9]. Several studies have been made on an SMT device. The correlation effect like Coulomb blockade and Kondo effect at low temperature [10-16], the Fano effect [17-19], Josephson tunneling [20-22], the Dicke effect [23,24] etc. are a few examples. The tunneling of electrons from the source to the central molecule or from the central molecule to the drain or vice versa distorts the central molecule. This distortion (phonon) interacts with electrons to give rise to a polaronic effect, particularly in organic or polar materials [25, 27].

Many theoretical and experimental research groups have examined the existence of vibrational side bands because of the electron-phonon (el-ph) interaction [28, 31]. A similar kind of observation was made by Chen et al. [32]. They have studied the effect of electron-phonon interaction on the differential conductance, tunneling current and spectral function. Transport properties through SMT have also been studied using many different theoretical and numerical methods like Slave-Boson mean-field non-crossing approach method [34], [33],renormalization method [35-39], kinetic equation method [40, 41], rate equation approach [42], and non-equilibrium Green's function approach [43-47]. Recently, Raju and Chatterjee [48] have studied the dissipation effect on SMT mounted on a non-interacting substrate. The substrate phonons have been assumed to interact with the local phonon of QD and this gives rise to a damping effect. This effect has been incorporated by introducing the Caldeira- Leggett (CL) term that brings in a linear dissipative coupling between the QD phonon and the substrate phonons. The total system is modeled by the Anderson-Holstein (AH) Hamiltonian plus the Caldeira- Leggett (CL) term. This Hamiltonian will be referred to as the AHCL Hamiltonian. Their study shows that when el-ph interaction is present, SMT parameters get renormalized. Costi [49] has used the Wilson renormalization technique and has shown that a strongly coupled QD placed in an external magnetic field could act as a spin filter. Dong et al. [50] have suggested that at zero temperature linear conductance gets suppressed when external magnetic field is present. Also when magnetic field is sufficiently high, side peaks can be observed in conductance. In a later work, Manasa et al. [51] have studied magneto-transport phenomena in an SMT device and determined the effect of electron-electron (el-el) interaction, electron-phonon interaction, and damping on the SMT device properties in an external magnetic field.

In the following chapter, we wish to study the phenomenon of non-equilibrium transport through a QD dimer. This device may be referred to a QD dimer transistor. We will examine the effects of magnetic field, dissipation, electron-electron interaction and electron-phonon interaction on Current, Spectral density, and differential conductance in such a system using AHCL Hamiltonian and the Keldysh Green function technique.

6.2 The Model

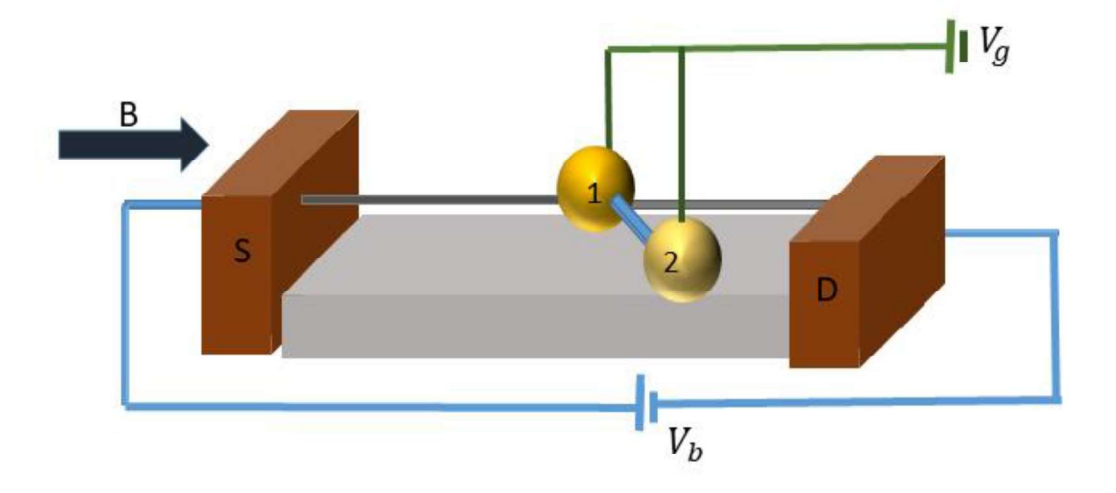


Figure. 6.1 Quantum Dot Dimer Configuration for QDD device

In Fig 6.1, a schematic diagram of a QD dimer (QDD) transistor (QDDT) device to be studied is given. It contains a source (S), a drain (D), and two QDs mounted on a dissipative substrate and placed in an external magnetic field. One QD is connected to both the source and the drain with metallic wires while the second QD is connected to the first QD only. Each QD has an individual lattice mode that interacts with local electrons through the el-ph coupling of Holstein type. Also the insulating substrate on which device is mounted acts as a heat-bath.

As already mentioned, phonons from the QDs and the substrate interact linearly through CL (Caldeira-Leggett) interaction and give rise to a dissipative effect to the tunneling current through the device. The effect of the magnetic field on the transport property is obvious [52, 53]; it lifts the spin degeneracy and makes the device suitable for a spin filter. The Hamiltonian for the system under consideration is given by

$$H = H_l + H_{ODD} + H_B + H_{tODD} + H_{ee}$$
 (6.1)

where H_l represents the source and the drain Hamiltonian, H_{QDD} denotes the Hamiltonian of QDD, H_B gives the Hamiltonian of the substrate, including the interaction between the phonons of the substrate and the QDs and H_{tQDD} describes the hybridization between the leads and the QDD.

 H_l can be written as

$$H_l = \sum_{\mathbf{k}, \sigma \in S, D} \varepsilon_{\mathbf{k}\sigma} n_{\mathbf{k}\sigma}, \tag{6.2}$$

The Hamiltonian H_l has been written in continuum state with $n_{k\sigma}$ corresponding to the number operator for source (S) and the drain (D).

 H_{ODD} can be written as

$$H_{QDD} = H_{QDD}^{0} + H_{vib}^{0} + H_{vib_e}^{0} , (6.3)$$

where H_{QDD}^0 is the pure electronic part of the QDD Hamiltonian, H_{vib}^0 is the pure phononic part of the QDD Hamiltonian and $H_{vib_e}^0$ is the local el-ph Hamiltonian. H_{QDD}^0 can be written as

$$H_{QDD}^{0} = \sum_{i,\sigma\in D} \varepsilon_{i} c_{i\sigma}^{\dagger} c_{i\sigma} - \sum_{\langle i,j\rangle,\sigma\in D} t_{ij} c_{i\sigma}^{\dagger} c_{j\sigma} + U \sum_{i} n_{i\uparrow} n_{i\downarrow} + \frac{1}{2} g\mu_{B} B S_{d}^{z},$$

$$(6.4)$$

where ε_i is the onsite energy, $n_{i\sigma}=c_{i\sigma}^{\dagger}c_{i\sigma}$ is the number operator for electrons at the i – th site with spin σ , $c_{i\sigma}(c_{i\sigma}^{\dagger})$ corresponds to annihilation (creation) operator, of electrons, t_{ij} is the intra-dot hopping parameter, U is the intra-dot el-el interaction strength, B is the magnetic field applied in the z direction, μ_B is the Bohr mageton S_d^z is the z-component of the total spin operator and S_d^z is the gyro-magnetic ratio. S_d^z is given by

$$H_{vib}^{0} = \sum_{i,\sigma \in D} \left[\frac{p_i^2}{2m_0} + \frac{1}{2} m_0 \omega_0^2 x_i^2 \right] , \qquad (6.5)$$

where m_0 is the mass of the QD oscillator, ω_0 is its frequency, S_d^z stands for the z-component of the total electron spin and B refers to the external magnetic field. $H_{vib\ e}^0$ is given by

$$H_{vib_e}^{0} = \sum_{i} g_{i} n_{i\sigma}(x_{i}) , \qquad (6.6)$$

where g_i is the electron-phonon (el-ph) coupling constant. Here we have taken el-ph coupling constant for both the quantum dots (QDs) to be equal to g. The Hamiltonian H_B of the substrate can be written as

$$H_B = H_B^0 + H_{vib-B}^0 , (6.7)$$

where H_B^0 is the Hamiltonian of a set of oscillators and is given by

$$H_B^0 = \sum_{j=1}^N \left[\frac{p_j^2}{2m_0} + \frac{1}{2} m_0 \omega_j^2 x_j^2 \right] , \qquad (6.8)$$

 ω_j being the frequency of the bath oscillator. H^0_{vib-B} is chosen as

$$H_{vib-B}^{0} = \sum_{\substack{j=1 \ \epsilon B \\ i=1 \epsilon QDD}}^{N,2} \beta_{j} x_{i} x_{j} , \qquad (6.9)$$

where β_j represent the coupling between the oscillators of QDD and the bath. H_{tQDD} can be written as

$$H_{tQDD} = V_r \sum (c_{S\sigma}^{\dagger} c_{1\sigma} + c_{1\sigma}^{\dagger} c_{S\sigma}) + V_r \sum (c_{D\sigma}^{\dagger} c_{1\sigma} + c_{1\sigma}^{\dagger} c_{D\sigma}). \tag{6.10}$$

where V_r denotes the lead-QDD hybridization strength. To decouple the interaction between the phonons of the QDD and the substrate, we first collect all the terms containing phonons. Thus we consider:

$$H_{B}^{0} + H_{vib}^{0} + H_{vib-B}^{0} + H_{vib-e}^{0} = \sum_{i,\sigma \in QDD} \left[\frac{p_{i}^{2}}{2m_{0}} + \frac{1}{2} m_{0} \omega_{0}^{2} x_{i}^{2} \right] + \sum_{j=1}^{2} \left[\frac{p_{j}^{\prime 2}}{2m_{0}} + \frac{1}{2} m_{0} \omega_{j}^{2} x_{j}^{\prime 2} \right] + \sum_{j=1}^{N,2} \varepsilon_{B} \beta_{j} x_{i} x_{j}^{\prime} + g \sum_{i} n_{i\sigma}(x_{i}) \quad (6.11)$$

By giving the transformation:

$$\widetilde{x'}_j = x'_j + \frac{\beta_j x_j}{m_j \omega_j}, \qquad (6.12)$$

we get

$$H_{B}^{0} + H_{vib}^{0} + H_{vib-B}^{0} + H_{vib_{e}}^{0} = \sum_{i,\sigma\in\mathcal{C}_{60}} \left[\frac{p_{i}^{2}}{2m_{0}} + \frac{1}{2}m_{0}\widetilde{\omega}_{0}^{2}x_{i}^{2} \right] + \sum_{j=1}^{N} \left[\frac{p'_{j}^{2}}{2m_{0}} + \frac{1}{2}m_{0}\omega_{j}^{2}\widetilde{\omega}_{j}^{2} \right] + g_{i}\sum_{j} c_{i\sigma}^{\dagger}c_{i\sigma}(x_{i}),$$

$$(6.13)$$

where

$$\widetilde{\omega}_0^2 = \omega_0^2 - \sum_j \frac{\beta_j^2}{m_0 \omega_j^2 m_j} = \omega_0^2 - \Delta \omega^2 ,$$
 (6.14)

where $\Delta\omega^2$ is the shift in the square of the quantum dot oscillator frequency caused by the linear oscillator-bath coupling .We assume that a spectral function $J(\omega)$ fully characterizes the oscillator bath:

$$J(\omega) = \sum_{j=1}^{N} \frac{\beta_j^2}{2m_j \omega_j^2} \delta(\omega - \omega_j).$$
 (6.15)

Replacing summation by the integration for large N. Therefore $\Delta\omega^2$ can be written as

$$\Delta\omega^2 = \frac{2}{m_0} \int d\omega \frac{J(\omega)}{\omega} \quad . \tag{6.16}$$

We choose Lorentz- Drude form for the spectral function:

$$J(\omega) = \frac{2m_0\gamma\omega}{1 + \left(\frac{\omega}{\omega_c}\right)^2} \tag{6.17}$$

where ω_c is the cut-off frequency and γ is the damping rate. We assume ω_c is much larger than the frequency of the system. Substituting Eq. (6.16) in Eq. (6.15), we get

$$\widetilde{\omega}_0^2 = \omega_0^2 - \frac{2}{m_0} \int d\omega \frac{J(\omega)}{\omega} = \omega_0^2 - 4\gamma \int d\omega \frac{1}{1 + \left(\frac{\omega}{\omega_c}\right)^2}$$

$$=\omega_0^2 - 4\gamma \omega_c tan^{-1} \left(\frac{\omega}{\omega_c}\right)_0^{\infty} = \omega_0^2 - 4\gamma \omega_c \frac{\pi}{2}$$

Or,

$$\widetilde{\omega}_0^2 = \omega_0^2 - 2\pi\gamma\omega_c \tag{6.18}$$

Thus our Hamiltonian reduces to

$$\overline{H} = \sum_{\mathbf{k},\sigma \in S,D} \varepsilon_{\mathbf{k}\sigma} n_{\mathbf{k}\sigma} + \sum_{\substack{i \\ \sigma \in QDD}} c_{i} c_{i\sigma}^{\dagger} c_{i\sigma} - \sum_{\substack{\langle i,j \rangle \\ \sigma \in QDD}} t_{ij} c_{i\sigma}^{\dagger} c_{j\sigma} + \hbar \widetilde{\omega}_{0}^{2} \sum_{i} b_{i}^{\dagger} b_{i}
+ g_{i} \sum_{i} c_{i\sigma}^{\dagger} c_{i\sigma} (b_{i} + b_{i}^{\dagger}) + \frac{1}{2} g \mu_{B} B S_{d}^{z}
+ V_{r} \sum_{i} \left(c_{S\sigma}^{\dagger} c_{1\sigma} + c_{1\sigma}^{\dagger} c_{S\sigma} \right)
+ V_{r} \sum_{i} \left(c_{D\sigma}^{\dagger} c_{1\sigma} + c_{1\sigma}^{\dagger} c_{D\sigma} \right),$$
(6.19)

where b_i and b_i^{\dagger} are the phonon annihilation and creation operators.

Next we proceed to decouple the el-ph interaction. To accomplish this we perform the lang-Firsov transformation [54]. The Hamiltonian then transforms to

$$\widetilde{H} = e^{S}\overline{H}e^{-S}$$

where

$$S = \frac{g_1}{\hbar\omega_0} \sum\nolimits_{i\sigma} n_{i\sigma} \left(b_i^\dagger - b_i \right) = \lambda \sum\nolimits_{i\sigma} n_{i\sigma} \left(b_i^\dagger - b_i \right), \qquad \lambda = \frac{g_1}{\hbar\omega_0}$$

The operators b_i transform to

$$\tilde{b}_i = \dots = b_i + [S, b_i] + \frac{1}{2!} [S, [S, b_i]] + \dots$$

$$= b_i - \lambda \sum_{\sigma} n_{i\sigma}$$
(6.20a)

Similarly operators $\ b_i^{\,\dagger}, \, c_{i\sigma}$ and $c_{i\sigma}^{\,\dagger}$ are transformed to

$$\tilde{b}_{i}^{\dagger} = \dots = b_{i}^{\dagger} + \left[S, b_{i}^{\dagger}\right] + \frac{1}{2!} \left[S, \left[S, b_{i}^{\dagger}\right]\right] + \dots$$

$$= b_{i}^{\dagger} - \lambda \sum_{\sigma} n_{i\sigma}$$

$$(6.20b)$$

$$\tilde{c}_{i\sigma} = \dots = c_{i\sigma} + [S, c_{i\sigma}] + \frac{1}{2!} [S, [S, c_{i\sigma}]] + \dots = \exp\left(-\lambda (b_i^{\dagger} - b_i)\right) c_{i\sigma}$$

$$= X c_{i\sigma}$$
(6.20c)

$$\tilde{c}_{i\sigma}^{\dagger} = \dots = c_{i\sigma}^{\dagger} + \left[S, c_{i\sigma}^{\dagger} \right] + \frac{1}{2!} \left[S, \left[S, c_{i\sigma}^{\dagger} \right] \right] + \dots = \exp\left(\lambda \left(b_i^{\dagger} - b_i \right) \right) c_{i\sigma}^{\dagger}$$

$$= X_i^{\dagger} c_{i\sigma}^{\dagger} \tag{6.20d}$$

So the Hamiltonian \widetilde{H} becomes

$$\widetilde{H} = \sum_{\mathbf{k},\sigma \in S,D} \varepsilon_{\mathbf{k}\sigma} n_{\mathbf{k}\sigma} + \sum_{i,\sigma \in QDD} \widetilde{\epsilon}_{i} n_{i\sigma} + \widetilde{U} \sum_{i} n_{i\uparrow} n_{i\downarrow}$$

$$+ \sum_{i} (\widetilde{V} c_{S\sigma}^{\dagger} c_{1\sigma} + \widetilde{V}^{\dagger} c_{1\sigma}^{\dagger} c_{S\sigma}) + \sum_{i} (\widetilde{V} c_{D\sigma}^{\dagger} c_{1\sigma} + \widetilde{V}^{\dagger} c_{1\sigma}^{\dagger} c_{D\sigma})$$

$$+ \hbar \widetilde{\omega}_{0} \sum_{i} \widetilde{b}_{i}^{\dagger} \widetilde{b}_{i} - t \sum_{\langle i,j \rangle} X_{i}^{\dagger} X_{j} c_{i\sigma}^{\dagger} c_{j\sigma} + \frac{1}{2} g \mu_{B} B S_{d}^{z},$$

$$(6.21)$$

where we have defined

$$\widetilde{U} = (U - \hbar \widetilde{\omega}_0 \lambda^2), \ \widetilde{\epsilon}_i = (\epsilon_i - \hbar \widetilde{\omega}_0 \lambda^2), \ \widetilde{V} = V_r X_i, \ \widetilde{V}^{\dagger} = V_r X_i^{\dagger},$$
 (6.22)

$$X = \exp\left(-\lambda \left(b_i^{\dagger} - b_i\right)\right), \quad X_i^{\dagger} = \exp\left(\lambda \left(b_i^{\dagger} - b_i\right)\right). \tag{6.23}$$

To treat the el-el interaction we perform the mean field approximation and the transformed Hamiltonian reads

$$\begin{split} \widetilde{H}_{m} &= \sum_{\boldsymbol{k}, \sigma \in S, D} \varepsilon_{\boldsymbol{k}\sigma} n_{\boldsymbol{k}\sigma} + \sum_{i, \sigma \in QDD} (\epsilon_{0} + \widetilde{U} < n_{i} >) n_{i\sigma} \\ &+ \sum_{\sigma} (\widetilde{V} c_{S\sigma}^{\dagger} c_{1\sigma} + \widetilde{V}^{\dagger} c_{1\sigma}^{\dagger} c_{S\sigma}) + \sum_{\sigma} (\widetilde{V} c_{D\sigma}^{\dagger} c_{1\sigma} + c_{1\sigma}^{\dagger} \widetilde{V}^{\dagger} c_{D\sigma}) \\ &+ \hbar \widetilde{\omega}_{0} \sum_{i} b_{i}^{\dagger} b_{i} - \sum_{\langle i, i \rangle} \widetilde{t} c_{i\sigma}^{\dagger} c_{j\sigma} + \frac{1}{2} g \mu_{B} B S_{d}^{z} \,. \end{split}$$
(6.24)

To calculate current, we first write the total number of electrons in the left lead which is given by

$$N_{s} = \sum_{k_{x},\sigma} c_{Sk_{x}\sigma}^{\dagger} c_{Sk_{x}\sigma}. \tag{6.25}$$

Now the current from the left lead is given by: $J_L = e\dot{N}_s$, where \dot{N}_s is given by

$$\dot{N}_{s} = -\frac{ie}{\hbar} \langle \left[N_{s}, \widetilde{H}_{m} \right] \rangle = -\frac{i}{\hbar} \langle \left[N_{s} H_{1} + H_{QDD} + H_{B} + H_{t} \right] \rangle$$

$$= \frac{i}{\hbar} \widetilde{V} \sum_{k_{x}, \sigma} \left[\langle c_{sk_{x\sigma}}^{\dagger} c_{1\sigma} \rangle - h.c \right]. \tag{6.26}$$

Thus the current from the source is given by

$$J_L = \frac{ie}{\hbar} \tilde{V} \sum_{k_x, \sigma} \left[\langle c_{sk_x \sigma}^{\dagger} c_{1\sigma} \rangle - h.c \right] , \qquad (6.27)$$

and can be written as:

$$J_L = \frac{ie}{\hbar} \frac{1}{\sqrt{L_x}} \sum_{k_x \sigma} \tilde{V} \left(G_{1\sigma, k_x \sigma}^{<} - G_{k_x, 1\sigma}^{<} \right) , \qquad (6.28)$$

where

$$G_{k\sigma,1}^{<}(t,t') = i\langle 0|c_{1\sigma}^{\dagger}(t')c_{sk\sigma}(t)|0\rangle, \tag{6.29}$$

$$G_{1,k\sigma}^{<}(t,t') = i\langle 0|c_{1\sigma}(t')c_{k\sigma}^{\dagger}(t)|0\rangle, \tag{6.30}$$

where $G_{1,k\sigma}^{<(>)}(t,t')$ represents greater (lesser) Keldysh Green function and the average is taken over electronic and phononic degrees of freedom. Now,

$$Rel G_{1\sigma,k_x\sigma}^{<} = \frac{1}{2} \left(i < c_{sk_{x\sigma}}^{\dagger} c_{1\sigma} > -i < c_{1\sigma}^{\dagger} c_{sk_x\sigma} > \right) . \tag{6.31}$$

Eq. (6.29) gives

$$J_L = \frac{2e}{\hbar} \sum_{k_x \sigma} \tilde{V} Rel(G_{1\sigma, sk_x \sigma}^{<}) . \qquad (6.32)$$

To obtain the time-ordered Green function we use equation of motion technique.

$$G_{1\sigma,k_{x}\sigma}^{<}(t,t') = i < c_{sk_{x}\sigma}^{\dagger}(t)c_{1\sigma}(t')$$

$$(6.33)$$

Differentiating Eq. 6.31 with respect to t', we obtain

$$-i\frac{\partial}{\partial t'}G_{1\sigma,k_{x}\sigma}^{<}(t,t') = \langle T\frac{\partial}{\partial t'}c_{k_{x}\sigma}^{\dagger}(t')c_{1\sigma}(t) \rangle$$

$$= \langle T[c_{k_{x}\sigma}^{\dagger}(t'),H_{m}]c_{1\sigma}(t) \rangle, \qquad (6.34)$$

where \widetilde{H}_m is given by equation (6.24). Substituting only those parts of Hamiltonian whose commutator is non-zero $c_{k_x\sigma}^{\dagger}(t')$ in Eq. (6.34) we get

$$-i\frac{\partial}{\partial t'}G^{<}_{1\sigma,k_{x}\sigma}(t,t')$$

$$= < T[c_{k_x\sigma}^{\dagger}(t'), \sum_{\pmb{k},\sigma \in S,D} \varepsilon_{\pmb{k}\sigma} n_{\pmb{k}\sigma} + \sum \left(\tilde{V} c_{S\sigma}^{\dagger} c_{1\sigma} + \tilde{V}^{\dagger} c_{1\sigma}^{\dagger} c_{S\sigma} \right)] c_{1\sigma}(t) >$$

$$= \tilde{V}^{\dagger} g_{1\sigma,1\sigma}^{<}(t,t') g_{L\sigma}(t,t') \tag{6.35}$$

Multiplying both side with $\exp(i\omega t)$ and integrating with respect to t we get

$$G_{1\sigma,k_x\sigma}^{<}(\omega) = \tilde{V}^{\dagger} g_{1\sigma,1\sigma}^{<}(\omega) g_{L\sigma}(k_x,\omega)$$
(6.36)

where

$$g_L(k_x, \omega) = \frac{1}{(\omega - \varepsilon_k)} \tag{6.37}$$

Since the equilibrium and non-equilibrium theory are topologically equivalent, Eq. (6.32) has precisely the same form in the non-equilibrium theory except for the fact that the intermediate time integral runs on the complex contour. According to Langreth rule for analytic continuation, the relation:

 $C(\tau) = A(\tau)B(\tau)$, can be written as

$$C^{<}(t,t') = \int \left[A^{<}(t,t_1)B^{(a)}(t_1,t') + A^{r}(t,t_1)B^{<}(t_1,t') \right] dt_1.$$
 (6.38)

Thus we can write

$$G^{<}_{1\sigma,k_{x}\sigma}(t,t') =$$

$$\tilde{V}^{\dagger} \int dt' (g^{r}_{1\sigma,1\sigma}(t-t')g^{<}_{L\sigma}(k_{x},t-t') + g^{<}_{1\sigma,1\sigma}(t-t')g^{a}_{L\sigma}(k_{x},t-t'))$$

$$(6.39)$$

In the energy space, we have

$$G^{<}_{1\sigma,k_{x}\sigma}(t-t') = \tilde{V}^{\dagger} \int \frac{d\epsilon}{2\pi} \left[(g^{r}_{1\sigma,1\sigma}(\epsilon)g^{<}_{L\sigma}(\epsilon) + g^{<}_{1\sigma,1\sigma}(\epsilon)g^{a}_{L\sigma}(k_{x},\epsilon) \right]$$

$$(6.40)$$

Using Eq. (6.40) in Eq. (6.32), we obtain

$$J_{L} = 2e\tilde{V}\tilde{V}^{\dagger}Rel\sum_{\sigma,k_{x}}\int \frac{d\epsilon}{2\pi} \left[(g_{1\sigma,1\sigma}^{r}(\epsilon)g_{L\sigma}^{<}(\epsilon) + g_{1\sigma,1\sigma}^{<}(\epsilon)g_{L\sigma}^{a}(k_{x},\epsilon) \right]$$
(6.41)

where $g^r_{1\sigma,1\sigma}(\epsilon)$ and $g^r_{L\sigma}(k_x,\epsilon)$ are the retartded Green functions for the QDD molecule and lead respectively and $g^a_{1\sigma,1\sigma}(\epsilon)$ and $g^a_{L\sigma}(k_x,\epsilon)$ are the advanced Green functions for the QDD molecule and lead respectively. Now we have

$$g_{L\sigma}^{<}(k_{x},\epsilon) = 2\pi i\hbar\delta(\epsilon - \epsilon_{k})f_{L}(\epsilon), \ Img \ g_{L\sigma}^{a}(k_{x},\epsilon) = \ 2\pi i\hbar\delta(\epsilon - \epsilon_{k}) \ (6.42)$$

and so J_L becomes

$$\begin{split} J_L &= \frac{2e\tilde{V}\tilde{V}^\dagger}{2\pi\hbar} \sum_{\sigma} \int d\epsilon \int dk_x \left[Im \left[(g^r_{1\sigma,1\sigma}(\omega)) \right] \delta(\epsilon - \epsilon_k) f_L(\epsilon) \right] \\ &+ \frac{2e\tilde{V}\tilde{V}^\dagger}{2\pi\hbar} \sum_{\sigma} \int d\epsilon \int dk_x \, \delta(\epsilon - \epsilon_k) \left[g^<_{1\sigma,1\sigma}(\omega) \right]. \end{split} \tag{6.43}$$

Let us define

$$\Gamma^{L}(\epsilon) = \tilde{V}\tilde{V}^{\dagger} \int dk_{\chi} \delta(\epsilon - \epsilon_{k}) = \tilde{V}\tilde{V}^{\dagger} \rho, \qquad (6.44)$$

so that Eq. (6.43) can be written as

$$J_{L} = \frac{e}{2\pi\hbar} \left[\int d\epsilon f_{L}(\epsilon) \Gamma^{L}(\epsilon) Img^{r}_{1\sigma,1\sigma}(\epsilon) + \int d\epsilon f_{L}(\epsilon) \Gamma^{L}(\epsilon) g^{<}_{1\sigma,1\sigma}(\epsilon) \right].$$

$$(6.45)$$

The expression for J_R is obtained in same way and we obtain

$$J_{R} = \frac{e}{2\pi\hbar} \left[\int d\epsilon f_{R}(\epsilon) \Gamma^{R}(\epsilon) Img^{r}_{1\sigma,1\sigma}(\epsilon) + \int d\epsilon f_{L}(\epsilon) \Gamma^{R}(\epsilon) g^{<}_{1\sigma,1\sigma}(\epsilon) \right]. \tag{6.46}$$

The current will be uniform in the steady state case. Therefore, $J_L = -J_R$. So the net current flowing through the device is given by

$$J = \frac{J_L - J_R}{2} . ag{6.47}$$

From Eqns. (6.43), (6.46) and (6.47), we have

$$J = \frac{e}{h} \left[\int d\epsilon [f_L(\epsilon) \Gamma^L(\epsilon)] - f_R(\epsilon) \Gamma^R(\epsilon)] A(\epsilon) \right]$$

$$+ \int d\epsilon [\Gamma^L(\epsilon) - \Gamma^R(\epsilon)] g^{<}_{1\sigma,1\sigma}(\epsilon) , \qquad (6.48)$$

where the Fermi distribution functions for the source and the drain have been denoted by $f_{L,R}(\epsilon)$ r and the bias voltage(((V_b)) and mid-voltage (V_m) are related to chemical potential by the relations $\mu_L - \mu_R = eVb$, ($\mu_L + \mu_R$)/2 = eVm. Since QDs are symmetrically coupled to source and drain leads, we write $\Gamma(\epsilon) = (\Gamma^L(\epsilon) + \Gamma^R(\epsilon))/2$, where $\Gamma^{R(L)}(\epsilon)$ is given by $2\pi\rho_{R(L)}|\tilde{V}|^2$ (Eqns.(6.44)), and it represents the density of energy states of the source and drain. The spectral function gives the excitations in the system and is written in the form of Green functions as

$$A(\epsilon) = i[g_{11}^r(\epsilon) - g_{11}^a(\epsilon)] = i[g_{11}^{<}(\epsilon) - g_{11}^{>}(\epsilon)]. \tag{6.49}$$

Now the total Green function contains both electronic and phononic contributions.

$$g^{<}_{1\sigma,1\sigma}(\tau) = i < c^{\dagger}_{1\sigma}(0)c_{1\sigma}(\tau) >_{\widetilde{H}} < X_{1}^{\dagger}(0)X_{1}(\tau) >$$
 (6.50)

To solve the phononic contribution $\langle X_1^{\dagger}(0)X_1(\tau) \rangle$, we consider

$$F(\tau) = \langle X_1^{\dagger}(0)X_1(\tau) \rangle = \frac{1}{Z}Tr[e^{-\beta\hbar}X_1^{\dagger}(0)X_1(\tau)]$$
 (6.51)

where

$$Z = \sum_{n} e^{-\beta \hbar \widetilde{\omega}_{0}} = \frac{1}{1 - e^{-\beta \hbar \widetilde{\omega}_{0}}},$$

$$X_1^{\dagger}(0) = e^{\lambda(b_1^{\dagger}(0) - b_1(0))}$$

and

$$X_1(\tau) = e^{\lambda \left(b_1^{\dagger}(\tau) - b_1(\tau)\right)}.$$

Using the value of Z, $X_1^{\dagger}(0)$, and $X_1(\tau)$ in Eq. (6.51), we have

$$F(\tau) = (1 - e^{-\beta\hbar\widetilde{\omega}_0 n}) \sum_{n} < n |e^{\beta\hbar\widetilde{\omega}_0 n} \left[e^{\lambda \left(b_1^{\dagger} - b_1\right) - \lambda \left(b_1^{\dagger} e^{i\widetilde{\omega}_0 \tau} - b_1 e^{i\widetilde{\omega}_0 \tau}\right)} \right] |n>$$

$$(6.52)$$

Now,

$$\left(1-e^{-\beta\hbar\widetilde{\omega}_0n}\right)\sum_n e^{-\beta\hbar\widetilde{\omega}_0n}e^{-\lambda^2} < n\left|\left[e^{\lambda b_1^\dagger}e^{-\lambda b_1}e^{-\lambda b_1^\dagger}e^{i\widetilde{\omega}_0\tau}e^{\lambda b_1e^{-i\widetilde{\omega}_0\tau}}\right]\right|n>$$

$$= (1 - e^{-\beta \hbar \widetilde{\omega}_{0} n}) \sum_{n} e^{-\beta \hbar \widetilde{\omega}_{0} n} e^{-\lambda^{2} (1 - e^{i\widetilde{\omega}_{0} \tau})} \times$$

$$< n \left| \left[e^{\lambda b_{1}^{\dagger} (1 - e^{i\widetilde{\omega}_{0} \tau})} e^{-\lambda b_{1} (1 - e^{-i\widetilde{\omega}_{0} \tau})} \right] \right| n >$$
(6.53)

Let us consider $u=\lambda(1-e^{-i\widetilde{\omega}_0\tau})$, $u^*=\lambda(1-e^{i\widetilde{\omega}_0\tau})$ and substituting Equation (6.53) in (6.52).

$$F(\tau) = \left(1 - e^{-\beta\hbar\widetilde{\omega}_0 n}\right) e^{-\lambda^2 \left(1 - e^{i\widetilde{\omega}_0 \tau}\right)} \sum_n e^{-\beta\hbar\widetilde{\omega}_0 n} < n \left| \left[e^{u^* b_1^{\dagger}} e^{-ub_1} \right] \right| n >$$

$$(6.54)$$

Using the relations

$$< n \left| \left[e^{u^* b_1^{\dagger}} e^{-u b_1} \right] \right| n > = L_n(|u|^2)$$
 ,

where $L_n(|u|^2)$ is the Laguerre polynomial. So equation (6.54) gives,

$$F(\tau) = \left(1 - e^{-\beta\hbar\widetilde{\omega}_0}\right)e^{-\lambda^2\left(1 - e^{i\widetilde{\omega}_0\tau}\right)} \sum_n e^{-\beta\hbar\widetilde{\omega}_0 n} L_n(|u|^2)$$
(6.55)

Using Laguerre polynomial properties we have

$$\sum_{0}^{\infty} z^{n} L_{n}(|u|^{2}) = \frac{e^{-|u|^{2}z/(z-1)}}{(1-z)} , \qquad (6.56)$$

where $z = \exp(-\beta \hbar \widetilde{\omega}_0)$. Therefore, we can write

$$\frac{z}{1-z} = \frac{\exp(-\beta\hbar\widetilde{\omega}_0)}{1-\exp(-\beta\hbar\widetilde{\omega}_0)} = \frac{1}{\exp(\beta\hbar\widetilde{\omega}_0) - 1} = N_{ph}$$
 (6.57)

and

$$|u|^2 = \lambda^2 (1 - e^{-i\widetilde{\omega}_0 \tau}) (1 - e^{i\widetilde{\omega}_0 \tau}) = \lambda^2 (1 - e^{i\widetilde{\omega}_0 \tau} + 1 - e^{-i\widetilde{\omega}_0 \tau}).$$

So $F(\tau)$ can be written as

$$F(\tau) = \exp\left(-\lambda^2 \left[\left(1 + N_{ph}\right) \left(1 - e^{i\widetilde{\omega}_0 \tau}\right) + N_{ph} \left(1 - e^{-i\widetilde{\omega}_0 \tau}\right) \right] \right) = \exp\left(-\phi(\tau)\right)$$
(6.58)

Defining $\phi(\tau) = \lambda^2 [(1 + N_{ph})(1 - e^{i\tilde{\omega}_0 \tau}) + N_{ph}(1 - e^{-i\tilde{\omega}_0 \tau})]$ and after some simplifications we have

$$\phi(\tau) = \lambda^2 \left[\left(1 + 2N_{ph} \right) - 2\sqrt{N_{ph}(N_{ph} + 1)} \cos\left(\widetilde{\omega}_0 \tau - i \frac{\beta \hbar \widetilde{\omega}_0}{2} \right) \right]$$
 (6.59)

which gives

$$F(\tau) = \exp\left[2\lambda^2 \sqrt{N_{ph}(N_{ph}+1)}\cos\left(\widetilde{\omega}_0\tau - i\frac{\beta\hbar\widetilde{\omega}_0}{2}\right)\right]e^{-\lambda^2(1+2N_{ph})}$$

$$=e^{-\lambda^2(1+2N_{ph})}e^{z'\cos\left(\widetilde{\omega}_0\tau-i\frac{\beta\hbar\widetilde{\omega}_0}{2}\right)},\qquad (6.60)$$

or,

$$F(\tau) = e^{-\lambda^2 (1+2N_{ph})} \sum_{l=-\infty}^{\infty} I_l(z') e^{il\widetilde{\omega}_0 \tau} e^{\frac{l\beta \hbar \widetilde{\omega}_0}{2}} = \sum_{l=-\infty}^{\infty} L_l(z) \quad , \tag{6.61}$$

where $z'=2\lambda^2\sqrt{N_{ph}(N_{ph}+1)}$ and $I_l(z')$ is the Bessel function. Using Eq. (6.61) in Eq. (6.50), we get

$$g_{1\sigma1\sigma}^{<}(\tau) = i < c_{1\sigma}(0)c_{1\sigma}^{\dagger}(t) > \tilde{g} < X_{1}(0)X_{1}^{\dagger}(t) > \tilde{g}^{<}(\tau) < X_{1}(0)X_{1}^{\dagger}(t) > \tilde{g}^{<}(\tau) < X_{1}(0)X_{1}^{\dagger}(t) > \tilde{g}^{<}(\tau) < \tilde{g$$

$$= \tilde{g}^{<}(\tau)e^{-\lambda^2(1+2N_{ph})} \sum_{l=-\infty}^{\infty} I_l(z')e^{il\tilde{\omega}_0\tau}e^{l\beta\hbar\tilde{\omega}_0/2}.$$
 (6.62)

In Fourier space we have

$$g^{<}(\epsilon) = \int d\tau e^{i\omega\tau} g_{1\sigma1\sigma}^{<}(\tau)$$

$$= \int d\tau e^{i\omega\tau} \tilde{g}^{<}(\tau) e^{-\lambda^{2}(1+2N_{ph})} \sum_{l=-\infty}^{\infty} I_{l}(z') e^{il\tilde{\omega}_{0}\tau} e^{\frac{l\beta\hbar\tilde{\omega}_{0}}{2}}$$

$$= \sum_{l=-\infty}^{\infty} I_{l}(z') e^{\frac{l\beta\hbar\tilde{\omega}_{0}}{2}} \tilde{g}^{<}(\epsilon + \tilde{\omega}_{0}l) e^{-\lambda^{2}(1+2N_{ph})}, \qquad (6.63)$$

or,

$$g^{<}(\epsilon) = \sum_{l=-\infty}^{\infty} L_l(z) \, \tilde{g}^{<}(\varepsilon + l\hbar \tilde{\omega}_0), \tag{6.64}$$

where l stand for number of phonon involved and the coefficient L_l depend on el-ph strength and temperature. At zero temperature, we have

$$L_n = \begin{cases} \frac{\lambda^{2l}}{l!} e^{-\lambda^2} & l \ge 0\\ 0 & l < 0 \end{cases}$$
 (6.65)

Similarly we can write for $g^{>}(\varepsilon)$.

$$g^{>}(\varepsilon) = \sum_{l=-\infty}^{\infty} L_l(z) \, \tilde{g}^{>}(\varepsilon - l\hbar \tilde{\omega}_0), \tag{6.66}$$

which gives

$$A(\varepsilon) = \sum_{l=-\infty}^{\infty} i L_l(z) [\tilde{g}^{>}(\varepsilon - l\hbar \tilde{\omega}_0) - \tilde{g}^{<}(\varepsilon + l\hbar \tilde{\omega}_0)].$$
 (6.67)

To calculate $\tilde{g}^{>}(\varepsilon)$ and $\tilde{g}^{<}(\varepsilon)$ we use Keldysh equation [57, 58, 59]

$$\tilde{g}_{11}^{<(>)}(\epsilon) = g_{11}^r(\epsilon)\tilde{\Sigma}^{<(>)}\tilde{g}_{11}^a(\epsilon). \tag{6.68}$$

where

$$\tilde{\Sigma}^{<} = (f_s(\epsilon) + f_D(\epsilon)) \text{ and } \tilde{\Sigma}^{>} = (2 - f_s(\epsilon) + f_D(\epsilon)),$$
 (6.69)

and $\tilde{g}_{11}^{r(a)}$ is calculated using equation of motion technique which gives

$$i\frac{\partial}{\partial t'} \left[\tilde{\mathbf{g}}_{11}^{\mathrm{r(a)}}(\varepsilon) \right]_{el} = \delta(\pm t \mp t') \mp i\theta(\pm t \mp t') \langle \left\{ c_1(t), \left[c_1^{\dagger}, \widetilde{H}_m \right] \right\} \rangle$$
 (6.70)

$$=\delta(\pm t \mp t')$$

$$\mp i\theta(\pm t \mp t') \left\langle \left\{ c_{1\sigma'}(t), \left[c_{1\sigma'}^{\dagger}(t'), \sum_{\mathbf{k}, \sigma \in S, D} \varepsilon_{\mathbf{k}\sigma} n_{\mathbf{k}\sigma} + \sum_{i, \sigma \in QDD} (\epsilon_0 + \widetilde{U} < n_i >) n_{i\sigma} + \sum_{\sigma} \left(\widetilde{V} c_{S\sigma}^{\dagger} c_{1\sigma} + \widetilde{V}^{\dagger} c_{1\sigma}^{\dagger} c_{S\sigma} \right) + \sum_{\sigma} \left(\widetilde{V} c_{D\sigma}^{\dagger} c_{1\sigma} + c_{1\sigma}^{\dagger} \widetilde{V}^{\dagger} c_{D\sigma} \right) - \sum_{\sigma} \widetilde{t} \left(c_{1\sigma}^{\dagger} c_{2\sigma} + c_{2\sigma}^{\dagger} c_{1\sigma} \right) \right\} \right\rangle$$

$$(6.71)$$

To simplify the above expression we calculate the following commutators.

$$\begin{split} \left[c_{1\sigma'}^{\dagger}, \sum_{i,\sigma \in QDD} (\epsilon_0 + \widetilde{U} < n_{\downarrow} >) n_{i\sigma}\right] &= \sum_{\sigma} \left[c_{d\sigma'}^{\dagger}, \widetilde{\epsilon}_d n_{d\sigma}\right] \\ &= \sum_{\sigma} (\epsilon_0 + \widetilde{U} < n_{\downarrow} >) \left[c_{1\sigma'}^{\dagger}, c_{1\sigma}^{\dagger} c_{1\sigma}\right] \end{split}$$

$$= -(\epsilon_0 + \widetilde{U} < n_{\downarrow} >) \sum_{\sigma} c^{\dagger}_{1\sigma\sigma'} \delta_{\sigma\sigma'} , \qquad (6.72)$$

$$\left[c_{1\sigma'}^{\dagger} \sum_{\sigma} \tilde{t} \left(c_{1\sigma}^{\dagger} c_{2\sigma} + c_{2\sigma}^{\dagger} c_{1\sigma}\right)\right] = \sum_{\sigma} \tilde{t} \left(\left[c_{1\sigma'}^{\dagger}, c_{2\sigma}^{\dagger} c_{1\sigma}\right] + h.c.\right) = -\sum_{\sigma} \tilde{t} c_{2\sigma}^{\dagger} \delta_{\sigma\sigma'}$$
(6.73)

$$\left[c_{1\sigma'}^{\dagger}, \sum_{\sigma} \left(\tilde{V}c_{S\sigma}^{\dagger}c_{1\sigma} + \tilde{V}^{\dagger}c_{1\sigma}^{\dagger}c_{S\sigma}\right) + \sum_{\sigma} \left(\tilde{V}c_{D\sigma}^{\dagger}c_{1\sigma} + c_{1\sigma}^{\dagger}\tilde{V}^{\dagger}c_{D\sigma}\right)\right] \\
= -\tilde{V}\sum_{\sigma} \left(c_{S\sigma}^{\dagger} + c_{D\sigma}^{\dagger}\right) \tag{6.74}$$

Substituting Eqns. (6.72),(6.73) and (6.74) in Eqn. (6.71), we have

$$i\frac{\partial}{\partial t'} \left[\tilde{g}_{11}^{r(a)}(\varepsilon) \right]_{el} = \delta(\pm t \mp t')$$

$$\mp i\theta(\pm t \mp t') < \{c_{1\sigma'}(t), -(\epsilon_0 + \tilde{U} < n_1 >) \sum_{\sigma} c_{1\sigma\sigma'}^{\dagger} \delta_{\sigma\sigma'}$$

$$-\sum_{\sigma} (\tilde{t}) c_{2\sigma}^{\dagger} \delta_{\sigma\sigma'} - \tilde{V} \sum_{\sigma} \left(c_{S\sigma}^{\dagger} + c_{D\sigma}^{\dagger} \right) >. \tag{6.75}$$

Multiplying both sides by $e^{i(\varepsilon \mp n\hbar \tilde{\omega}_0)\tau}$ and integrating over τ , we get

$$(\varepsilon \mp n\hbar\widetilde{\omega}_{0})g_{11}^{r(a)}(\varepsilon)$$

$$= 1 + (\epsilon_{0} + \widetilde{U} < n_{1} >)\widetilde{g}_{11}^{r(a)}(\varepsilon \mp n\hbar\widetilde{\omega}_{0}) + \widetilde{t}\widetilde{g}_{12}^{r(a)}(\varepsilon \mp n\hbar\widetilde{\omega}_{0})$$

$$+\widetilde{V}(\widetilde{g}_{1Sk}^{r(a)}(\varepsilon \mp n\hbar\widetilde{\omega}_{0}) + \widetilde{g}_{1Dk}^{r(a)}(\varepsilon \mp n\hbar\widetilde{\omega}_{0})) , \qquad (6.76)$$

which gives

$$\tilde{g}_{11}^{r(a)}(\varepsilon \mp n\hbar \widetilde{\omega}_0)$$

$$=\frac{1+\tilde{t}\tilde{g}_{12}^{r(a)}(\varepsilon\mp n\hbar\tilde{\omega}_{0})+\tilde{V}(\tilde{g}_{1,Sk}^{r(a)}(\varepsilon\mp n\hbar\tilde{\omega}_{0})+\tilde{g}_{1,Dk}^{r(a)}(\varepsilon\mp n\hbar\tilde{\omega}_{0}))}{\left[(\varepsilon\mp n\hbar\tilde{\omega}_{0})-\tilde{\epsilon}_{0}-\tilde{U}\langle n_{d\downarrow}\rangle\right]}\;,$$

$$(6.77)$$

where $\tilde{g}_{1,Sk\sigma}^{r(a)}(\varepsilon \mp n\hbar \tilde{\omega}_0)$ is the Fourier transform of $\tilde{g}_{1,S\sigma}^{r(a)}(t,t')$. Similarly we have the equation of motion for $\tilde{g}_{1,Sk\sigma}^{r(a)}(t,t')$.

$$i\frac{\partial}{\partial t'}\tilde{g}_{1,Sk\sigma}^{r(a)}(t,t') = \mp i\theta(\pm t \mp t')\langle\{c_{1}(t),[c_{sk}^{\dagger},\tilde{H}]\}\rangle$$

$$= \mp i\theta(\pm t \mp t')\langle\{c_{d}(t),[c_{k}^{\dagger},\sum_{k\sigma}\varepsilon_{k}n_{k\sigma}+\sum_{k\sigma}(\tilde{V}c_{Sk\sigma}^{\dagger}c_{1}+h.c)]\}\rangle$$

$$= \mp i\theta(\pm t \mp t')\varepsilon_{k}\langle\{c_{d}(t),c_{k}^{\dagger}(t')\}\rangle \mp i\theta(\tau)\tilde{V}^{\dagger}\langle\{c_{1}(t),c_{1}^{\dagger}(t')\}\rangle$$

$$= \varepsilon_{k}\tilde{g}_{1,Sk\sigma}^{r(a)}(t,t') + \tilde{V}^{\dagger}\tilde{g}_{11}^{r(a)}(t,t') .$$

$$(6.79)$$

Again multiplying by $e^{i(\varepsilon \mp n\hbar \tilde{\omega}_0)(\tau)}$ and integrating over τ , we obtain after rearrangement

$$\tilde{g}_{1,sk\sigma}^{r(a)}(\varepsilon \mp n\hbar \tilde{\omega}_0) = \left[\frac{\tilde{V}^{\dagger}}{(\varepsilon - \varepsilon_k)}\right] \tilde{g}_{11}^{r(a)}(\varepsilon \mp n\hbar \tilde{\omega}_0) \quad . \tag{6.80}$$

Similarly, we get

$$\tilde{g}_{1,Dk\sigma}^{r(a)}(\varepsilon \mp n\hbar \tilde{\omega}_0) = \left[\frac{\tilde{V}^{\dagger}}{(\varepsilon - \varepsilon_k)}\right] \tilde{g}_{11}^{r(a)}(\varepsilon \mp n\hbar \tilde{\omega}_0) \quad . \tag{6.81}$$

and,

$$i\frac{\partial}{\partial t'}\widetilde{g}_{1,2\sigma}^{r(a)}(t,t') = \mp i\theta(\pm t \mp t')\langle \left\{c_1(t),\left[c_2^{\dagger},\widetilde{H}\right]\right\}\rangle$$

$$= \mp i\theta(\pm t \mp t') \left\langle \left\{ c_1(t), \left[c_k^{\dagger}, \sum_{\sigma} \epsilon_0 c_2^{\dagger} c_2 + \sum_{k\sigma} (\tilde{t} c_1^{\dagger} c_2 + h.c) \right] \right\} \right\rangle$$
(6.82)

$$= \epsilon_0 \tilde{g}_{1,2\sigma}^{r(a)}(t,t') + \tilde{t} \tilde{g}_{11}^{r(a)}(t,t'). \tag{6.83}$$

Again multiplying by $e^{i(\varepsilon \mp n\hbar \tilde{\omega}_0)(\tau)}$ and integrating over τ , we obtain after rearrangement

$$\tilde{g}_{1,2\sigma}^{r(a)}(\varepsilon \mp n\hbar \tilde{\omega}_0) = \left[\frac{\tilde{t}}{(\varepsilon - \epsilon_0)}\right] \tilde{g}_{11}^{r(a)}(\varepsilon \mp n\hbar \tilde{\omega}_0) \qquad (6.84)$$

Now, substituting Eqns. (6.80), (6.81) and (6.84) in Eqn. (6.77) we have $\tilde{g}_{11\downarrow\uparrow}^{r(a)}(\epsilon)$

$$= \frac{\varepsilon - \tilde{\epsilon}_0 \pm \mu_B B - \widetilde{U} < n > -eV_g}{\left(\varepsilon \pm \mu_B B - \widetilde{\epsilon}_0 - \widetilde{U} < n > -eV_g\right) \left(\left(\varepsilon - \widetilde{\epsilon}_0 \pm \mu_B B - \widetilde{U} < n > -eV_g \pm i\Gamma\right)\right) - t^2}.$$
(6.86)

From Eq. (6.86) we can determine greater and lesser Green function using Keldysh equation Eqn. (6.68). From there, the Spectral function can be calculated using relation (6.67), which on substituting in Eq. (6.48) gives us the expression for tunneling current J for symmetric coupling i.e. $\Gamma^L(\epsilon) = \Gamma^R(\epsilon)$,

$$J = \frac{e\Gamma}{h} \left[\int d\epsilon [f_s(\epsilon) - f_D(\epsilon)] A(\epsilon) \right]. \tag{6.48}$$

where $f_S(\varepsilon)$ and $f_D(\varepsilon)$ at zero temperature is give by

$$f_S(\varepsilon) = heaviside\left(\left(eV_m + \frac{eV_b}{2}\right) - \varepsilon\right).$$
 (6.87)

$$f_D(\varepsilon) = heaviside\left(\left(eV_m - \frac{eV_b}{2}\right) - \varepsilon\right).$$
 (6.88)

Using Eqs. (6.48), (6.87) and (6.88) we finally obtain the desired expression for the spectral function and the tunneling current. We also calculate the spin polarization parameter: $P_{\sigma,-\sigma} = (J_{\sigma} - J_{-\sigma})/(J_{\sigma} + J_{-\sigma})$ and the Differential Conductance (DC) which is defined as: G = dJ/dV.

6.3 Results and Discussion

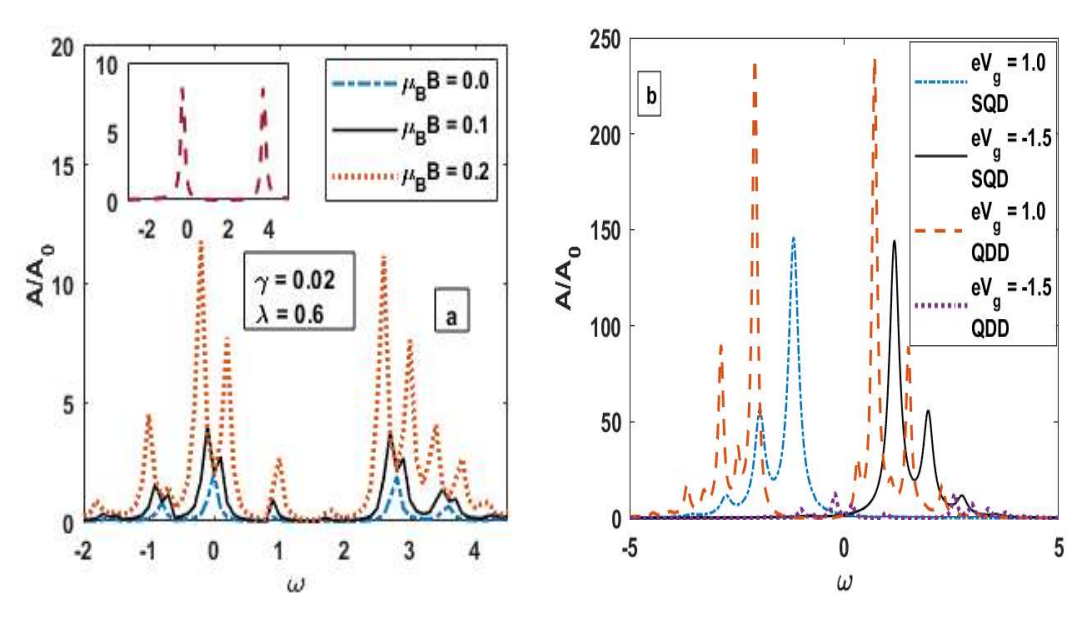


Fig. 6.2. (a) Spectral Function A vs ω for (a) QDD; (b) Comparison of A between QDD and SQD.

0.5 and $eV_m = 0.1$. In Fig. 6.2, the behavior of spectral function (SF) of QDD, is studied when dissipation, magnetic field, el-ph and el-el interaction is present. In the absence of damping effect (γ), B and el-ph interaction we see two lorentzian peaks (inset). When damping effect and electron-phonon interaction are considered, we observe side peaks along with lorentzian peaks due to polaronic effect. As magnetic field is introduced, we see split in theses peaks and as magnetic field increases, we see increase in spectral function. In Fig 6.2(b), comparison between QDD and single quantum dot SQD has been studied for two different gate voltages. The spectral function for QDD is maximum when gate voltage $eV_g = 1$ and minimum when gate voltage $eV_g = -1.5$.

In Fig 6.3, plot for spin resolved spectral function is given. For up-spin, spectral function A_{\uparrow} increases as magnetic field increases Fig 6.3(a) and a left shift in ω -scale is observed. Fig 6.3 (b) shows the spectral function for down-spin A_{\downarrow} . The down-spin SF A_{\downarrow} also increases with increase in magnetic field but comparatively less than A_{\uparrow} . Furthermore, A_{\downarrow} shifts towards right in ω -scale. Also form Fig 6.2 and Fig 6.3, we observe that the spectral function A is the sum of A_{\uparrow} and A_{\downarrow} .

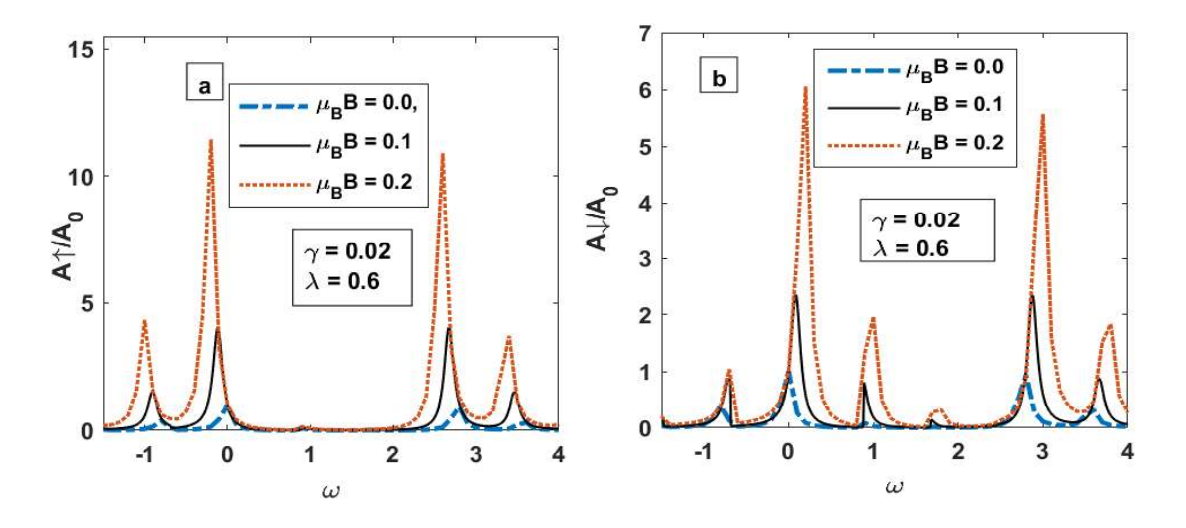


Fig. 6.3. A_↑ and A_↓versus ω for various μ_B B values.

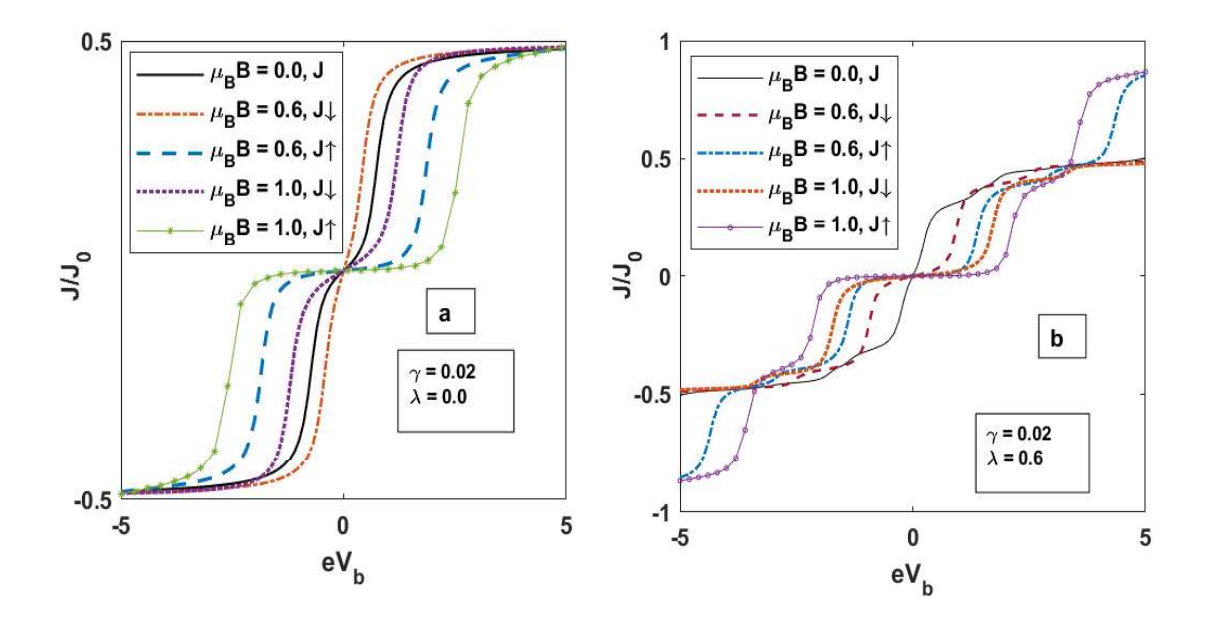


Fig. 6.4 (a) Spin resolved tunneling current $(J_{\uparrow} \text{ and } J_{\downarrow})$ versus bias Voltage V_b for various magnetic field B values when el-ph interaction is absent; (b) J_{\uparrow} and J_{\downarrow} versus V_b for various magnetic field B value when el-ph interaction is present.

In Fig 6.4 (a), up-spin and down-spin tunneling currents are plotted with bias voltage V_b in the absence of el-ph interaction. When B = 0, the tunneling current J has ohmic nature for a finite interval of V_b and saturate afterward. This saturation in J comes with the increase in V_b . As V_b increases, the Fermi level of the source goes up. As a result, more number of electrons flow on to QDs. As QDs can accumulate a fixed number of electrons, the current eventually reaches a saturation value. As B is introduced, the spin degeneracy is lifted and each QD develops energy levels, one for up spin with a lower energy and other for down spin with a higher energy. For $\mu_B B = 0.6$, the down-spin energy level shifts upward, and there exist an easy path for the electrons to tunnel from source to drain and hence J_{\downarrow} has higher value than J. When magnetic field increased to $\mu_B B = 1.0$ the energy level of quantum dot shifts further up, which make QDs energy level approx. equal or greater than the fermi level of source. So a higher

bias voltage is needed for the tunneling of electrons from source to QDs. It's because as bias voltage increases, the source Fermi level moves up and that of the drain moves down. In the case of up-spin current, the energy level for the up spin goes down with increase in magnetic field. So for the tunneling of the up-spin current, the value of bias voltage must be high. As we increase el-ph interaction (Fig 6.4 (b)), the total energy of the system gets renormalized and electrons require higher bias voltage to tunnel. Also, the tunneling current for spin-up electrons turns out to be higher than that of spin-down electrons, indicating a finite probability of hopping of the spin-down electrons to the second quantum dot.

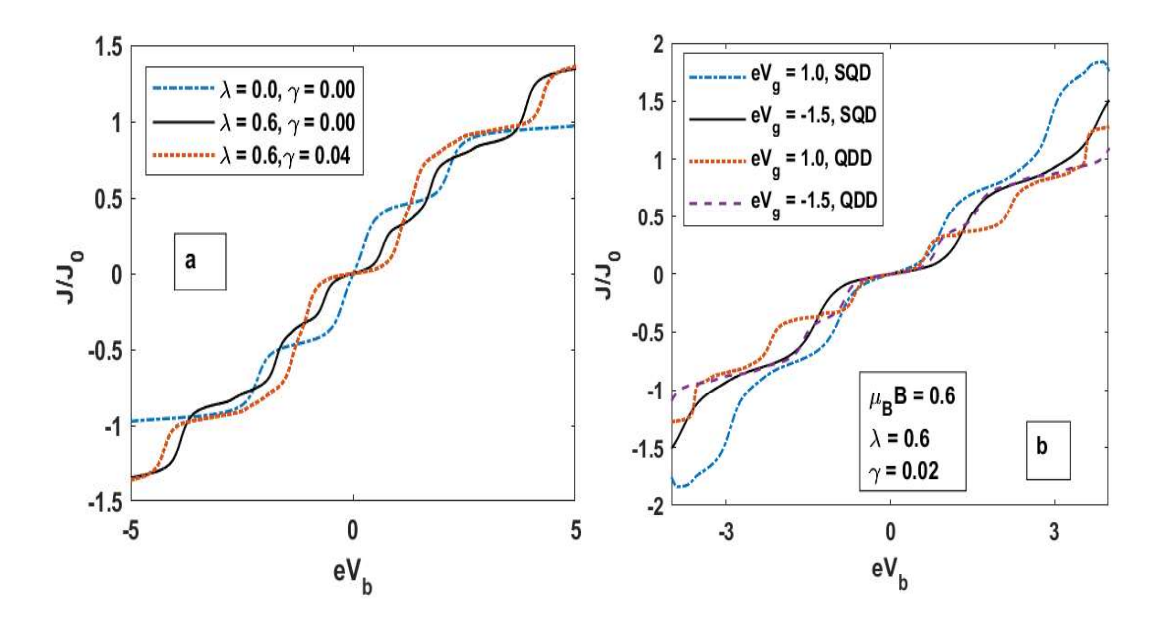


Fig. 6.5. (a) J vs V_b for various λ and γ values; (b) Comparison of J vs V_b —behaviour between SQD and QDD for different values of V_q .

In Fig 6.5(a), the tunneling current J is plotted with the bias voltage eV_b for various values of el-ph and substrate-QDs interaction parameters. As explained above, when el-ph and substrate-QDs interaction are present, the tunneling current is maximum. In Fig. 6.5(b), the comparison of currents J in QDD and

SQD is shown when the magnetic field is present. We observe that the tunneling current in SQD is higher, which shows that the second QD in QDD provides a leakage path for electrons, which reduces the net current.

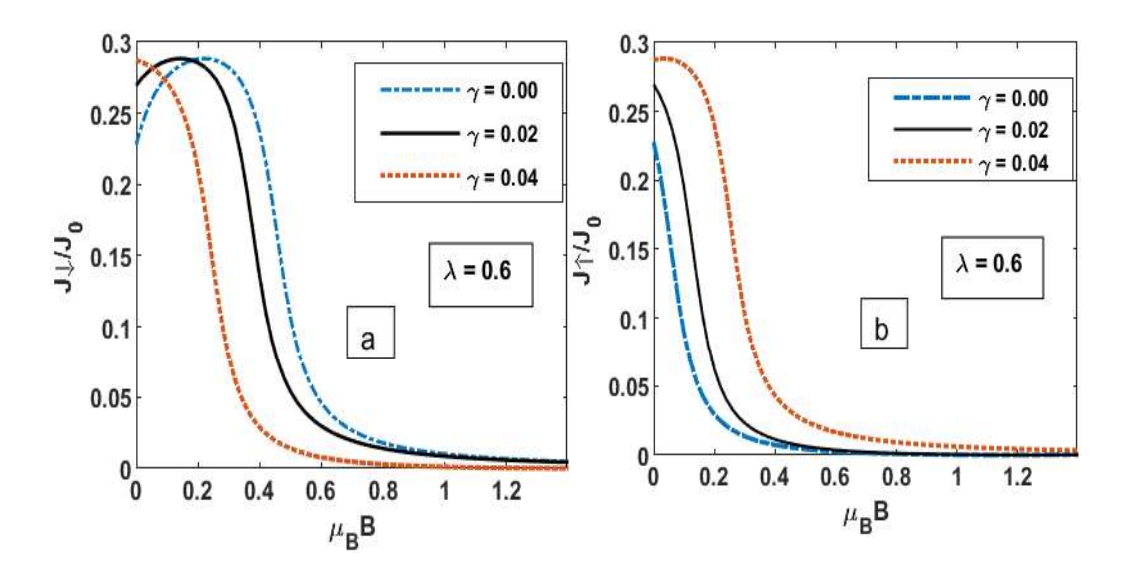


Fig. 6.6 (a) J_{\downarrow} versus B for various γ values; (b) J_{\uparrow} versus B for various γ values.

In Fig 6.6, Spin-dependent tunneling currents (J_1 and J_1) with the magnetic field are plotted for various damping constant values. In the absence of QDs-substrate interaction, the down-spin tunneling current J_1 reaches a maximum value and starts decreasing afterward. This behavior is understandable. As explained above, when the B is small, the energy level of the down-spin state and the source Fermi level are nearly equal, giving rise to the current. As the magnetic field increases, the energy levels of the QDs move up, causing a decrease in the current (Fig 6.6 (a)). In the case of up-spin current (Fig 6.6(b)), the energy level of the up-spin state moves down when the magnetic field is tuned, and it becomes difficult for the electrons to tunnel from QDs to drain. As the substrate-QDs interactions are introduced, the energy levels of QDs are renormalized. To be more specific, the up and down-spin state's energy levels move higher, causing an increase in the up-spin tunneling current and a decrease in the down-spin tunneling current.

In the present problem, we have neglected the inter-dot el-el interaction, and considered only the intra-dot el-el interactions. The tunneling current with respect to el-el interaction shows initial peaks for weak el-el interaction strength and zero magnetic field. For stronger el-el interaction strength, the tunneling current is almost constant.

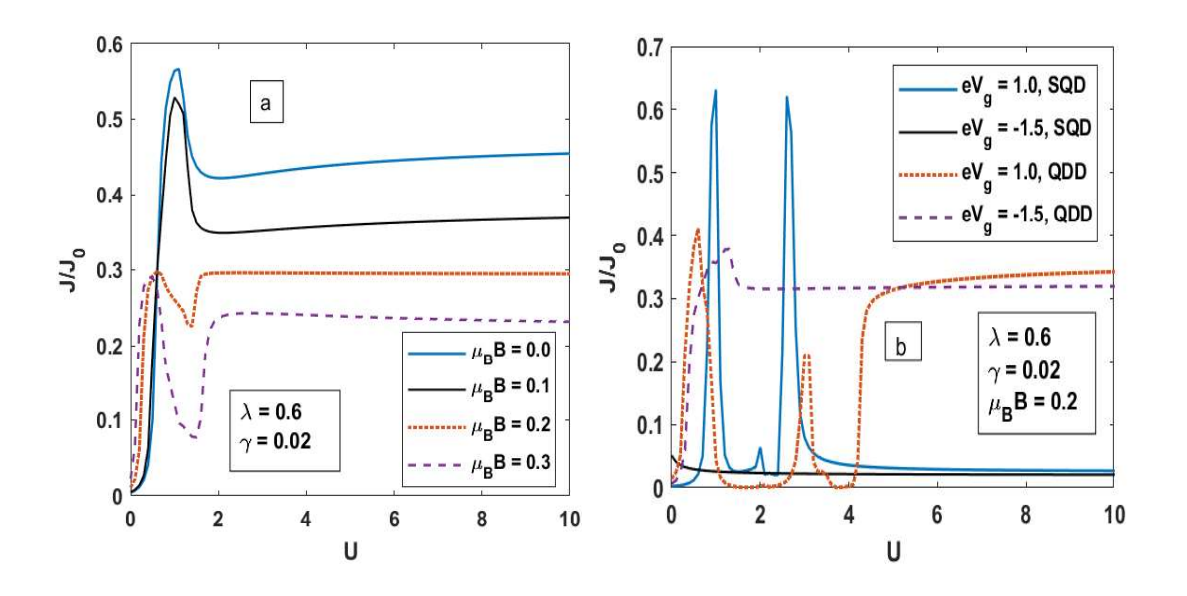


Fig. 6.7 J versus U for various B values; (b) Comparison of J vs U — behaviour between SQD and QDD for different values of V_g .

As magnetic field exceeds a certain value, a minimum is observed in J after the maximum. This minimum becomes lower as B is increased. After the minimum, the current of course increases with U and attains a constant value (Fig 6.7(a)). This constant value is lower for a higher magnetic field. Fig 6.7(b), shows the J vs U —behaviour in QDD is compared with that in SQD for different gate voltage values. For $eV_g = 1$, we observe peaks in SQD at weak el-el interaction. As U increases, J acquires a constant value. A similar behavior is shown by QDD but now the peaks are smaller but J saturates to a higher value. For $eV_g = -1.5$, in SQD, J decreases monotonically with increasing U and saturates to a constant while QDD first shows a peak and then decreases to a constant value.

Fig 6.8, shows plot of J with V_g for various λ and γ values. We see peaks for both negative and positive values of gate voltage. When we increase el-ph interaction, the peaks reduce and when the substrate-QDs interactions are considered along with el-ph interaction, the peaks shift towards right. In Fig 6.8 (b) we compare the behaviour in SQD with that in QDD for different values of B. When B = 0, J has only one peak for SQD and two peaks for QDD. For a finite magnetic field, J has more peaks with reduced height because of splitting caused by magnetic field. Also the peaks in SQD are higher than QDD

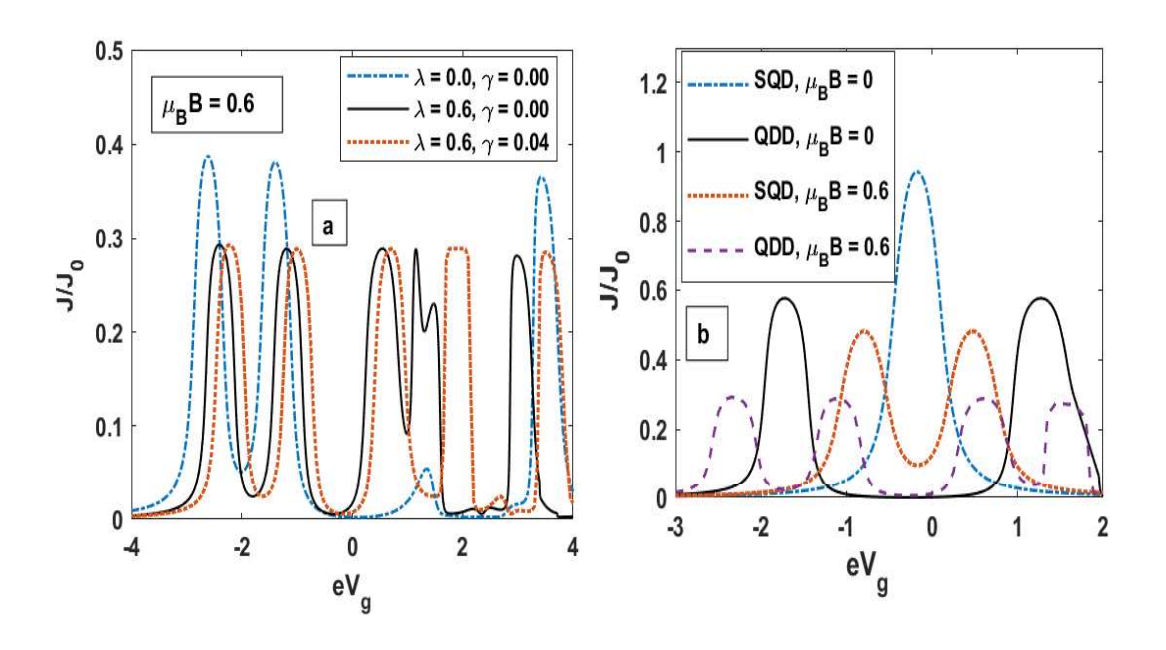


Fig. 6.8 J vs V_g for various λ and γ values; (b) Comparison of J vs V_b —behaviour between SQD and QDD for various B values.

. In Fig 6.9, J_{\uparrow} and J_{\downarrow} are plotted versus λ for a few values of B. There are two ways in which el-ph interaction affects the system. Firstly, it lowers the energy of the system, which favors the current flow and secondly it reduces the mobility of the electron because of polaron formation. Mathematically, because of the factor $\lambda^2 e^{-\lambda^2}$, we can see Gaussian like behavior of tunneling current when

magnetic field is absent. When magnetic field is present, the degeneracy in spin is removed and the current flows with a specific spin direction through two subbands. When the el-ph interaction is weak, down-spin current is high and electrons can easily go from the source to the drain. As the el-ph interaction increases, the polaronic effect also increases, which reduces the mobility of electrons, causing a decrease in the current. Tunneling current for up spin is low initially, but with the increase electron-phonon effect current increases. This is understandable because with increase in electron-phonon interaction the energy level of up spin increases and overcome polaronic effect. So for an interval, we see rise in tunneling current, afterwards polaronic effect dominates again and up spin tunneling current decreases which reduces the current flow

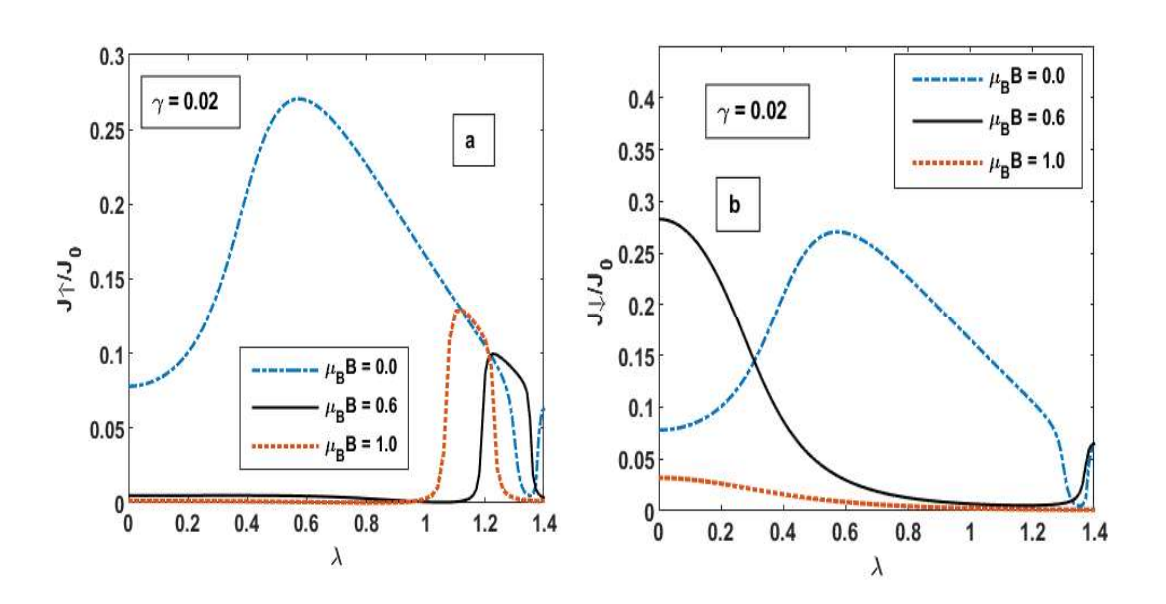


Fig. 6.9 (a) J_{\downarrow} vs λ for various *B* values; (b) J_{\uparrow} vs λ for various *B* values.

In Fig 6.10, three-dimensional plots of J with λ and γ are given for B=0 and $B \neq 0$. For B=0, J shows a maxima at a certain λ value (Fig 6.10(a)). For $B \neq 0$, the curve is a little flattened and J shows lower values (Fig 6.10(b)).

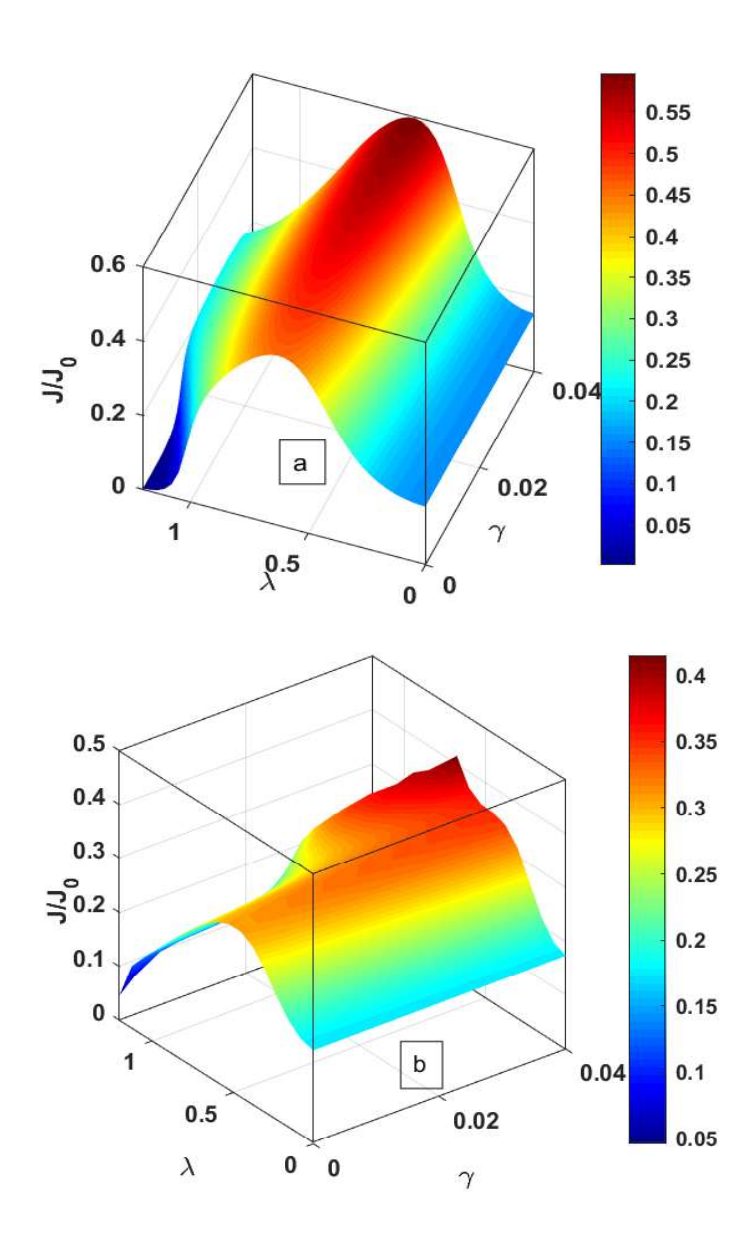


Fig. 6.10. Three-dimentional plot of J in $(\lambda - \gamma)$ – plane for: (a) B = 0; (b) $B \neq 0$.

In Fig. 6.11, contour plots of J in the $(V_m - V_b)$ – plane are given for various sets of U and B values. When both B = 0 and U = 0, J shows a smooth behaviour (Fig 6.11(a)). As el-el interaction is introduced, deformation in the contour plot can be seen for postive values of V_m and higher values of V_b (Fig 6.11(b)). For $B \neq 0$ and U = 0, we can observe the split which shows the splitting because of

magnetic field(Fig 6.11(c)) When both are non zero B and U are non-zero, both splitting and deformation occur in the contour plot at higher values of V_m and V_b (Fig 6.11(d)).

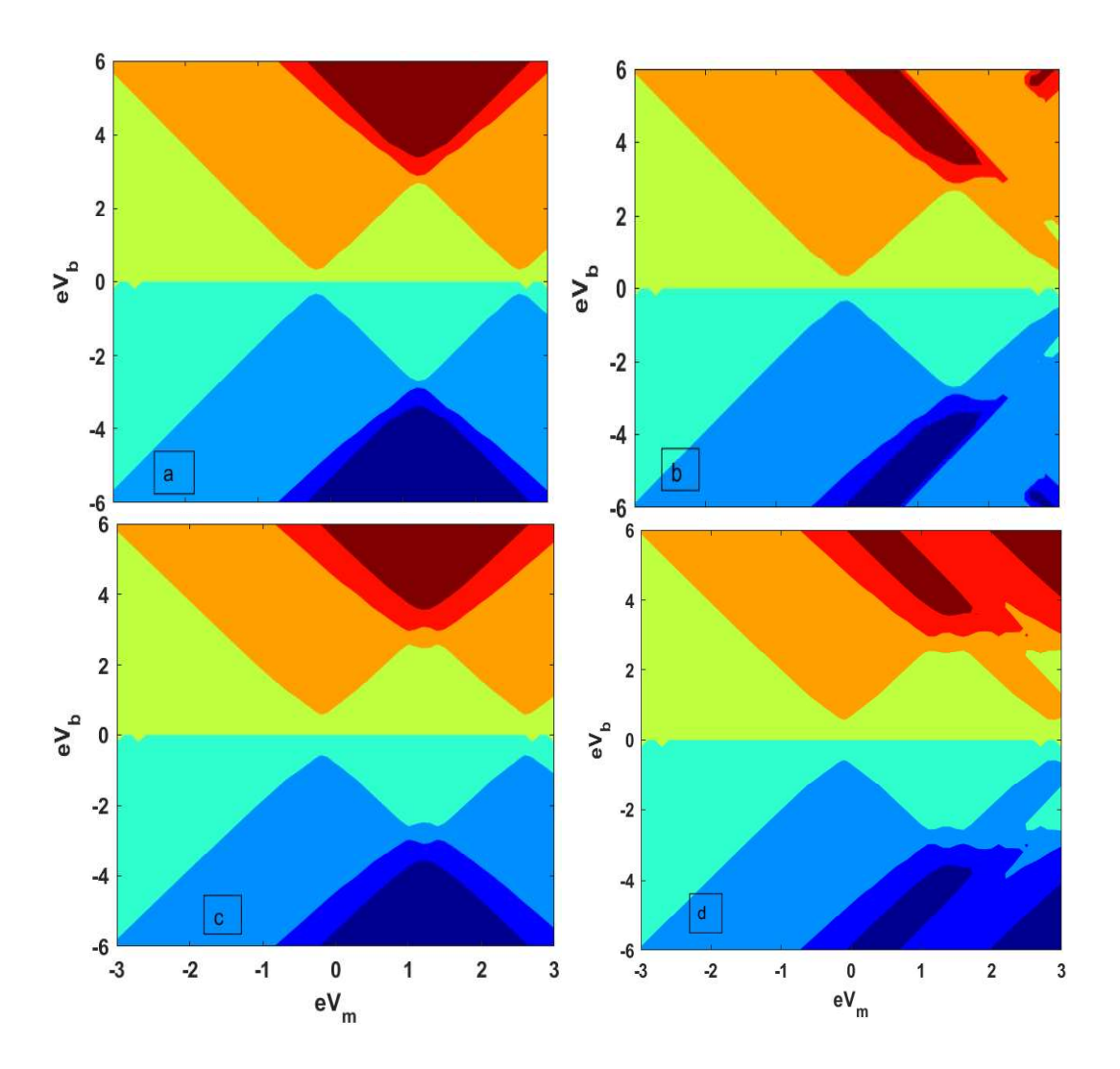


Fig. 6.11. Contour plot of tunneling current (J) in eV_m and eV_b —plane (a) when magnetic field and electron-electron interaction is absent ($\mu_B B = 0$, U = 0), (b) when magnetic field is absent and electron-electron interaction is present ($\mu_B B = 0$, $U \neq 0$) (c) when magnetic field is present and electron-electron interaction is absent ($\mu_B B \neq 0$, U = 0);(d) when magnetic field and electron-electron interaction is present ($\mu_B B \neq 0$, $U \neq 0$).

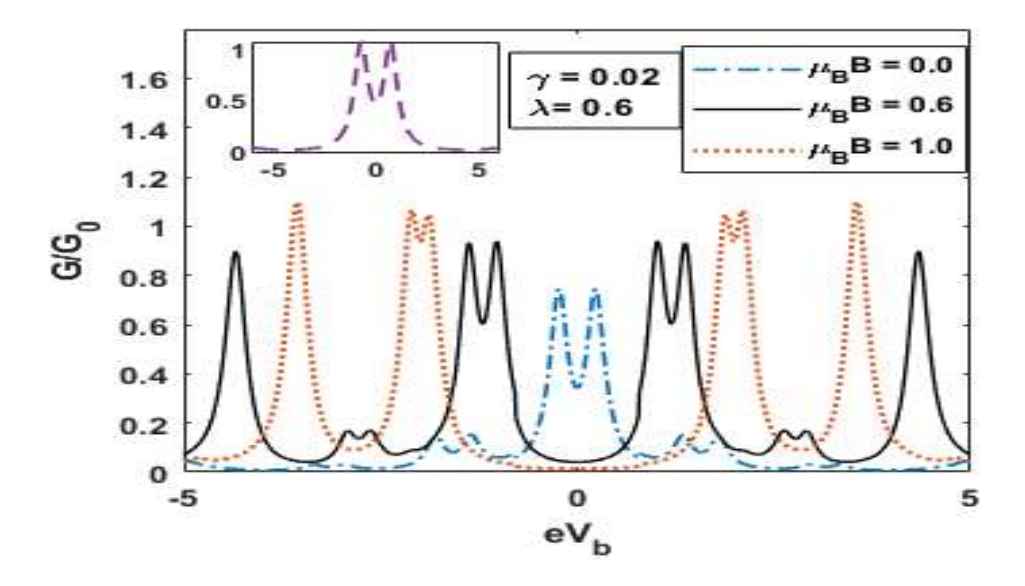


Fig. 6.12 Differential Conductance (G) versus V_b for different value of B.

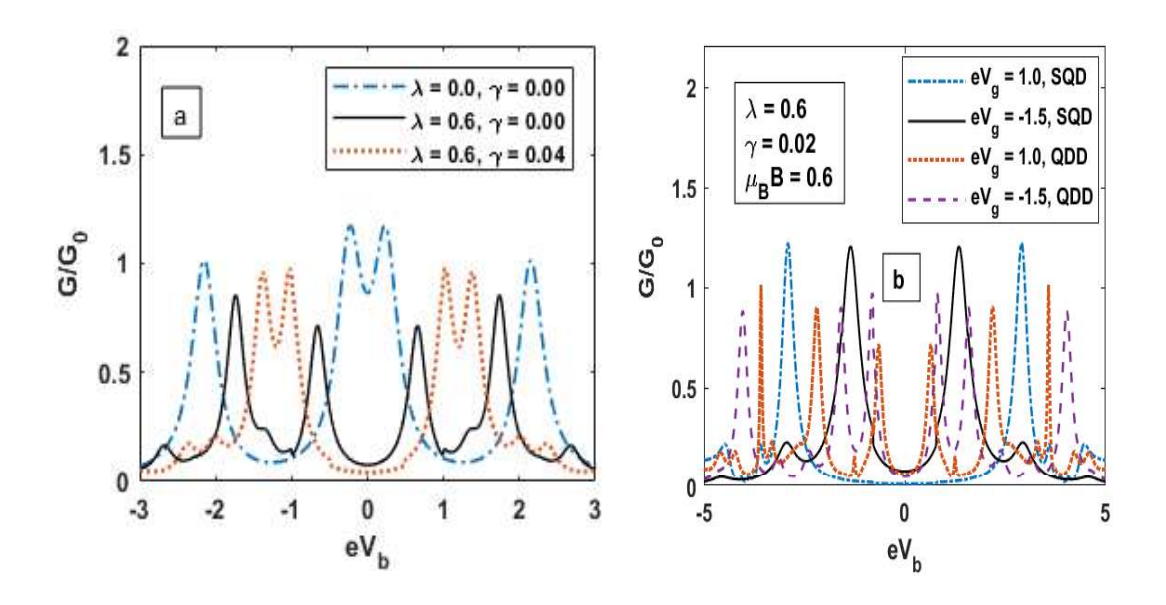


Fig. 6.13 G versus V_b for various λ and γ values (b) Comparison of G vs V_b – behaviour between SQD and QDD for various V_g values

In Fig 6.12, the behavior of Differential Conductance (DC) (G) with respect to V_b is given. For $\lambda = 0$, $\gamma = 0$ and B = 0, DC shows two peaks, which indicate the possible excitation in the system in this case (inset). These peaks are modified

along with some side peaks for the finite value of λ , γ and $\mu_B B = 0$. As a magnetic field is introduced, each peak splits. As we further increase the magnetic field, DC peaks go higher, causing an increase in DC.

In Fig. 6.13, we plot DC with bias voltage V_b. When substrate –QDs and el-ph interactions is absent, we encounter two peaks. As el-ph interaction is introduced, the peak height reduces and the space between them increases. The space between peaks further increases Fig 6.13(a)). When substrate- QDs is introduced .Fig. 6.13(b) shows that SQD peaks are much higher than QDD peaks. Also as the gate voltage increases, peaks in the case of SQD move further apart, while in the case of QDD, they come close.

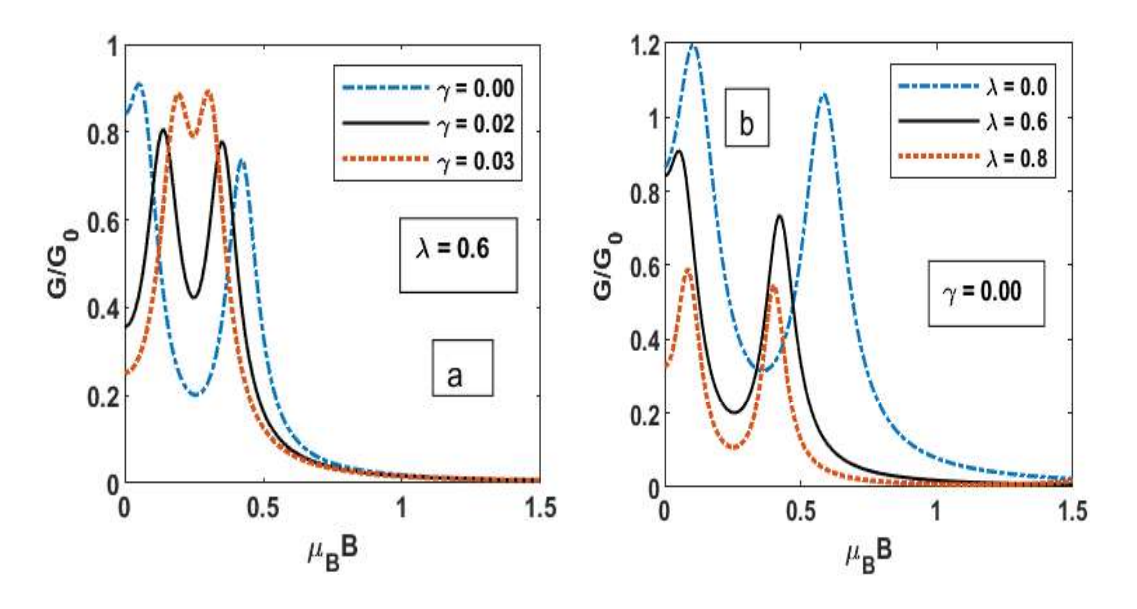


Fig. 6.14 G versus B for various: (a) λ values; (b) B for various γ values.

Fig 6.14 gives the variation of DC with respect to magnetic field. For $\gamma = 0$, DC has two uneven peaks. These peaks signify the contribution of up-spin and down-spin charges (see Fig 6.15). As γ increases, the peak heights arising from the two contributions become almost equal. We can see similar behaviour for different values of λ , when γ is absent (Fig. 6.14(b)).

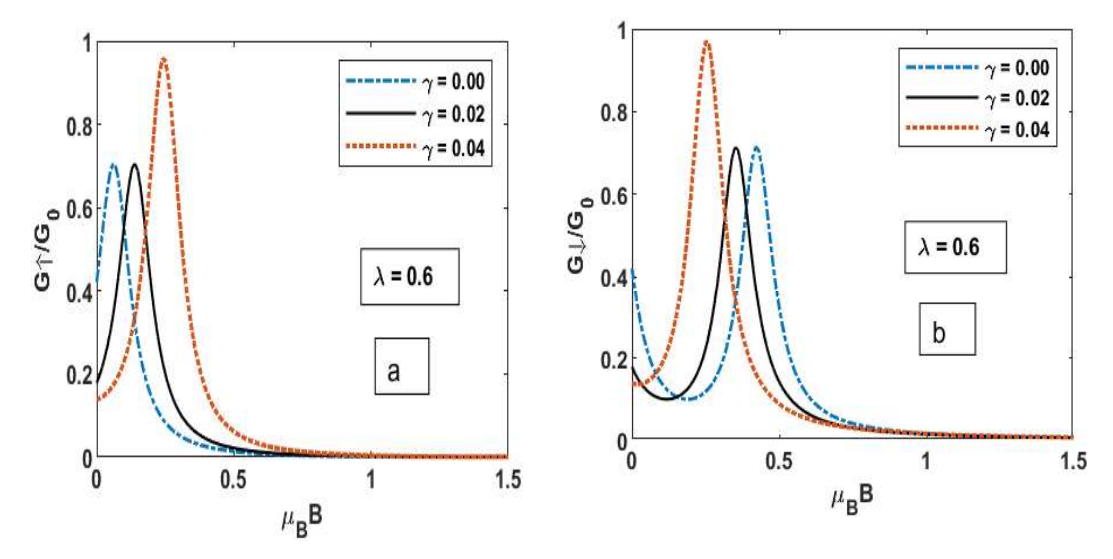


Fig. 6.15 (a,b) Spin resolved (G_{\downarrow} and G_{\uparrow})Differential Conductance versus B for various γ values.

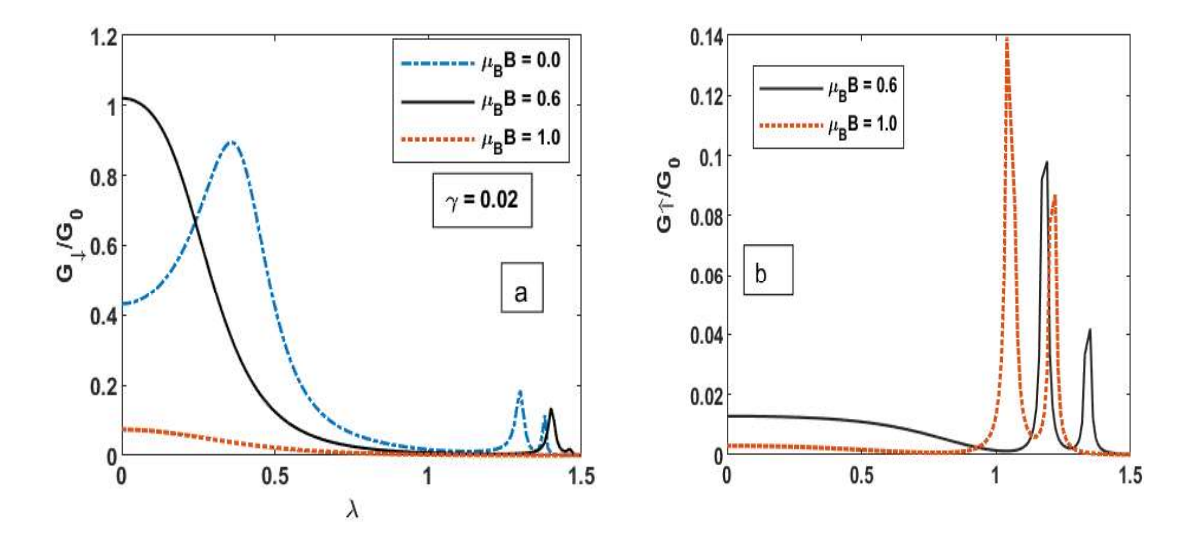


Fig. 6.16 (a,b) J_{\downarrow} and J_{\uparrow} versus λ for different magnetic field value ($\mu_B B$).

In Fig 6.16, spin polarized Differential Conductance is plotted with el-ph interaction for various values of the magnetic field. DC for spin- down electrons shows higher peaks for the lower value of electron-phonon interaction, for higher value of λ peaks are smaller. In case of up-spin there are no initial peaks, peaks can be observed only higher values of λ .

Fig. 6.17 give the plot of three-dimentional DC with respect to λ and γ . The nature of the plot is quite similar to the tunneling current case (Fig 6.10). for $B \neq 0$, DC shows two maxima, which arises due to the contribution of up and down spin electrons.

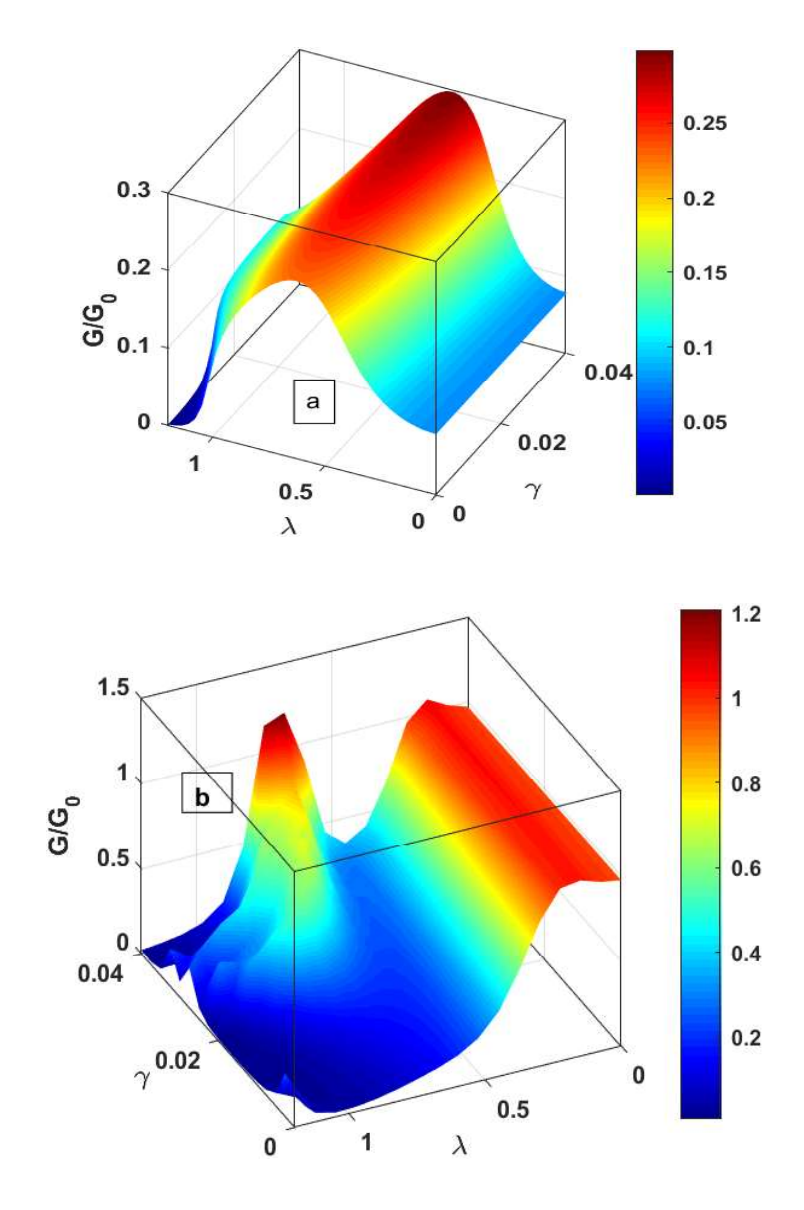


Fig. 6.17 Three-dimentional plot of DC (G) in λ and γ — plane for : (a) B=0; (b) $B\neq 0$.

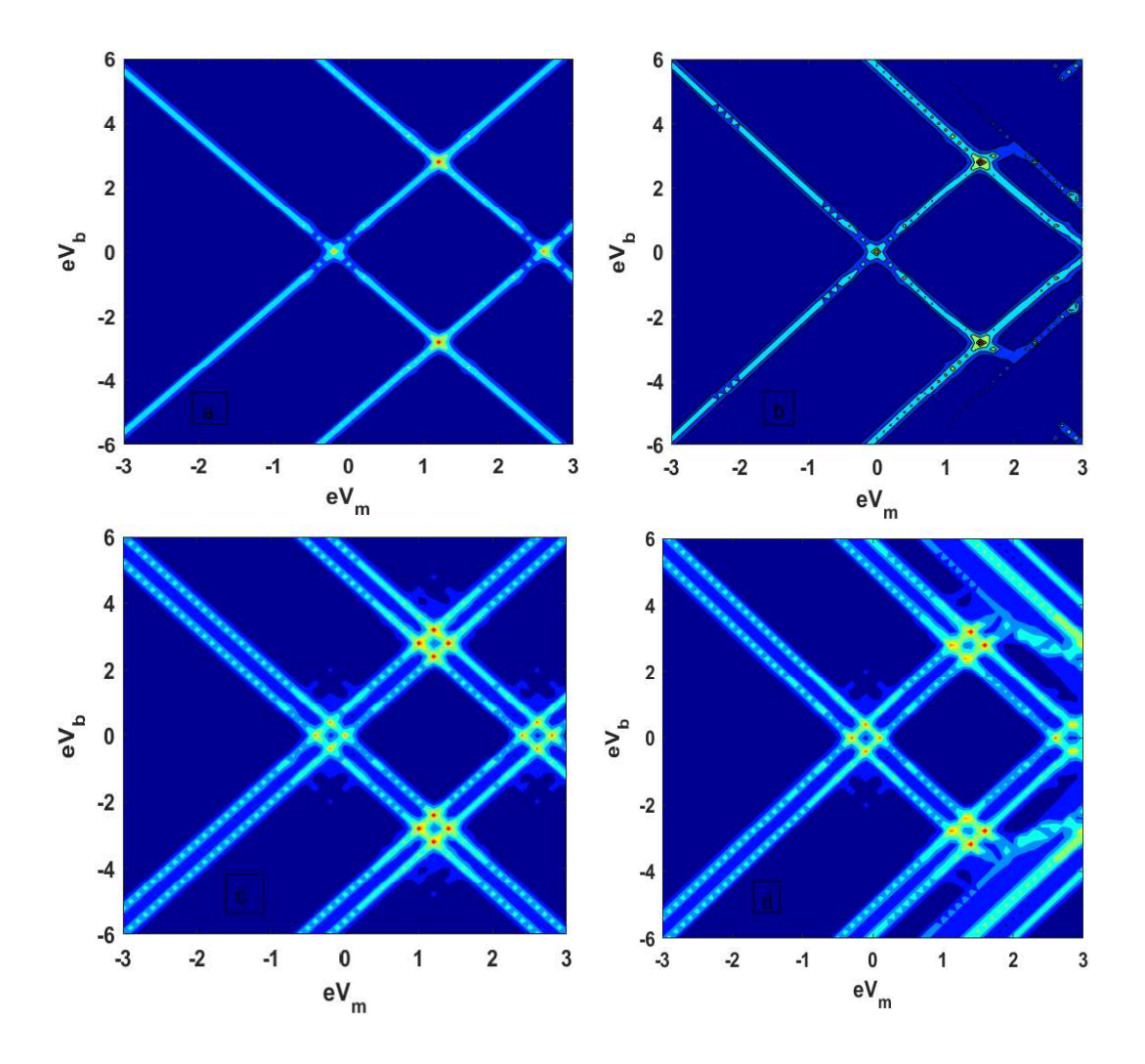


Fig. 6.18. Contour plot of Differential Conductance (G) in eV_m and eV_b —plane (a) when magnetic field and electron-electron interaction is absent ($\mu_B B = 0$, U = 0), (b) when magnetic field is absent and electron-electron interaction is present ($\mu_B B = 0$, $U \neq 0$) (c) when magnetic field is present and electron-electron interaction is absent ($\mu_B B \neq 0$, U = 0);(d) when magnetic field and electron-electron interaction is present ($\mu_B B \neq 0$, $U \neq 0$).

Fig. 6.18 gives the contour plot of DC in the in $(V_m - V_b)$ -plane. When B = 0 and U = 0, DC is smooth everywhere (Fig 6.18(a)). In presence of electron-electron interaction, when magnetic field is zero, we see deformation in higher value of bias voltage and mid voltage Fig 6.18(b). If magnetic field is present, we see a split in lines, which manifest contibution of both up and down spin Fig 6.18(c).

Again when electron-electron interaction and magnetic field is present we have both splitting and distortion in contour Fig 6.18 (d)

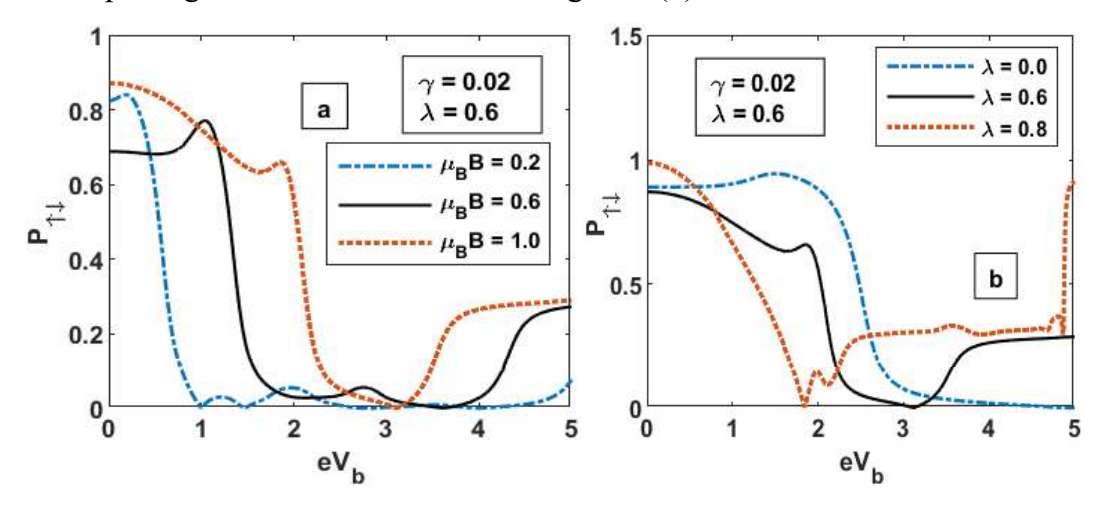


Fig. 6.19. Spin polarization $(P_{\uparrow\downarrow})$ versus V_b for few: (a) B; (b) λ values.

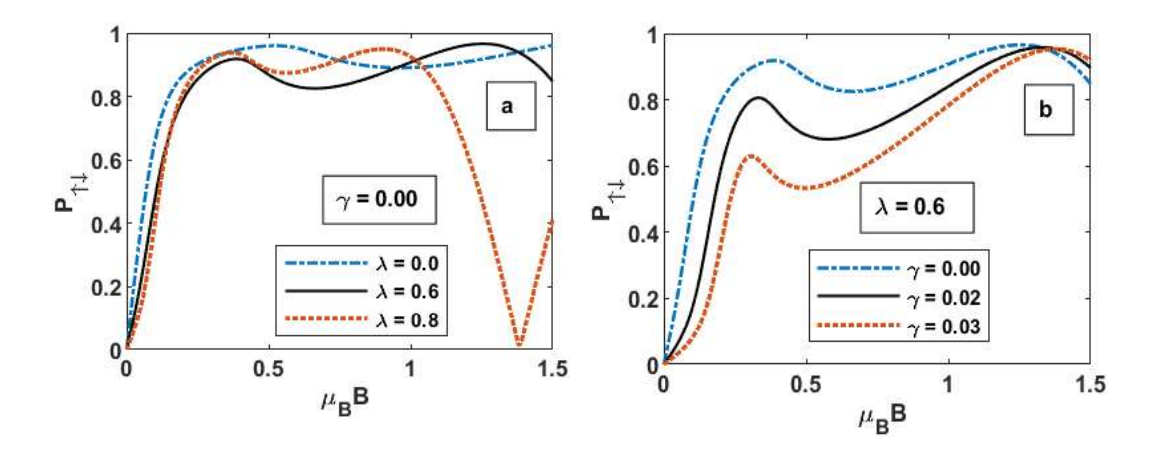


Fig. 6.20. $P_{\uparrow\downarrow}$ versus *B* for few: (a) λ .; (b) γ values.

In Fig 6.19 we have studied spin polarization (SP) with V_b for several B and λ values. The nature of spin polarization can be predicted from Fig (6.4, 6.5) where we have studied the variation of up-spin and down-spin tunneling current. The variation of SP with V_b depends on B and λ . When B is small, SP decreases for a smaller value of bias voltage and remains almost zero for a finite interval of bias

voltage. Though for higher bias voltage values, it again starts increasing. As we increase B, SP decreases for higher bias voltage. And the interval in which SP is zero also reduces Fig 6.19(a). When studying for various el-ph strength values Fig 6.19(b), we observe that with the increase λ , SP reaches minima for lower bias voltage value. And afterward, as bias voltage increases, SP starts increasing. SP vs B is plot is shown in Fig 6.20 for various (a) λ .; and (b) γ values. SP initially increases, attains maxima for two different magnetic field values, and finally falls off to zero. As λ increases, peaks seem to come closer and zero for lower B values (Fig 6.20(a). For various γ values, Fig 6.20(b), the initial peak decreases with increases in γ , though the secondary peak remain unaffected.

6.4 Conclusion

In this chapter, we have presented our work on the non-equilibrium transport through a QD dimar which is mounted on a dissipative and is connected to a source and a drain and the transport is studied in the presence of magnetic field, substate-QDs interaction, el-el and el-ph interaction. The model is studied using Anderson-Holstein-Caldeira-Leggett Hamiltonian (AHCL) and the tunneling Current density (1), spin polarization parameter, differential conductance and spectral function are calculated using the Keldysh Green function formalism. When magnetic field is present, the spin degeneracy is lifted, leading to a split in energy levels and the spectral function of QDs. When both damping and el-ph interaction are present, the ground state energy gets renormalized and we observe a higher value of the spectral function and tunneling current for the spin-up electrons, indicating a finite probability of the spin-down electrons hopping to the second QD. In the plots of differential conductance (G), we again observe a split when magnetic field is present. We also observe that the peak height increases as the magnetic field increases. When compared with SQD, we find that that the current and DC is higher in case of SQD which shows that the second QD in QDD

provides a leakage path for electrons. Finally, the spin polarization coefficient is calculated for QDD as a function of V_b and B. We find that spin polarization increases with increase in magnetic field and have higher value for low bias voltage. We have aslo shown the variation of J and G with el-ph interaction and mid voltage. The above model may be important for making more complicated devices and there functioning.

6.5 References

- C. Joachim, J. K. Gimzewski, R. R. Schlittler, and C. Chavy, Phys. Rev.Lett. 74, 2102 (1995); J. K. Gimzewski and C. Joachim, Science 283, 1683(1999).
- 2. A. Yazdani, D. M. Eigler, and N. Lang, Science 272, 1921 (1996).
- 3. S. Tans, A. Verschueren, and C. Dekker, Nature (London) **393**, 49 (1998).
- 4. J. W. G. Wild€oer, L. C. Venema, A. G. Rinzler, R. E. Smalley, and C. Dekker, Nature (London) **391**, 59 (1998); D. Porath, A. Bezryadin,
- S. de Vries, and C. Dekker, Nature (London) **403**, 635 (2000).
- M. A. Reed, C. Zhou, C. J. Muller, T. P. Burgin, and J. M. Tour, Science 278, 252 (1997); J. Chen, M. A. Reed, A. M. Rawlett, and J. M. Tour, Science 286, 1550 (1999).
- Y. Xue, S. Datta, S. Hong, R. Reifenberger, J. I. Henderson, and C. P.Kubiak, Phys. Rev. B 59, R7852 (1999).
- 7. Ma, Sh. Guan, and C.-H. Lai, Phys. Rev. B **74**, 205401 (2006)
- 8. Abdelghaffar, N., Aïmen, B., Bilel, H., Wassim, K. & Adel, K. 18, 1558–1748 (2018).
- 9. Makoto, Y. et al. Sci. Rep 7, 1589 (2017).
- 10. Chen, Z. Z., Lu, H., Lü, R. & Zhu, B. F. *J. Phys.: Condens. Matter* **18**, 5435–5446 (2006).

- 11. Gonzalez, G., Leuenberger, M. N. & Mucciolo E. R. *Phys. Rev. B* **78**, 054445–12 (2008).
- Klein, D. L., Roth, R., Lim, A. K. L., Alivisatos, A. P. & McEuen, P. L. *Nature* 389, 699–701 (1997).
- Pipit, U. V., Yasuo, A., Masanori, S., Toshiharu, T. & Yutaka,
 M. Mater. Res. Express 4, 024004 (2017).
- 14. Goldhaber-Gordon, D. et al. Nature 391, 156–159 (1998).
- 15. Ho, W. J. Chem. Phys. 117, 11033-11061 (2002).
- 16. Yu, L. H. & Natelson, D. Nano Lett. 4, 79-83 (2003).
- 17. K Kobayashi, H Aikawa, S Katusmoto and Y Iye, Phys.Rev. Lett. **88**, 1 (2002)
- 18. PAOrellana,ML Ladron de Guevera and FClaro, Phys.Rev. B **70**, 233315 (2004)
- 19. ML Ladron de Guevara, F Carlo and PAOrellana, Phys.Rev. B **67**, 195335 (2003)
- 20. J D Pillet, C H L Quay, P Morfin, C Bena, A Levy Yeyati and P Joyez, Nat. Phys. **6**, 965 (2010)
- 21. S De Franceschi, LKouwenhoven, C Schonenberger and W Wernsdorfer, Nat. Nanotechnol. **5**, 703 (2010)
- 22. G Rajput, R Kumar and Ajay, Superlatt. Microstruct. 73, 193 (2014)
- 23. T Vorrath and T Brandes, Phys. Rev. B **68**, 035309(2003)
- 24. E Vernek, P A Orellana and S E Ulloa, Phys. Rev. B **82**,165304 (2010)
- 25. Heeger, A. J., Kivelson, S., Schrieffer, J. R. & Su, W. P.Rev. Mod. Phys. **60**, 781–850 (1988).
- 26. Koch, T., Loos, J., Alvermann, A., Bishop, A. R. & Fehske. J. Phys.: Conf. Ser. **220**, 012014–9 (2010).
- 27. Loos, J., Koch, T., Alvermann, A., Bishop, A. R. & Fehske, J. Phys.: Condens. Matter. **21**, 395601–18 (2009).
- 28. Paaske, J. & FlensbergPhys. Rev. Lett, **94**, 176801–4 (2005)
- 29. Park, H. et al. Nature **407**, 57–60 (2000)

- 30. Lüffe, M. C., Koch, J. & von Oppen, F. Phys. Rev. B 77, 125306–7 (2008).
- 31. Braig, S. & Flensberg, K. Phys. Rev. B 68, 205324–10 (2003).
- 32. Chen, Z. Z., Lü, R. & Zhu, B. F. Phys. Rev. B 71, 165324–9 (2005).
- 33. Meir, Y., Wingreen, N. S. & Lee, P. A. *Phys. Rev. Lett.* **70**, 2601 (1993)
- 34. Wingreen, N. S. & Meir, Y.Phys. Rev. B 49, 11 040 (1994).
- 35. Hewson, A. C. & Meyer, D. J. Phys. Cond. Matter 14, 427 (2002).
- 36. Jeon, G. S., Park, T. H. & Choi, H. Y. Phys. Rev. B 68, 045106 (2003).
- 37. Khedri, A., Costi, T. A. & Meden, V. Phys. Rev. B 96, 195155 (2017).
- 38. Khedri, A., Costi, T. A. & Meden, V. Phys. Rev. B **96**, 195156 (2017).
- 39. Khedri, A., Costi, T. A. & Meden, V. Phys. Rev.B **98**, 195138 (2018).
- 40. Boese, D. & Schoeller, H. Europhys. Lett. 54, 668 (2001)
- 41. McCarthy, K. D., Prokof'ev, N. & Tuominen, M. T. *Phys. Rev. B* **67**, 245415–6 (2003)
- 42. Mitra, A., Aleiner, I. & Millis, A. Phys. Rev. B 69, 245302–21 (2004).
- 43. Keldysh., L. V. Sov. Phys. JETP 20, 1018–1026 (1965).
- 44. Datta, S. Electronic Transport in Mesoscopic Systems. (Cambridge University Press, 1997).
- 45. Haug, H. & Jauho, A. P. Quantum Kinetics in Transport and Optics of Semiconductors (Springer, 1996).
- 46. Song, J., Sun, Q. F., Gao, J. & Xie, X. C. Phys. Rev B. **75**, 195320 (2007).
- 47. Datta, S. Quantum Transport: Atom to Transistor. (Cambridge University Press, 2005).
- 48. Narasimha, R. C. & Ashok, C. Scientific Reports 6, 18511 (2016).
- 49. Costi., T. A. Phys. Rev. B **64**, 241310(R) (2001).
- 50. Bing, D. & Lei, X. L. Phys. Rev. B **63**, 235306 (2001).
- 51. Kalla, M., Chebrolu, N. R. & Chatterjee, A. Sci. Rep. 9, 16510 (2019)
- 52. Cornaglia, P. S. & Grempel, D. R. Phys. Rev. B 71, 245326–6 (2005).
- 53. Hui, P. Phys. scr. **78**, 065703 (2008).

- 54. Lang, I. G. & Firsov, Y. A.. Sov. Phys. JETP 16, 1301 (1962).
- 55. K. Kawamura and T. Aono, Jpn. J. Appl. Phys., Part 1 36, 3951 (1997).
- 56. G. D. Mahan, Many-Particle Physics, 3rd ed. sPlenum Press, New York, (2000).
- 57. Jauho, A. P., Wingreen, N. S. & Meir, Y. *Phys. Rev. B* **50**, 5528–5544 (1994).
- 58. Meir, Y., Wingreen, N. S. & Lee, P. A. Phys. Rev. Lett. **66**, 3048 (1991).
- 59. Swirkowicz, R. et al. Phys. Rev. B 68, 195318 (2003).

CHAPTER 7

Conclusion

In chapter 1, we define some basic terminology of spintronics and single molecular transistor, along with their principal of working and applications. In chapter 2, we have studied the Rashba spin-orbit interaction effect on the spin and charge transport for a two-dimensional tight-binding electronic system when randomized impurities are present. There we used Matsubara green's function technique and computed a lower-order Feynman diagram to calculate the relaxation time from impurity-electron scattering events and calculated spin and charge conductivity, using Kubo formalism. We worked in a low temperature and impurity regime to better understand the system. Our findings predict that concerning the chemical potential u, longitudinal charge, and spin conductivities along with relaxation time display a peak, at some critical value of chemical potential µ. Beyond that critical value, the decrease in relaxation time with chemical potential is relatively slow, though the corresponding depletion in charge conductivity and spin conductivity will be much faster. We have also shown that the spin conductivity peaks are much higher than the charge conductivity peaks. These peaks increase with the RSOI effect for spin conductivity and charge conductivity and decrease with an increase in impurity strength. Though, the peak value remains unchanged in the case of relaxation time, when RSOI is changed. Further, we have shown in chapter 2 that spin conductivity, charge conductivity, and relaxation time increase with RSOI interaction and decrease in the presence of impurities.

In continuation with chapter 2, in chapter 3, along with Rashba, we have taken Dresselhaus spin-orbit interaction term and examined how the interplay between both spin-orbit interactions affects the system when randomized impurities are present. We used Matsubara green's function technique and computed a lower-order Feynman diagram to calculate the relaxation time caused by impurity-electron scattering. To calculate spin and charge conductivity, we have used Kubo formalism similar to chapter 2. Our finding in chapter 3 shows that for all Rashba and Dresselhaus strength values, charge and spin conductivity along with relaxation time as a function of chemical potential exhibits peaks. The charge conductivity with Rashba strength increases with an increase in Dresselhaus strength. In contrast, the spin conductivity with Rashba strength decreases with an increase in Dresselhaus strength. It has also been shown that spin conductivity is zero whenever Rashba and Dresselhaus strength become equal. Furthermore, we have also seen that spin to charge ratio with Rashba strength decreases until the Dresselhaus strength equates to Rashba strength; afterward, spin to charge ratio increases with Rashba strength.

In chapter 4, we have calculated spin Hall conductivity and spin Hall angle at zero temperature. Our results propose that SHC displays peak when studied with chemical potential, and the value of these peaks decreases with increasing DSOI strength, as DSOI strength broaden the energy bands. A similar observation was seen when SHC is investigated as a function of RSOI.

We have also shown that in the presence of both SOI effects, SHC almost remains unaffected with low impurity and decreases when impurity strength is high. Also, SHC is maximum when the difference between the strength of RSOI and DSOI increases.

Conclusively, we have calculated the spin to charge ratio. We have shown that if any one of the following SOI dominates (RSOI or DSOI), the ratio increases, and as both SOI coupling become equal in strength, the ratio goes to zero.

In chapter 5, we further study SOI effect on the torque dependent longitudinal and transverse spin conductivity and spin hall angle at finite temperature in the

presence of impurity using formalism similar to chapter 2, 3 and 4. Our finding in the following chapter shows that LCC, LSC, and SHC all display peak structure as a chemical potential function for finite temperature. The peak value of conductivities decreases with an increase in DSOI strength, as DSOI strength triggers more scattering events.

From the finding of chapters 2 and 3, we knew that LSC and LCC increase monotonically with RSOI strength at T = 0 K. However, they seem to saturate to some constant value when, the DSOI effect is absent at finite temperature. In the presence of DSOI strength, we see a downturn nature, i.e., conductivities start decreasing after a certain point. This downturn effect increases with an increase in DSOI strength. For SHC, we found that the downturn nature is present in the presence or absence of temperature and DSOI. We have also observed that the rate at which LSC and SHC decrease with impurity strength depends on RSOI and DSOI strength differences.

Finally, in chapter 5, we have shown that the spin to charge ratio increases when the difference between RSOI and DSOI increases. And the ratio is zero when both RSOI and DSOI strength become equal.

In chapter 6, we investigate magneto-transport through a quantum dot dimer placed on a substrate, when electron-phonon interaction, electron-electron interaction magnetic field, and substrate- quantum dot interaction is present. The model is analyzed using Anderson-Holstein-Caldeira-Leggett Hamiltonian (AHCL), and to determine tunneling Current, spectral function, spin polarization parameter and Differential Conductance Keldysh Green's function method is used. When both damping due to the substrate and el-ph interaction are present, the ground state energy gets renormalized and tunneling current and differential conductance increase. Also Difference Conductance shows peaks which splits and increases in height as the magnetic field increases.

In this chapter, we have also compared Quantum Dot Dimer with Single Quantum Dot and found that Current and Difference Conductance is maximum for SQD while the minimum for QDD.

Lastly, in chapter 6, we have studied the Spin polarization coefficient with bias voltage and magnetic field. We find that spin polarization increases with increase in magnetic field and have higher value for low bias voltage. We have also shown the variation of J and G with el-ph interaction and mid voltage. The above model may be important for making more complicated devices and there functioning.

List of publications

Publications based on which the present thesis has been written

- 1) "Spin torque induced spin current in a two-dimensional tight-binding system with Rashba coupling in the presence of random impurities". (chapter 2)
- H. Sharma, S. Sil, and A. Chatterjee, J Mag Mag Mat, 500, 166329, (2020).
- 2) "Spin transport in a two-dimensional tight-binding system with Rashba and Dresselhaus spin-orbit interactions in the presence of static random disorder". (Chapter 3)
- H. K Sharma, S. Sil and A. Chatterjee, J Mag Mag Mat, 529, 167711, (2021).
- 3) Torque-dependent Spin-Hall conductivity and Hall angle in a two-dimensional tight-binding system with Rashba and Dresselhaus spin-orbit interactions in the presence of static random disorder. (Chapter 4)
- H. K Sharma, S. Sil and A. Chatterjee (in Review).

Paper to be published

- 1) Torque-dependent Longitudinal and transverse spin conductivity and Hall angle in a two-dimensional tight-binding system with Rashba and Dresselhaus spin-orbit interactions in the presence of static random disorder at low temperature. (Chapter 5)
- H. K Sharma, S. Sil and A. Chatterjee (To be communicated).

- 2) Non-Equilibrium Quantum transport through a Quantum Dot Dimer in presence of electron-electron interaction and electron-phonon interaction, magnetic field and quantum dissipation. (Chapter 6)
- H. K Sharma, M. Kalla and A. Chatterjee (To be communicated)

Publications (not part of the thesis work):

- "Electronic and magnetic properties of a two-electron Gaussian GaAs quantum dot with spin-Zeeman term: A study by numerical diagonalization".
 Hemant K. Sharma, Aalu Boda, Bahadir Boyacioglu, Ashok Chatterjee J Mag Mag Mat, 469, 171, (2020).
- 2) "Nature of localization-delocalization transition in a two-level system interacting with a phonon bath: A variational treatment with an improved wave function" **Hemant K. Sharma**, M. Yadaiah, Soma Mukhopadhyay and Ashok Chatterjee, IJTP **59**, 596 (2020)

Transport phenomenon in low dimensional quantum system

by Hemant Kumar Sharma

Submission date: 28-Dec-2021 04:55PM (UTC+0530)

Submission ID: 1736081948

File name: Hemant_Thesis_for_plagarism.pdf (3.72M)

Word count: 23831 Character count: 105805

> Prof. ASHOK CHATTERIES SCHOOL OF PHYSICS UNIVERSITY OF HYDERABAD HYDERABAD - 500 046, INDIA

Transport phenomenon in low dimensional quantum system

ORIGINALITY REPORT

SIMILARITY INDEX

INTERNET SOURCES

PUBLICATIONS

STUDENT PAPERS

PRIMARY SOURCES

Hemant Kumar Sharma, Shreekantha Sil, Ashok Chatterjee. "Spin transport in a twodimensional tight-binding system with Rashba and Dresselhaus spin-orbit interactions in the presence of static random disorder", Journal of Magnetism and Magnetic Materials, 2021

Publication

Hemant Kumar Sharma, Shreekantha Sil, Ashok Chatterjee. "Spin torque induced spin current in a two-dimensional tight-binding system with Rashba coupling in the presence of random impurities", Journal of Magnetism and Magnetic Materials, 2020 Publication

Manasa Kalla, Narasimha Raju Chebrolu, Ashok Chatterjee. "Magneto-transport properties of a single molecular transistor in the presence of electron-electron and electron-phonon interactions and quantum of Physics dissipation". Scientific Reports, 2010 UNIVERSITY OF HYDERABAD HYDERABAD - 500 046. INDIA dissipation", Scientific Reports, 2019

4	Ch. Narasimha Raju, Ashok Chatterjee. "Quantum dissipative effects on non-equilibrium transport through a single-molecular transistor: The Anderson-Holstein-Caldeira-Leggett model", Scientific Reports, 2016 Publication	<1%
5	P. Kleinert. "Theory of the spin-Hall effect revisited", physica status solidi (c), 12/2006	<1%
6	Submitted to Arab Open University Student Paper	<1%
7	Junren Shi, Ping Zhang, Di Xiao, Qian Niu. "Proper Definition of Spin Current in Spin-Orbit Coupled Systems", Physical Review Letters, 2006 Publication	<1%
8	Manasa Kalla, Narasimha Raju Chebrolu, Ashok Chatterjee. "Quantum transport in a single molecular transistor at finite temperature", Scientific Reports, 2021	<1%
9	Miao Wang, Kai Chang. "Anisotropic spin transport in two-terminal mesoscopic rings: Rashba and Dresselhaus spin-orbit interactions", Physical Review B, 2008 Publication	<1%
10	Tutul Biswas. "Zitterbewegung of electrons in quantum wells and dots in the presence	<1%

of an in-plane magnetic field", Journal of
Physics Condensed Matter, 05/09/2012
Dublication

	Publication	
11	Submitted to University of St Andrews Student Paper	<1%
12	F. Mancini. "The Hubbard model within the equations of motion approach", Advances In Physics, 7/1/2004 Publication	<1%
13	Gaolin Fang. "", IEEE Transactions on Systems Man and Cybernetics - Part A Systems and Humans, 1/2007 Publication	<1%
14	Manasa Kalla, Ashok Chatterjee. "Magneto- transport in an interacting single molecular transistor using Anderson-Holstein model", AIP Publishing, 2018 Publication	<1%
15	S. Sil, P. Entel. "Electronic Transport in Magnetic Domain-wall Structure", Phase Transitions, 2003 Publication	<1%
16	Th. Pruschke, M. Jarrell, J.K. Freericks. " Anomalous normal-state properties of high- superconductors: intrinsic properties of strongly correlated electron systems? ", Advances in Physics, 1995 Publication	<1%

17	J. S. Sheng, Kai Chang. "Spin states and persistent currents in mesoscopic rings: Spin-orbit interactions", Physical Review B, 2006 Publication	<1%
18	S. Bandyopadhyay. "Infrared absorption in a quantum wire: A technique to measure different types of spin-orbit interaction strengths", Applied Physics Letters, 2006 Publication	<1%
19	Zhe Zhang, Xuejuan Zhong. "Time-cost trade-off resource-constrained project scheduling problem with stochastic duration and time crashing", International Journal of Applied Decision Sciences, 2018 Publication	<1%
20	www.ncbi.nlm.nih.gov Internet Source	<1%
21	Kuntal Bhattacharyya, Ashok Chatterjee. "Polaronic and bound polaronic effects in the energy states of an electron in a two- dimensional parabolic quantum dot in the presence of Rashba spin-orbit interaction", AIP Publishing, 2019 Publication	<1%
22	Markus Ehlert, Cheng Song, Mariusz Ciorga, Thomas Hupfauer et al. "All-electrical detection of spin Hall effect in	<1%

semiconductors", physica status solidi (b), 2014

Publication

23	Submitted to National University of Singapore Student Paper	<1%
24	opus4.kobv.de Internet Source	<1%
25	Qing-feng Sun, X. C. Xie, Jian Wang. "Persistent spin current in nanodevices and definition of the spin current", Physical Review B, 2008 Publication	<1%
26	Environmental Science and Engineering, 2014. Publication	<1%
27	High-Tc Superconductors and Related Materials, 2001. Publication	<1%
28	Submitted to Queen's University of Belfast Student Paper	<1%

Exclude quotes On Exclude bibliography On

Exclude matches

< 14 words

